Development of comprehensive analysis tools for Supernova neutrino detection in multiple experiments

by

Vsevolod Orekhov

Doktorarbeit in Physik
vorgelegt dem Fachbereich Physik, Mathematik und Informatik (FB 08)
der Johannes Gutenberg-Universität Mainz
am 13.02.2024

Prüfungsdatum: 03.09.2024

Ich versichere, dass ich die Arbeit selbstständig verfasst und keine anderen als die angegebenen Quellen und Hilfsmittel benutzt sowie Zitate kenntlich gemacht habe.

Mainz, den 13.02.2024

Vsevolod Orekhov
Institut für Physik
Staudingerweg 7
Johannes Gutenberg-Universität D-55099 Mainz
vorekhov@uni-mainz.de

Table of content

Table of content

Abstract

A galactic Supernova explosion is a unique neutrino source: detecting the neutrinos from deep inside the star will help us understand both the physics of the core collapse and properties of the neutrinos themselves. If a SN neutrino burst arrived at Earth today or in the near future, it would be detected by a variety of ton to kiloton scale neutrino detectors based on different technologies and target media. By combining the analysis of the explosion in multiple experiments, one could significantly improve the precision of determining the neutrino flux and spectral parameters such as the mean energy and spectral index. In this work an analysis framework was developed in order to be able to fit simultanously the supernova neutrino signals from different detectors. It was shown that by combining three large neutrino detectors such as JUNO, DUNE and IceCube one could achieve percent level precision on the determination of the neutrino spectral parameters. For a canonic supernova at a known distance of 10 kpc, the total energy of the explosion could be measured with 7.1 % uncertainty. On the example of an 8.8 $M_{\odot}$ supernova, a time-dependent analysis of the signal was carried out. The time evolution of the neutrino spectral parameters was fitted, using an adapted analytical model to describe the time development of mean energy, spectral index and flux. The fit results gave a possibility to measure and estimate some astrophysical parameters of the supernova, such as the accretion time $\tau_a = 0.14 \pm 0.01$ s. The resulting fit parameters can be used as well to indirectly constrain physical properties of the proto neutron star. Assuming that the distance to the event is known at 2% level (as for SN1987A), the combination of JUNO, IceCube and DUNE can determine the radii of the flavor-dependent neutrino spheres to 6% for $\bar{\nu}_e$, 2.2% for ν_e and 13% for ν_x level accuracy. Moreover the temperatures of the PNS neutrino spheres can be extracted at: 6% for T_{ν_e}, 1% for $T_{\bar{\nu_e}}$ and for T_{ν_x} 7% level.

1 Overview

A core-collapse supernova explosion is a fascinating astrophysical event. In case it happens within our galaxy it is sufficiently bright to be visible in the sky during the day time. Such an event would offer a great opportunity to reveal the underlying physics of the core-collapse and answer number of question of physical and astrophysical nature, such as the supernova explosion mechanism, the total energy emitted in neutrinos, their spectra, neutron star or black hole formation, and many more.
The only time neutrinos have been observed from a core-collapse supernova was the SN1987A in the Large Magellanic Cloud. At the time four detectors reported the detection of the neutrino interactions. And although the number of these events didn't surpass three dozen, it was enough to confirm the basic model of the core-collapse and derive a lot of constraints on physics and astrophysics. On the Earth today there are, and in the near future there will be, plenty of the detectors with different media and neutrino detection method which will be able to catch the supernova neutrinos in abundance. These detectors have their own specialities and will one by one offer only a limited view of the collapse. Therefore in order to profit from all the information available, one would need to do a multidetector analysis. This kind of analysis requires analysis tools and sensitivity studies for various detectors. The creation of such a framewok is at the centre of this work.
Basic neutrino properties and supernova physics, its evolution and collapse you can find in section 2.
Three detectors were chosen, namely JUNO, DUNE and IceCube. These are huge neutrino detectors scattered around the globe, with different media, including scintillator, liquid argon and ice, which will be operating alltogether in the near future. You can find their descriptions in chapter 3.
As a common simulation framework, the SNOwGLoBES software package was used (Chapter 4). SNOwGLoBES is a public software that allows to simulate supernova neutrino spectra and basic detector responses for numerous materials. To set it up correctly the neutrino proton elastic scattering including scintillation quenching for protons was added for the JUNO-like detector, an interaction channel that was missing from the SNOwGLoBES framework before.
The developed analysis framework with the fit procedure are presented in a chapter 5. The χ^2 analysis showed that the JUNO-like detector is mostly sensitive to the $\bar{\nu_e}$ and ν_x flavors, because of the inverse beta decay, neutrino-proton elastic scattering processes and neutral current interaction on ^{12}C. On the other hand a DUNE-like detector is mostly sensitive to the ν_e's. The addition of the IceCube-like detector to these two constrain $\bar{\nu_e}$'s even better due to the dominant IBD channel. The combination of all the detectors allows to determine the neutrino spectral parameters, such as mean

energy, pinching factor and normalisation, with percent level precision.
It takes time for the supernova to collapse. The explosion can be described in three phases: neutronization, accretion and cooling phases. Using the combination of three detectors provides much better information on the time dependence and underlying collapse. The strategy behind the analytical fit and time-dependent analysis is described in chapter 6. As an example, a 8.8 $M_{\odot}$ supernova explosion, modelled by the Hüdepohl group [1], at 10 kpc canonical distance was analysed. The time evolution of the neutrino flux parameters (such as mean energy, pinching or normalisation) can be analytically described, by the model described by Vissani et al. in Ref.[2]. A simultaneous fit of the spectral parameters derived for regular time intervals permits both to constrain the time evolution of their values and to access underlying astrophysical parameters like the temperature and time constants of PNS cooling as well as the radii of the PNS neutrino spheres.
Results are summarised and an outlook is given in Chapter 7.

2 Basic concepts

2.1 Neutrinos

The existence of the neutrino as an elementary particle with a very small mass, a spin 1/2 and electrical charge equal to zero, was proposed by a German physicist Wolfgang Pauli in 1930. It was introduced in order to explain electron energy spectrum in β-decays of nuclei. According to Pauli the energy released in radioactive decay is carried away by an electron or positron and a neutrino (ν) or antineutrino ($\bar{\nu}$):

$$A_1 \rightarrow A_2 + e + \nu$$

First theory, based on Pauli hypothesis, was created by an Italian physicist Enrico Fermi in 1934 almost immediately after the discovery of the neutron by James Chadwick. The term "neutrino" also belongs to Fermi – translated from italian little neutron. In Fermi theory a new type of interaction was introduced, its range of interaction should be much smaller than the nuclear radius, an interaction that was later called "weak". The weak interaction causes the transformation of a neutron into a proton(or a proton into a neutron, which is possible inside the nucleus) with the simultaneous birth of an electron(positron) and an antineutrino(neutrino). Intensity of the weak interaction is described by dimensional constant G_F - Fermi constant. $\mathrm{G}_F = \mathrm{erg}^{-2}$. An the value is $10^{-5}/\mathrm{m}_p^2$, where m_p is the proton mass.
Knowing the Fermi constant, one could estimate the cross-section of a (anti)neutrino proton interaction, inverse beta decay (IBD):

$$\bar{\nu} + p \rightarrow e^+ + n$$

Considering the dimensions, it is easy to estimate the answer: $\sigma \approx G_F^2 E_\nu^2$. For the 1 MeV neutrino energy the cross-section is extremely small: about $10^{-43} cm^2$. With such cross-section, the neutrino free path in matter turns out to be equal to 10^{20}cm.

$$\mathrm{L} = \frac{1}{n\sigma} \approx 10^{20} \text{ cm}$$

This value is 10^{11} times larger than the radius of the Earth. It is clear why it was called weak..

2.2 Discovery of neutrino

The first to detect neutrino interaction with matter were Cowan and Reines, 1956 [3]. The source of neutrinos (more precisely antineutrinos) in their experiment was the nuclear reactor - the most powerful source of neutrinos on the Earth. They used

the IBD-reaction which produces positron and neutron. The setting consisted of two polyethylene tanks with water, each of a 200 l volume. Cadmium salt was added to the water to increase the efficiency of neutron capture. Prompt gammas produced in positron annihilation and delayed after neutron capture were detected in tanks with a liquid scintillator. The detector site was surrounded by paraffin and lead to reduce background.
Signals from the photomultiplier tubes(PMTs), which observed the tanks with the scintillator, were fed to a oscilloscope. In 200 hours there were detected approximately 500 events. The cross-section of the neutrino interaction was found to be in a good agreement with the prediction of Fermi theory: $\sigma \approx 10^{-42} cm^2$, $E_\nu \approx 3$ MeV.

2.3 Neutrino properties

According to the modern classification neutrino belongs to lepton family(leptons are the particles which do not participate in strong interaction). There are three charged leptons: e, μ, τ and three neutral: ν_e, ν_μ, ν_τ. The carriers of the weak interaction between leptons and quarks are heavy charged- W and neutral Z-bosons. W and Z-bosons have ∼80 GeV and ∼91 GeV correspondingly, radius of the weak interaction ($\sim 1/M_W$)$\sim 10^{-16}$cm. The reactions in which the incident lepton changes sign are called charge-current(CC) reactions and happen through W-boson exchange; the reactions in which the lepton does not change sign are called neutral-current(NC) interactions and they happen with the Z-boson exchange.
Different species of neutrino(ν_e, ν_μ, ν_τ) are different particles. So, for instance, in the interaction of ν_μ with matter the muons would be borned and not electrons or tau-leptons. Such character of the weak interaction(conservation of electron, muon and tau lepton numbers) was confirmed in many experiments and put in the foundation of the Standard Model of the particle physics.
Although the mass of the neutrinos is extremely small, it is not equal to zero. It was proven by the discovery of neutrino oscillations. Historically the first measurements that pointed towards oscillations were performed with solar neutrinos. The experimentally determined flux of solar ν_e was, depending on the energy, about one third to half the value predicted in solar models. The interpretation is of course that the ν_e oscillate into ν_μ and ν_τ. The flavour states $|\nu_e\rangle$, $|\nu_\mu\rangle$ and $|\nu_\tau\rangle$ are not identical to the states $|\nu_1\rangle$, $|\nu_2\rangle$ and $|\nu_3\rangle$ which posses a well-defined mass. One can write the flavour states as orthogonal linear combinations of the mass states:

$$\begin{pmatrix} |\nu_e\rangle \\ |\nu_\mu\rangle \\ |\nu_\tau\rangle \end{pmatrix} = \begin{pmatrix} U_{e1} & U_{e2} & U_{e3} \\ U_{\mu 1} & U_{\mu 2} & U_{\mu 3} \\ U_{\tau 1} & U_{\tau 2} & U_{\tau 3} \end{pmatrix} \begin{pmatrix} |\nu_1\rangle \\ |\nu_2\rangle \\ |\nu_3\rangle \end{pmatrix} \tag{2.1}$$

This matrix is called PMNS (Pontecorvo, Maki, Nakagawa, Sakata) matrix. To understand how the elements of U can be determined, one could consider only two generations of neutrinos, $|\nu_e\rangle$ and $|\nu_\mu\rangle$:

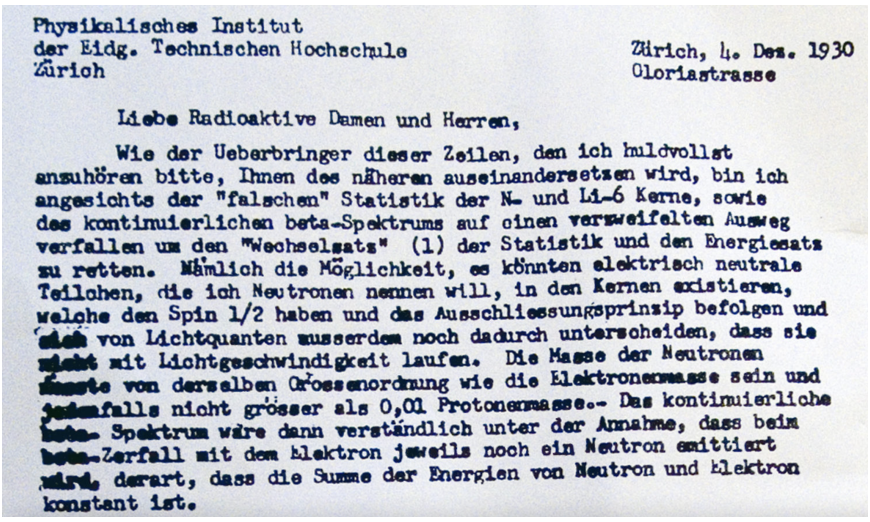

Physikalisches Institut
der Eidg. Technischen Hochschule
Zürich

Zürich, 4. Dez. 1930
Gloriastrasse

Liebe Radioaktive Damen und Herren,

Wie der Ueberbringer dieser Zeilen, den ich huldvollst anzuhören bitte, Ihnen des näheren auseinandersetzen wird, bin ich angesichts der "falschen" Statistik der N- und Li-6 Kerne, sowie des kontinuierlichen beta-Spektrums auf einen verzweifelten Ausweg verfallen um den "Wechselsatz" (1) der Statistik und den Energiesatz zu retten. Nämlich die Möglichkeit, es könnten elektrisch neutrale Teilchen, die ich Neutronen nennen will, in den Kernen existieren, welche den Spin 1/2 haben und das Ausschliessungsprinzip befolgen und sich von Lichtquanten ausserdem noch dadurch unterscheiden, dass sie nicht mit Lichtgeschwindigkeit laufen. Die Masse der Neutronen müsste von derselben Grössenordnung wie die Elektronenmasse sein und jedenfalls nicht grösser als 0,01 Protonenmasse.- Das kontinuierliche beta- Spektrum wäre dann verständlich unter der Annahme, dass beim beta-Zerfall mit dem Elektron jeweils noch ein Neutron emittiert wird, derart, dass die Summe der Energien von Neutron und Elektron konstant ist.

Figure 2.1: Letter of W. Pauli proposing the existence of neutrino.

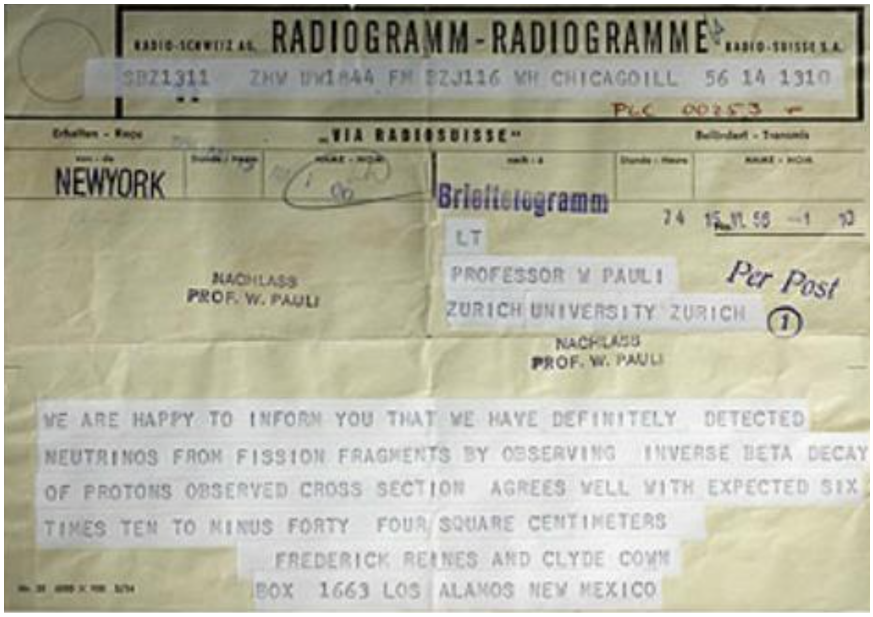

RADIO-SCHWEIZ AG. RADIOGRAMM-RADIOGRAMME RADIO-SUISSE S.A.

SBZ1311 ZHV UW1844 FM BZJ116 WH CHICAGOILL 56 14 1310

Pcc 00253

„VIA RADIOSUISSE"

NEWYORK

Brieftelegramm

LT

PROFESSOR W PAULI

Per Post

ZURICH UNIVERSITY ZURICH (1)

NACHLASS PROF. W. PAULI

NACHLASS PROF. W. PAULI

WE ARE HAPPY TO INFORM YOU THAT WE HAVE DEFINITELY DETECTED NEUTRINOS FROM FISSION FRAGMENTS BY OBSERVING INVERSE BETA DECAY OF PROTONS OBSERVED CROSS SECTION AGREES WELL WITH EXPECTED SIX TIMES TEN TO MINUS FORTY FOUR SQUARE CENTIMETERS

FREDERICK REINES AND CLYDE COWN

BOX 1663 LOS ALAMOS NEW MEXICO

Figure 2.2: Radiogramm to W.Pauli about the discovery of the neutrino

$$\begin{pmatrix} |\nu_e\rangle \\ |\nu_\mu\rangle \end{pmatrix} = \begin{pmatrix} \cos\theta & \sin\theta \\ -\sin\theta & \cos\theta \end{pmatrix} \begin{pmatrix} |\nu_1\rangle \\ |\nu_2\rangle \end{pmatrix} \tag{2.2}$$

Neutrinos are produced as flavour states by the weak interaction, e.g. a $|\nu_e\rangle = \cos\theta|\nu_1\rangle + \sin\theta|\nu_2\rangle$ by a charged current electron-quark interaction. The time evolution of the mass states leads after a time t to the following wave function of the electron neutrino:

$$|\nu_e(t)\rangle = cos\Theta e^{-iE_1 t/\hbar}|\nu_1\rangle + sin\Theta e^{-iE_2 t/\hbar}|\nu_2\rangle \tag{2.3}$$

Neutrinos are ultra-relativistic, hence their energy is:

$$E_{\nu_i} = \sqrt{p^2c^2 + m_{\nu_i}^2 c^4} \approx pc(1 + \frac{1}{2}\frac{m_{\nu_i}^2 c^4}{p^2c^2}) \tag{2.4}$$

The probability to find an electron neutrrino after the time t is therefore:

$$P_{\nu_e \to \nu_e} = \langle \nu_e(t)|\nu_e(t)\rangle|^2 = cos^4\Theta + sin^4\Theta + 2cos^2\Theta sin^2\Theta cos(\frac{1}{2}\frac{\Delta m_{21}^2 c^4}{\hbar c}\frac{L}{pc}) =$$

$$= 1 - sin^2 2\Theta sin^2(\frac{1}{4}\frac{\Delta m_{21}^2 c^4}{\hbar c}\frac{L}{pc}). \tag{2.5}$$

where $\Delta m_{21}^2 = m_{\nu_2}^2 - m_{\nu_1}^2$ is the difference of the squares of the masses of the states ν_1 and ν_2, and L = ct is the distance between production and detection travelled by the neutrino in the time t. Hence if one measure the survival probability, you can determine the amplitude $sin^2 2\Theta$(and hence the elements of the PMNS-matrix) and the mass-squared difference Δm_{21}^2, which is proportional to the oscillation frequency. The characteristic scale of oscillations is the distance between two minima or maxima, which is denoted as oscillation length:

$$L_{osc} = 4\pi\frac{\hbar pc^2}{\Delta m_{21}^2 c^4}$$

On Fig.2.3 the typical oscillation curve for the transition probability is presented.

2.4 Core-collapse Supernova

2.4.1 Introduction

Supernovae(SNe) are very powerful explosions which end the life of some stars. Typically, huge masses are ejected into the interstellar space with a kinetic energy around 10^{51} erg. The ejecta contain heavy elements that are important for the chemical evolution of the universe and life in it. Some SNe produce a compact remnant, black hole or a neutron star, which could be observed (Giunti & Kim, 2007, p.511 [4]). A

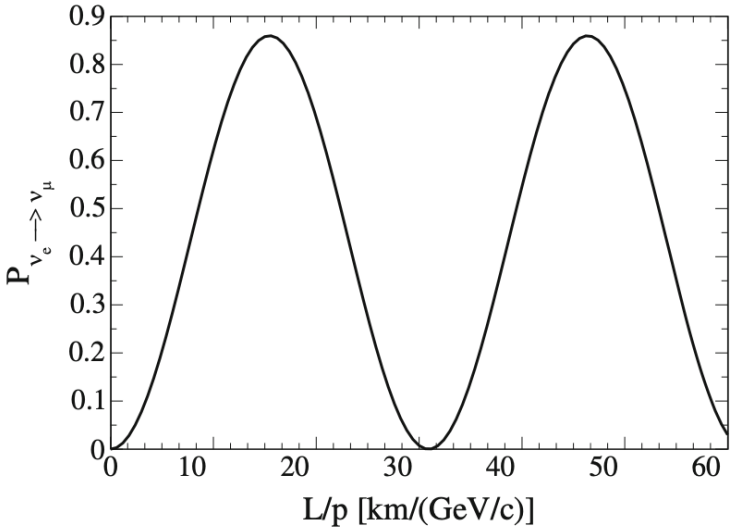

Figure 2.3: Typical oscillation curve for the transition probability of electron neutrinos in muon neutrinos. The chosen parameters are $\Theta = 34\ ^\circ$ and $m^2_{\nu_2} - m^2_{\nu_1} = 8{\cdot}10^{-5}\mathrm{eV}^2/c^4$. Hence the transition probability is zero for the L/p$\approx$ 31 km/(MeV/c) and maximal ($\sin^2 2\Theta = 0.86$) for half this value. The oscillation length for a momentum of 3 MeV/c is $L_{osc} \approx 93$ km.

prominent feature of the collapse is that $\sim$ 99 % of the gravitational binding energy of the resulting remnant is converted to neutrinos with energies of a few tens of MeV over a timescale of a few tens of seconds. This highly efficient energy loss via neutrinos occurs because the neutrinos interact only via the weak interaction and can escape easily [5].
The study of SNe was initiated by W.Baade and F. Zwicky in the early 1930s [6]. They suggested that that the source of the enormous amount of energy released in SNe is the gravitational collapse of a star to a neutron star and that SNe may be sources of cosmic rays. In the following years a sistematic search of SNe was organised and it led to the present knowledge of thousands of SNe ([4], p.511).
Some star sollapses that have happened in a Milky Way, our galaxy, have been observed with the bare eye during the last 2000 years. The most famous is the 1054 supernova, which produced the Crab nebula and the Crab pulsar. The 1006 SN was the brightest of all times. The last galactic SNe were observed in 1572(Tycho Brahe) and 1604(Joannes Kepler). SNe happening in the other galaxies were observed with the telescopes in the last few centures. It was possible because their luminosity was comparable to that of an entire galaxy. Last SN that occured in our neighbourhood was SN1987A, the core collapse happened on 23 February 1987 in the Large Magellanic Cloud. It is the best studied SN and it is the only SN which was detected also through its neutrino burst. This first observation of neutrinos produced with the extragalactic star explosion started important studies of SN dynamics, but also neutrino

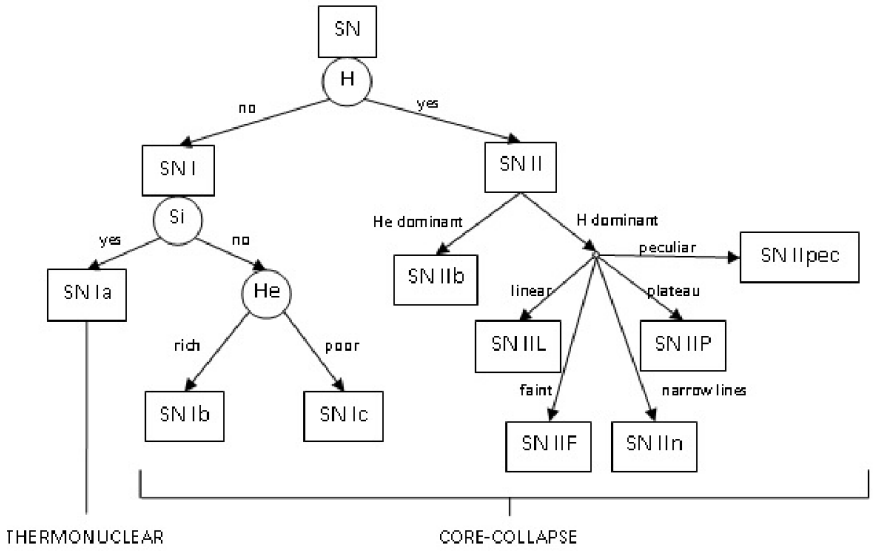

Figure 2.4: The classification scheme of supernovae.

properties, such as neutrino masses ([4], p.511).

2.4.2 Types of Supernova

Supernovae are divided into different types, which are being characterised by their spectroscopic characteristic close to maximum luminosity and properies of their light curve, which contains information about the composition of the SN progenitor star. Nowadays exist two categories of the SNe called type 1 and type 2. They are characterised by the presence or the absence of the Hydrogen lines. However, the mechanism that generates SNe is the most important characterisic, that distinguishes SNe of type Ia from SNe of type Ib, Ic and II, as you can see on Fig 2.4. It becomes clear if you observe the light spectrum several months after maximum luminosity, when the ejecta become optically thin, so one could see inner regions of it. The spectrum of SNe Ia is dominated by the Fe emission lines, whereas SNe Ib, Ic and II by O and C emission lines. Typically, the optical emission of both types of the SNe start with the rise in luminosity during the first couple of weeks due to the expansion of the luminous surface. Type I SNe have narrow peak, whereas type II have broad luminosity peaks, for about of 100 days. Then it decreases for a year ([4], p.512).
Type Ia supernovae are assumed to be generated by carbon-oxygen white dwarfs that have a close star companion from which white dwarf can acrete mass. White dwarfs are the result of the stars that ended their thermonuclear fuel burn. Their mass is comparable with the solar mass, radius approximately 5000 km and density around 10^6g cm^{-3}. Degenerate electrons pressure supports them against pull of gravity. In 1931 Chandrasekhar discovered that white dwarfs have a maximum mass $\sim 1.4 M_\odot$, above which the star collapses [7]. When the mass reaches this limit, the star becomes

unstable, because the pressure of the degenerate electron gas can no longer sustain the gravitational weight. The white dwarf begins to collapse, triggering the fusion of carbon and oxygen to heavy nuclei, like ^{56}Ni, which releases huge amount of energy, causing thermonuclear explosion of the star([4], p.513-514).
SNe of type Ia are all generated under similar physical conditions, such as the exploding star mass is close to Chandrasekhar limit, so there is a little variation in the absolute luminosity of these explosions, making them nearly ideal distance indicators. What variation there is seems to be well correlated with the rise time and decline time of the supernova light: the slower the decline, the higher the absolut luminosity. It allows the use of type Ia SNe as standard candles for the measurement of the distance of galaxies as far as 100 Mpc or more([4], p.514).
It is believed that type II SNe are generated by the core collapse of red(or blue as SN1987A) giant stars with the masses more than 8 solar mass. Since the size and mass of collapsing stars can be very different, the visible effects of its explosion have a wide range of variability, which leads to a further classification of type II SNe into the subtypes[Ref]: IIL if the decrease of the luminosity is approx. linear in time; IIP if the time evolution of the luminosity shows a plateu; IIF if the SN is faint; IIb if helium dominates over hydrogen; IIn if the spectrum shows narrow line emissions; IIpec if the SN has peculiar characteristics. Supernova SN1987A was an extreme case of type IIP SN, since the luminosity increased for about 3 months after the collapse and the supernova was rather faint([4], p.515).

2.4.3 Supernova rates

It is very important to know, how often SN, or core collapse SN can occur. SN rates depend mostly on the galaxy type. One could see it on the Fig. 2.5. No core-collapse SNe of type Ib/c an II have been observed in elliptical galaxies, which are very old and hence do not have or have little active star formation, that would produce massive stars that later could end their life with the supernova explosion. Crucial question for the neutrino astronomy is: what is the rate of the SN core-collapse explosions in our galaxy, which could emit neutrino bursts, that could be detected in neutrino detectors with high or relatively high statistics ([4], p.515).
Estimates of the core-collapse SNe rate are shown in the Table 2.1.
The absence of observation of neutrinos from core-collapse SNe in our galaxy since the Baksan Underground Scintillator Telescope began observation in June 1980 imply an upper limit of 13 SNe per century in the Milky Way at 90% CL [22]. Estimates shown in Table 2.1 are based upon observations of the rate of occurence of supernovae in other galaxies; the extragalatic rates incorporate large corrections to account for the covering effect of dust and gas, that could hide SNe, and of viewing angle. The rate of stellar collapses could also be estimated from the rate of formation of galactic pulsars, which are magnetised and rotating neutron stars. Narayan [23] found a mean time between the formation of neutron stars:

$$20yr \leq T \leq 60yr,$$

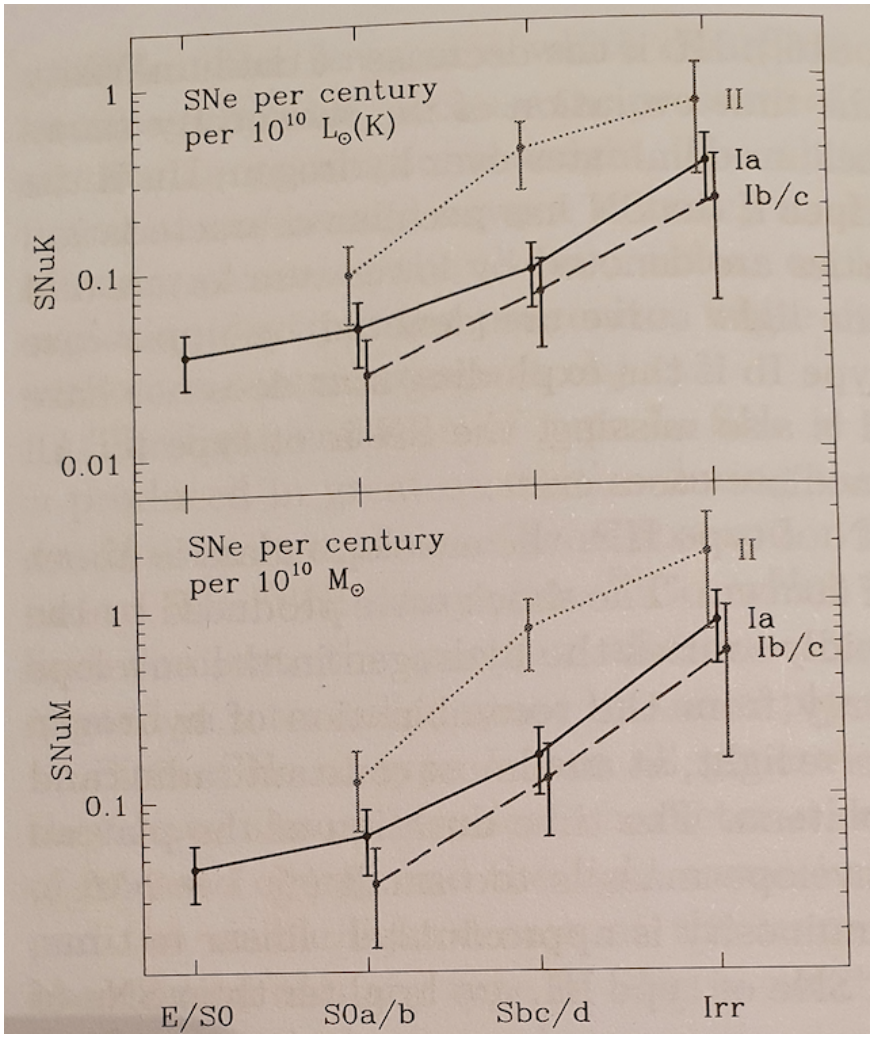

Figure 2.5: SN rates as a function of the galactic morphological index.[8]

Rate $[10^{-2}y^{-1}]$	Reference
5.8 ± 2.4	Tamman (1982) [9]
$1.2^{+1.7}_{-0.7}$	Ratnatunga & van den Bergh (1989) [10]
3^{+2}_{-1}	Strom (1990) [11]
4.0 ± 2.0	Muller et al. (1992) [12]
2.0 ± 1.1	Cappellaro et al. (1993) [13]
3.0 ± 1.5	van den Berg (1993) [14]
$2.5^{+0.8}_{-0.5}$	Tammann et al. (1994) [15]
5.7 ± 1.7	Strom (1994) [16]
1.3 ± 0.9	Cappellaro et al. (1997) [17]
3.4 ± 2.8	Timmes et al. (1997) [18]
8.4 ± 2.8	Dragicevich et al. (1999) [19]
1.5 ± 1.0	Cappellaro & Turatto (2000) [20]
1 - 2	Reed (2005) [21]

Table 2.1: Estimates of the rate of core-collapse SNe in the Milky Way

with a preffered value of 56 yr ([24], p.434).

2.4.4 Core collapse supernova dynamics

When a Type II supernova is about to explode, the fusion of silicon to form iron first becomes possible at the center of the star. At this time the star has already passed through successive stages of burning hydrogen, helium, carbon, oxygen and neon and has taken on an onion-like structure with the innermost regions containing the heaviest nuclei and the outer layer contains pure hydrogen. Fusion continues at the boundary between the iron core and the silicon shell, relentlessly adding mass to the core. Inside the core, there is no any production of energy anymore by nuclear reactions, it's just become a sphere under a huge pressure. A typical massive star takes several million years from the birth on the main sequence until it has developed an iron core ([24], p.425).
Core-collapse SNe are the final explosion of the stars with mass larger than 8-9 solar masses. The explosion is due to the shock wave created when the core collapses to a proton-neutron star, which ejects the stellar envelope. Stars lighter than about 9 $M_\odot$ end their life as white dwarfs. As illustrrated in Fig 2.6 and Fig 2.7 if stars had mass larger than $40M_\odot$, they can end their life in a supernova explosion if they have a sufficient initial metallicity, i.e. abundance of heavy elements. ([4], p.515)
During their life they suffer mass losses through stellar wind. The core of low and medium metallicity stars with the masses between about 25 and 40 solar masses initially collapses to a proton neutron star, generating a weak SN IIp, and later collapses to a black hole because of the increase of mass of the proto-neutron star due to fallback of the envelope. Stars with mass in excess of about 10 solar masses are thought to undergo all the stages of nuclear fusion of hydrogen, helium, carbon, oxygen, neon,

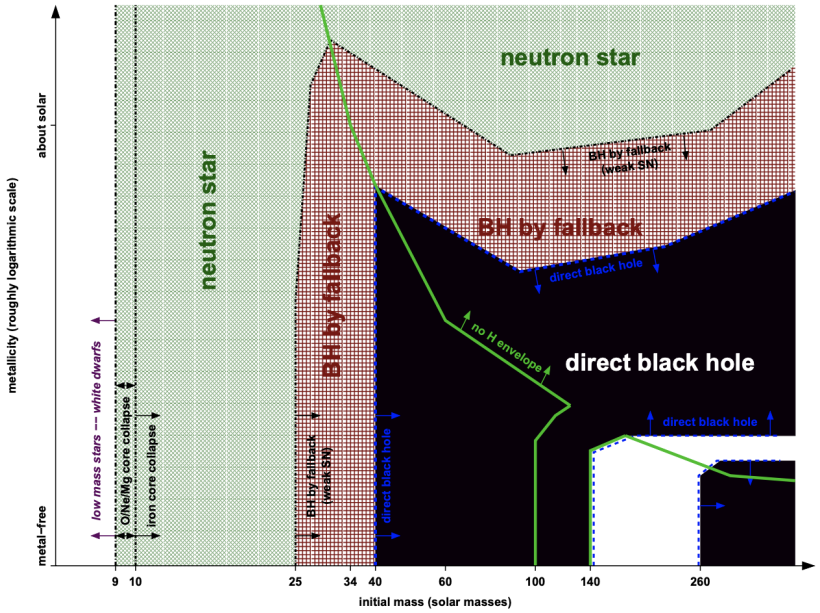

Figure 2.6: Remnants of massive single stars as a function of initial mass(x axis) and initial metallicity(y axis) [25]. The line marked *no H envelope* separates the regimes where the stars keep their hydrogen envelope(left and low right) from those where the hydrogen envelope is lost(upper right and small strip at the bottom between 100 and 140M$\odot$). The line marked **direct black-hole** indicates the border of the regime of direct black-hole formation(black). This domain is interrupted by a strip of pair instability supernovae that leave no remnant(white). Outside the direct black-hole regime, at lower mass and higher metallicity, lies the regime of black-hole formation by fallback. Outside of this, lies the region corresponding to the formation of neutron stars. The lowest-mass neutron stars may be made by O/Ne/Mg core collapse instead of iron core collapse(vertical dash-dotted lines at the left). At even lower masses, the cores do not collapse and only white dwarfs are made(white strip at the very left).

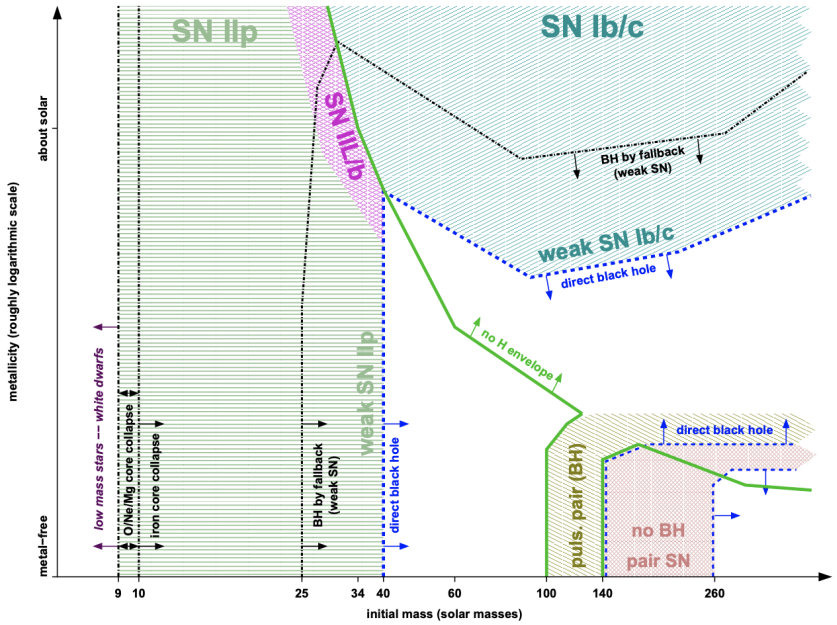

Figure 2.7: Supernovae types of nonrotating massive single stars as a function of initial metallicity and initial mass [25]. The lines and axes have the same meaning as in Fig. 2.6

silicon until the star has an onion-like structure. ([4], p.517).
The mass of the inner core containing mostly iron-like elements is near the Chandrasekhar mass limit, the maximum mass a star can have and support itself against gravity by the degeneracy pressure of electrons. Speaking in numbers, $M_{Ch} = 5.8\ Y_e^2 M_\odot \approx 1.4 M_\odot$, where $Y_e \approx Z/A$ is the electron ratio per baryon. The temperature at the center of the core is ≤ 0.7 MeV. The core is supported by the Fermi pressure of the highly degenerate electron gas, $E_F \approx 8$ MeV, and its highest density is near 10^{10}g cm^{-3}. The core is compressed by its own gravity. This compression raises the temperature in the center, which might be expected to raise the pressure and slow the collapse. However, at these extreme temperatures, the heating has the opposite effect. Pressure now is determined by two factors: number of the particles in a system and their average energy. In the core of the star everything contributes to this pressure i.e. electrons, nuclei and photons. After the core is heated, some fraction of iron nuclei are broken up into smaller nuclei, increasing number of particles and raising nuclear component of the pressure. Simultaneously, the energy from the photons is being absorbed by the dissociation of nuclei; since energy is released when an iron nucleus is formed, the same quantity of the energy must be used to break the nucleus apart. The loss in pressure that is required to disassociate the iron nuclei is greater than the gain in nuclear pressure. Therefore the collapse accelerates ([24], p.425).

$$\gamma + {}^{56}Fe \rightarrow 13\alpha + 4n$$

The core begins to collapse because of the net pressure loss due to the photodesintegration of iron [27]. The collapse is also being accelerated due to rapid capture of free electrons on nuclei and on free protons and in calculated models the SNe are being destabilised primarily by it. The speed of collapse increases to a notable fraction of free-fall, densities rise, nuclei merge into nuclear matter, which because of the electron capture contains approximately two neutrons for every proton. Only resistance of nuclear matter halts the collapse from further compression. If nuclear matter were not sufficiently stiff, the core would collapse directly into a black hole. The collision of falling matter with outgoing matter at the moment of bounce back creates an outward moving shock which ultimately produces the visible explosion which we call Supernova. The earliest neutrinos produced in the collapse are believed to be entirely electron capture neutrinos. There are too few positrons available to produce any significant amount of electron antineutrinos and the temperatures are much too lowto produce thermally any neutrinos of other flavors. ([24], p.426).
The electron neutrinos produced by the electron capture processes and initially leave the core freely, carrying away energy and lepton number, since their mean free path is longer than the radius of the core.

$$e^- + N(Z, A) \rightarrow N(Z-1, A) + \nu_e,$$
$$e^- + p \rightarrow n + \nu_e$$

The density of the inner core reaches the density of nuclear matter, about 10^{14}g cm^{-3}, after about one second from the start of instability, and the pressure of degenerate

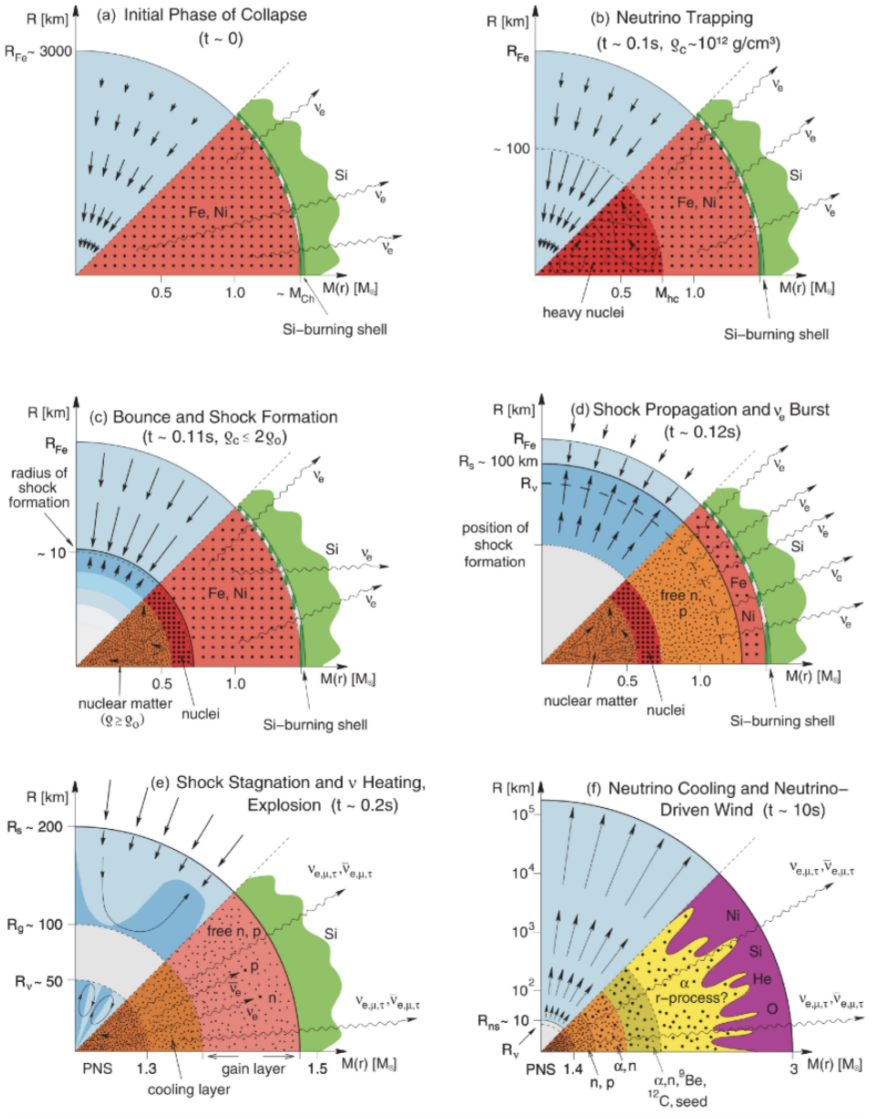

Figure 2.8: Stages of the SN core-collapse [33].

nonrelativistic nucleons abruptly stops the collapse. The inner core settles into hydrostatic equilibrium, forming a proto-neutron star with a radius approximately 10 km. In the meanwhile a supersonic shock wave caused by the halting and rebound of the inner core forms at its surface. The shock propagates outward through the outer iron core, which is still collapsing, with an initial velocity of an order of 100 km msec^{-1}. The infalling gas at a near free-fall velocity is abruptly decelerated within the shock. Below th shock it falls much slower on the surface of the proton-neutron star, accreting it. Therefore, the proto-neutron star develops an unshocked core and a shocked mantle. The core has a radius of the order of 10 km with a density of the order of 10^{14}gcm^{-3}, as a nucleus. The mantle has a radius of 100 km, with a density decreasing from the nuclear density of the core to about 10^{9}gcm^{-3} at the surface of the proto-neutron star, where the density has a steep decrease of several orders of magnitude ([4], p.521).
The energy of the propagating shock is dissipated by the photodissociation of nuclei into protons and neutrons. Free protons have high electron capture rate, which causes the transformation of most protons into neutrons with huge production of electron neutrinos. These neutrinos accumulate behind the shock, which is dense and opaque to them, until the shock reaches a zone with a density about 10^{11}gcm^{-3}(**shock breakout**) a few milliseconds after the bounce and the electron neutrinos behind the shock are released in a few milliseconds. This neutrino emission is usually called a **promt electron neutrino burst** or **neutronization burst** or **breakout pulse**, to be distinguished from the thermal production of all neutrino flavours ([4], p.522).
The energy loss due to photodissociation of nuclei and neutrino emission weakens the shock. In the so-called **prompt** SN explosion scenario, the weakened shock is still able to expel the envelope of the star generating the SN explosion on a time scale of the order of 100 msec. If the shock stalls a SN explosion can be achieved only if the shock is revived by some mechanism that is able to renew its energy. The mechanism which is currently believed to be able to do that is the energy deposition by the huge neutrino flux produced thermally in the proton-neutron star[Ref]. If the shock is revived, a so-called **delayed** supernova explosion is produced on a time scale of the order of 0.5s after the bounce ([4], p.522).
All flavours of neutrinos are produced in the core of the proton-neutron star, which has a temperature about 40 MeV, through electron-positron pair annihilation,

$$e^- + e^+ \to \nu + \bar{\nu}$$

electron-nucleon bremsstrahlung,

$$e^{\pm} + N \to e^{\pm} + N + \nu + \bar{\nu}$$

nucleon-nucleon bremsstrahlung,

$$\mathrm{N} + \mathrm{N} \to \mathrm{N} + \mathrm{N} + \nu + \bar{\nu}$$

plasmon decay,

$$\gamma \to \nu + \bar{\nu}$$

and photoannihilation

$$\gamma + e^{\pm} \rightarrow e^{\pm} + \nu + \bar{\nu}$$

Electron neutrinos are also produced by electron capture process and electron antineutrinos are produced positron capture on neutrons($e^+ + n \rightarrow p + \bar{\nu_e}$). In spite of their weak interaction origin, these neutrinos are trapped in a SN core because of the very high matter density. Neutrinos can free-stream out of mantle of a proton-neutron star only at a distancefrom the center where the matter density is low enough($\approx 10^{11}\mathrm{gcm}^{-3}$) so that the neutrino free path is larger than the radius of the core. The sphere from which neutrinos stream out freely is called the **neutrinosphere**, and it lies whithin the mantle of the proto-neutron star. There are three energy-dependent neutrinospheres: for ν_e, $\bar{\nu_e}$ and ν_x (ν_x neutrinos are: $\nu_\mu, \bar{\nu_\mu}, \nu_\tau, \bar{\nu_\tau}$). Each energy-dependent neutrinosphere emits a black-body thermal flux of neutrinos. The estimated radii are around 50-100 km. After a shock breakout each neutrinosphere produces a thermal flux of the corresponding neutrino flavour ([4], p.523-524). The opacities of ν_e and $\bar{\nu_e}$ are dominated by the charge current interaction processes:

$$\nu_e + p \rightarrow n + e^-$$
$$\bar{\nu_e} + n \rightarrow p + e^+$$

It is not difficult to understand roughly equal partition between different neutrino and antineutrino species. A neutron star that was formed as a result of stellar collapse consists primarily of neutrons at close to nuclear density and is supported by the degeneracy pressure of the neutrons. The degenerate star has about 2 $\times 10^{57}$ baryons. Matter begins as one-half neutrons and one-half protons and winds up as neutron matter, somewhat less than $10^{57}\nu_e$'s must be emitted to shed lepton number. Even for a generous assumed average energy of 15 MeV, this amount to only about 25 $\times 10^{51}$ ergs, or about 10% of the total energy emitted. Most of these ν_e's diffuse out from center of the star, where they have degeneracy energies $\approx$150 MeV. Thus, their degradation in energy as they escape from the star produces a cascade of about 10 pair neutrinos for each ν_e that carries away one unit of lepton number ([24], p.426).
Since the mantle of the proton-neutron star is neutron rich, the opacity of ν_e of a given energy is larger than the opacity of $\bar{\nu_e}$ with the same energy, and the corresponding ν_e neutrinosphere has a larger radius than the $\bar{\nu_e}$ neutrinosphere. This means that for a fixed energy $\bar{\nu_e}$ are emitted by a deeper and hotter layer than ν_e's, leading to a $\bar{\nu_e}$ mean energy larger than ν_e's. Moreover the spectra do not have perfect black-body shape, but are **pinched**, i.e. both the low- and high-energy tails are suppressed with respect to the tails of a black-body thermal spectrum with the same mean energy ([4], p.525).
In the delayed SN explosion scenario the stalled shock lies at a radius of about 100-300 km, outside the neutrinosphere. The post-shock temperature is about 1.5 MeV. The capture of a small fraction, about 5-10% [26], of the thermal flux of the neutrinos could revive the shock, leading to the explosion ([4], p.527).
While the shock is stalled, matter continues to accrete on the proto-neutron star going through the shock. This phase of the supernova exlosion is a so-called **accretion**

phase. The shocked hot material behind the shock, composed mostly of free nucleons, electrons and photons, is heated by the accretion and produces neutrinos and antineutrinos of all flavours. These neutrinos can free stream out of the star and cause so-called **hump** in the neutrino luminosity curve. The average neutrino energy is low during the hump, because the dense matter is opaque to high energy neutrinos. As the shock gradually revives at about 0.5s after the bounce, the matter density decreases and the average neutrino energy increases ([4], p.528).
The delayed explosion scenario is a sort of standard model of core-collapse SN explosion.

3 Supernova neutrino detectors

Currently on the Earth exist a few neutrino detectors, which are able to detect the burst supernova neutrinos, and in the near future come some more. They all have different detector material and they are sensitive to different neutrino species. In case of a supernova explosion in a reasonable distance from our planet, altogether they will be able to detect thousands of neutrino events (millions, if you count $\bar{\nu}_e$ via IBD in IceCube for example). Therefore on order to get the best analysis result possible, one would need to profit from them all. Hence, there is an obvious solution, the multidetector analysis. By combining the analysis of the possible explosion in multiple next generation neutrino experiments, one could significantly improve the precision of determining the neutrino spectra parameters such as the mean energy and spectral index. This analysis requiers tools and sensitivity studies which were done and you can explore them in the following chapters. In this chapter though you can find the description of the chosen detectors, namely JUNO, DUNE and IceCube. This combination was made because JUNO, as a scintillator detector has great energy resolution, and hence can provide the energy information together with spectra information, DUNE is very sensitive to the ν_e, and the IceCube is able to catch huge amount of $\bar{\nu}_e$ via IBD and can give overall rates information. Hence these detectors give very good spectral and rates information, which, combined, provide us with the fluxes. And now to the overview.

3.1 The JUNO experiment

3.1.1 Overview

The Jiangmen Underground Neutrino Observatory (JUNO) is a multi-purpose neutrino experiment. It was proposed in 2008 to determine the neutrino mass hierarchy by detecting reactor antineutrinos from the Daya Bay nuclear power plant (NPP) ([28] - [31]), thus formerly known as "Daya Bay II experiment". The mass hierarchy determination requires equal baselines from the detector to all reactor cores to avoid cancellation of the oscillation dephasing effect. The site location is optimized to have the best sensitivity for the mass hierarchy determination, which is at 53 km from both the Yangjiang and Taishan NPPs [32]. The neutrino detector is a liquid scintillator (LS) detector with a 20 kton fiducial mass, deployed in a laboratory 700 meter underground ([33], p. 28).
Measuring the neutrino burst from the next nearby supernova (SN) is a premier target of low- energy neutrino physics and astrophysics. For a typical galactic distance of 10 kpc and typical SN parameters, JUNO will register about 5000 events from inverse

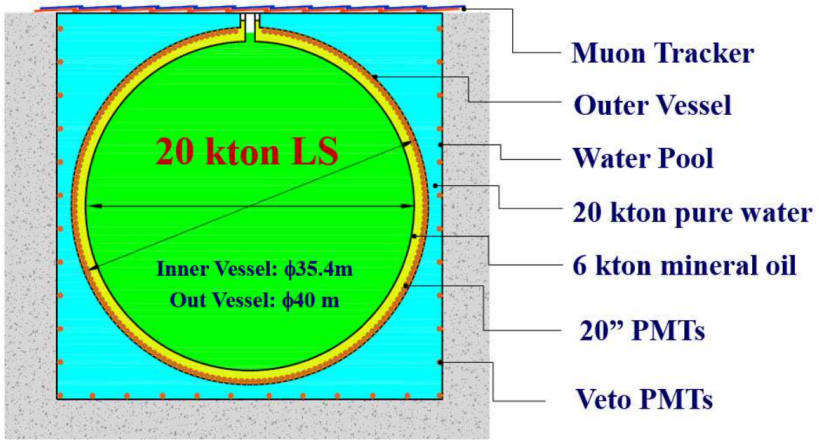

Figure 3.1: Schematic view of the JUNO detector.

beta decay (IBD), which is comparable to Super-Kamiokande, and many events from complementary channels, notably 2000 events from all-flavor elastic neutrino-proton scattering. With more than 300 events from neutrino- electron scattering, JUNO will also be the best detector for SN electron neutrinos. Such a high-statistics signal can determine a detailed neutrino "light curve" spectrum, and complete flavor information. In combination with other neutrino detectors, gravitational-wave detectors, and observations in various electromagnetic channels, a detailed astrophysical multi-messenger picture will emerge ([33], p.68).

3.1.2 Expirement site

The JUNO experiment locates in Jinji town, Kaiping city, Jiangmen city, Guangdong province. The geographic location is east longitude 112° 31'05" and north latitude 22° 07'05". The experimental site is 43 km to the southwest of the Kaiping city, a county-level city in the prefecture-level city Jiangmen in Guangdong province. There are five big cities, Guangzhou, Hong Kong, Macau, Shenzhen, and Zhuhai, all in $\sim$ 200 km drive distance, as shown in Fig. 3.2. The experimental site is at $\sim$ 53 km from the Yangjiang NPP and Taishan NPP. Yangjiang NPP has six reactor cores of 2.9 GW each (thermal power). All cores are the 2nd generation pressurized water reactors CPR1000, which is a derivative of Framatone M310, with improvements on safety, refueling, and conventional island design. The total thermal power of the Yangjiang and Taishan NPPs would be 35.73 GW. Daya Bay complex includes Daya Bay NPP, Ling Ao NPP, and Ling Ao-II NPP in a spread of 1.1 km, each with 2 cores of 2.9 GW. The Daya Bay and Ling Ao cores are Framatone M310 and the Ling Ao-II cores are CPR1000. The Daya Bay complex is 215 km away from the JUNO detector, and will contribute about 2.8% of the reactor antineutrino events. The thermal power of all cores and the baselines are listed in Table below. The distances from the detector site

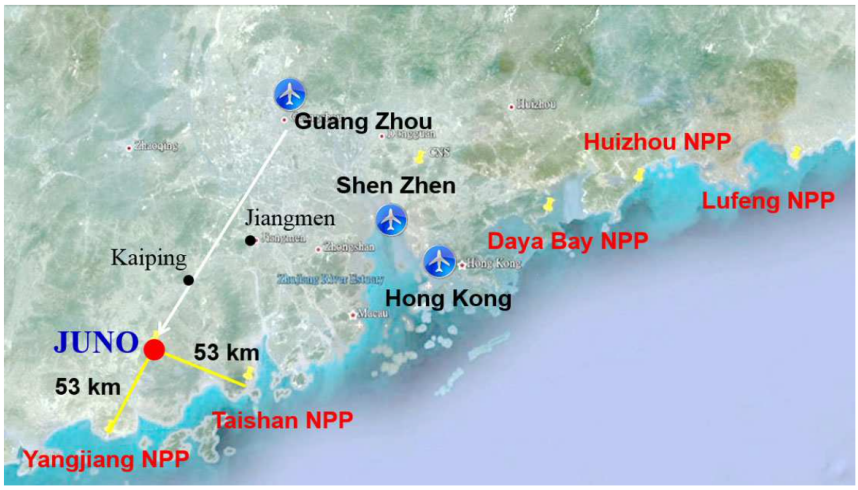

Figure 3.2: Location of the JUNO site.

Cores	YJ-C1	YJ-C2	YJ-C3	YJ-C4	YJ-C5	YJ-C6
Power (GW)	2.9	2.9	2.9	2.9	2.9	2.9
Baseline(km)	52.75	52.84	52.42	52.51	52.12	52.21
Cores	TS-C1	TS-C2	TS-C3	TS-C4	DYB	HZ
Power (GW)	4.6	4.6	4.6	4.6	17.4	17.4
Baseline(km)	52.76	52.63	52.32	52.20	215	265

Figure 3.3: Summary of the thermal power and baseline to the JUNO detector for the Yangjiang (YJ) and Taishan (TS) reactor cores, as well as the remote reactors of Daya Bay (DYB) and Huizhou (HZ) [33].

to the Yangjiang and Taishan cores are surveyed with a Global Positioning System (GPS) to a precision of 1 meter. All these NPPs are constructed and operated by the China General Nuclear Power Group (CGNPG). The detector will be deployed in an underground laboratory under the Dashi hill. The elevation of the hill above the detector is 268 m, and that of the dome and the floor of the underground experimental hall is -433 m and -460 m, respectively. The detector is located in a cylindrical pit. The elevation of the detector center is -481.25 m. Therefore, the vertical overburden for the detector is more than 700 m. The activities of the ^{238}U, ^{232}Th, and ^{40}K in the rock around the experimental hall are measured to be 130, 113, and 1062 Bq/kg, respectively. The muon rate and average energy in the JUNO detector are expected to be 0.0030 Hz/m2 and 215 GeV estimated by simulation with the surveyed mountain profile taken into account ([33], p.29).

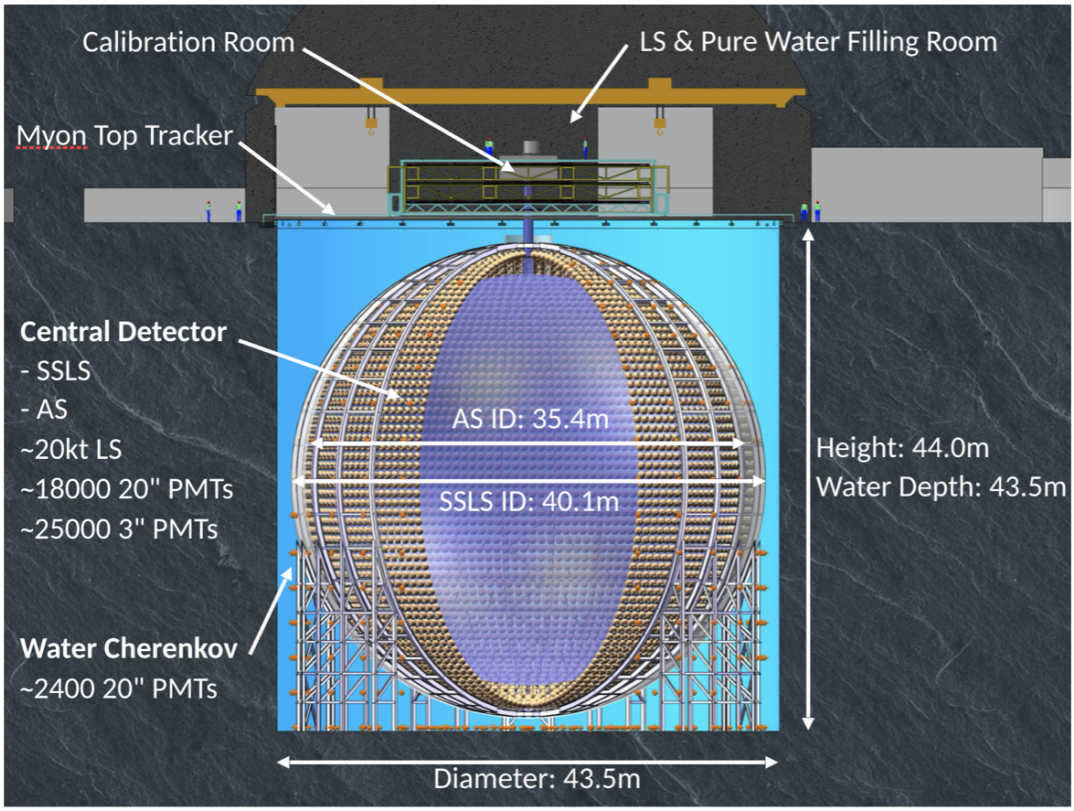

Figure 3.4: Detailed schematic view of the JUNO detector.

3.1.3 JUNO detector

The JUNO detector consists of a central detector, a water Cherenkov detector and a muon tracker. The central detector is a liquid scintillator (LS) detector of 20 kton fiducial mass with an designed energy resolution of 3%/ E(MeV). The central detector is submerged in a water pool in order to be shielded from natural radioactivity from the surrounding rocks and air. The water pool is equipped with photomultiplier tubes (PMTs) to detect the Cherenkov light from the cosmic muons, acting as a veto detector. On top of the water pool, there is another muon detector, which aims measure the muon tracks([33], p.30).
To reach the required energy resolution, some improvements from Daya Bay have to be accomplished: the PMT photocathode covergage $\geq$ 75%, the PMT photocathode quantum efficiency $\geq$ 35%, the attenuation length of the liquid scintillator $\geq$ 20 m at 430 nm, which corresponds to an absorption length of 60 m with a Rayleigh scattering length of 30 m. The liquid scintillator has similar recipe as the Daya Bay LS without gadolinium loading. Linear alkylbenzene (LAB), a straight alkyl chain of 10-13 carbons attached to a benzene ring, is used as the detection medium due to its excellent transparency, high flash point, low chemical reactivity, and good light yield. The

liquid scintillator also consists of 3 g/L 2,5-diphenyloxazole (PPO) as the fluor and 15 mg/L p-bis-(o-methylstyryl)-benzene (bis-MSB) as the wavelength shifter. Twenty thousand ton LS is contained in a spherical container of radius of 17.7 m. The light emitted by the LS is watched by about 17,000 20-inch PMTs. PMTs are installed on a spherical structure of a radius of 19.5 m, and submerged in a buffer liquid to protect the LS from the radioactivity of the PMT glass. The photocathode coverage can reach 75% to 78% for various options of positioning the PMTs. The muon detection efficiency is expected to be similar as that of the Daya Bay water Cherenkov detector, which is 99.8% ([33], p.31).

3.1.4 Detection of the supernova neutrinos with JUNO

In order to estimate the expected neutrino rates in JUNO, it was assumed that a linear alkylbenzene (LAB) based liquid scintillator and a fiducial mass of 20 kiloton, implying about $1.5 \cdot 10^{33}$ target protons. For a typical galactic SN at 10 kpc, there will be more than 5000 neutrino events solely from the IBD channel. Such a high-statistics observation definitely allows us to probe the time- dependent features of SN neutrinos. A total energy of $3 \cdot 10^{53}$ erg is assumed to be equally distributed in neutrinos and antineutrinos of three flavors. As the average neutrino energies are both flavor- and time-dependent, the event rates was calculated for three representative values $\langle E_\nu \rangle =$ 12 MeV, 14 MeV and 16 MeV, and in each case the average energy is taken to be equal for all the flavors. The total numbers of neutrino events for the main channels in JUNO are summarized in Fig. 3.6, where no neutrino flavor conversions are considered. The neutrino event spectra with respect to the visible energy in six main reaction channels are shown in Fig.3.7 ([33], p.74-75).

1. The IBD is the dominant channel for SN neutrino detection in both scintillator and water-cherenkov detectors, in which a large number of free protons are available. In the IBD reaction $\bar{\nu}_e + p \rightarrow n + e^+$, the neutrino energy threshold is $\mathrm{E}_\nu^{th} = \Delta + \mathrm{m} \approx$ 1.806 MeV, where $\Delta = m_n$ - $m_p \approx 1.293$ MeV is the neutron-proton mass difference. The energy of the incident neutrino can be reconstructed from the positron energy via $E_\nu \approx E_e + \Delta$. The energy deposition and the annihilation of the positron with an ambient electron into 0.511-MeV γ's give rise to a prompt signal. In addition, the neutron is captured on a free proton with an average lifetime of about 200 μs, producing a 2.2-MeV γ. Hence the time coincidence of the prompt and delayed signals increases greatly the tagging power.

2. As an advantage of the scintillator detector, the charged-current (CC) interaction on ^{12}C takes place for both ν_e and $\bar{\nu_e}$ via

$$\nu_e + {}^{12}\mathrm{C} \rightarrow e^- + {}^{12}\mathrm{N}$$
$$\bar{\nu}_e + {}^{12}\mathrm{C} \rightarrow e^+ + {}^{12}\mathrm{B}$$

The subsequent beta decay of ^{12}N and ^{12}B will lead to a prompt-delayed coincidental signal. These charge-current reactions will hence provide a possibility to detect ν_e and $\bar{\nu_e}$ separately.

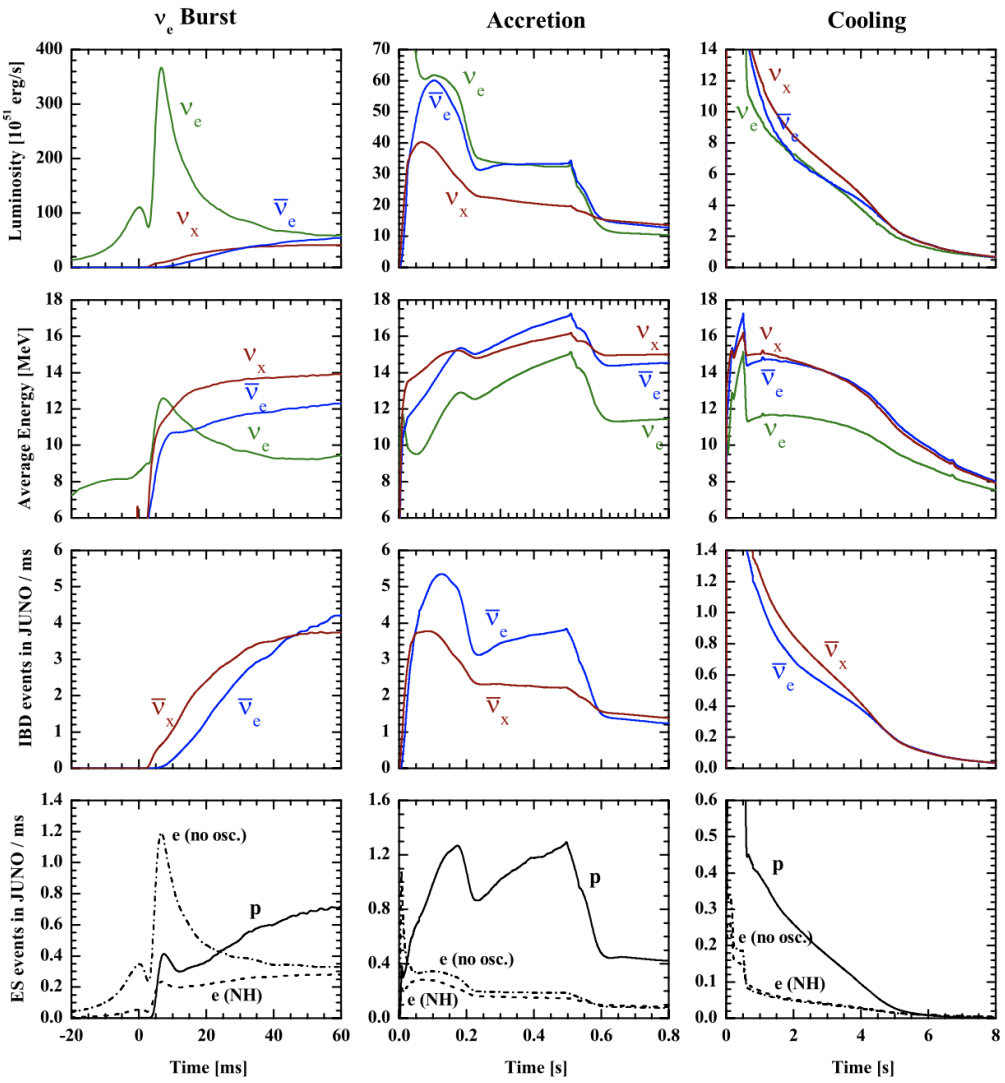

Figure 3.5: Three phases of neutrino emission from a core-collapse SN, from left to right: (1) Infall, bounce and initial shock-wave propagation, including prompt ν_e burst. (2) Accretion phase with significant flavor differences of fluxes and spectra and time variations of the signal. (3) Cooling of the newly formed neutron star, only small flavor differences between fluxes and spectra. [33].

Channel	Type	Events for different $\langle E_\nu \rangle$ values		
		12 MeV	14 MeV	16 MeV
$\overline{\nu}_e + p \to e^+ + n$	CC	4.3×10^3	5.0×10^3	5.7×10^3
$\nu + p \to \nu + p$	NC	0.6×10^3	1.2×10^3	2.0×10^3
$\nu + e \to \nu + e$	ES	3.6×10^2	3.6×10^2	3.6×10^2
$\nu + {}^{12}\mathrm{C} \to \nu + {}^{12}\mathrm{C}^*$	NC	1.7×10^2	3.2×10^2	5.2×10^2
$\nu_e + {}^{12}\mathrm{C} \to e^- + {}^{12}\mathrm{N}$	CC	0.5×10^2	0.9×10^2	1.6×10^2
$\overline{\nu}_e + {}^{12}\mathrm{C} \to e^+ + {}^{12}\mathrm{B}$	CC	0.6×10^2	1.1×10^2	1.6×10^2

Figure 3.6: Numbers of neutrino events in JUNO for a SN at a typical distance of 10 kpc, where ν collectively stands for neutrinos and antineutrinos of all three flavors and their contributions are summed over. For the elastic neutrino-proton scattering, a threshold of 0.2 MeV for the proton recoil energy is chosen [33].

3. The neutral-current (NC) interaction on ^{12}C is very important to probe neutrinos of non-electron flavors, where ν collectively denotes neutrinos and antineutrinos of all three flavors. A 15.11-MeV γ from the deexcitation of $^{12}\mathrm{C}^*$ to its ground state is a clear signal of SN neutrinos.

$$\nu + {}^{12}\mathrm{C} \to \nu + {}^{12}\mathrm{C}^*$$

4. In the elastic scattering (ES) of neutrinos on electrons, the scattered electrons carry the directional information of incident neutrinos, and thus can be used to locate the SN. This is extremely important if a SN is hidden in the galactic gas and dust clouds and the optical signal is obscured. The elastic scattering

$$\nu + e^- \to \nu + e^-$$

is most sensitive to ν_e because of its largest cross section, which is particularly useful in detecting the prompt ν_e burst. It is challenging for a liquid scintillator detector to determine the SN direction by reconstructing the direction of the scattered electron, unless the PMT time response is quick enough and the detector is preciselycalibrated and understood. For high-energy electrons, it might be possible to obtain some directional information from the Cherenkov light.

5. The elastic scattering of neutrinos on protons is a promising channel to measure SN neutrinos of all and particularly non-electron flavors.

$$\nu + p \to \nu + p$$

The total cross section of the reaction is about four times smaller than that of the IBD one. But the contributions from all the neutrinos and antineutrinos of three flavors will compensate for the reduction of cross section. In this channel, the proton recoil energy $T_p \leq 2E_\nu^2/m_p$ is highly suppressed by the nucleon mass, so the precise

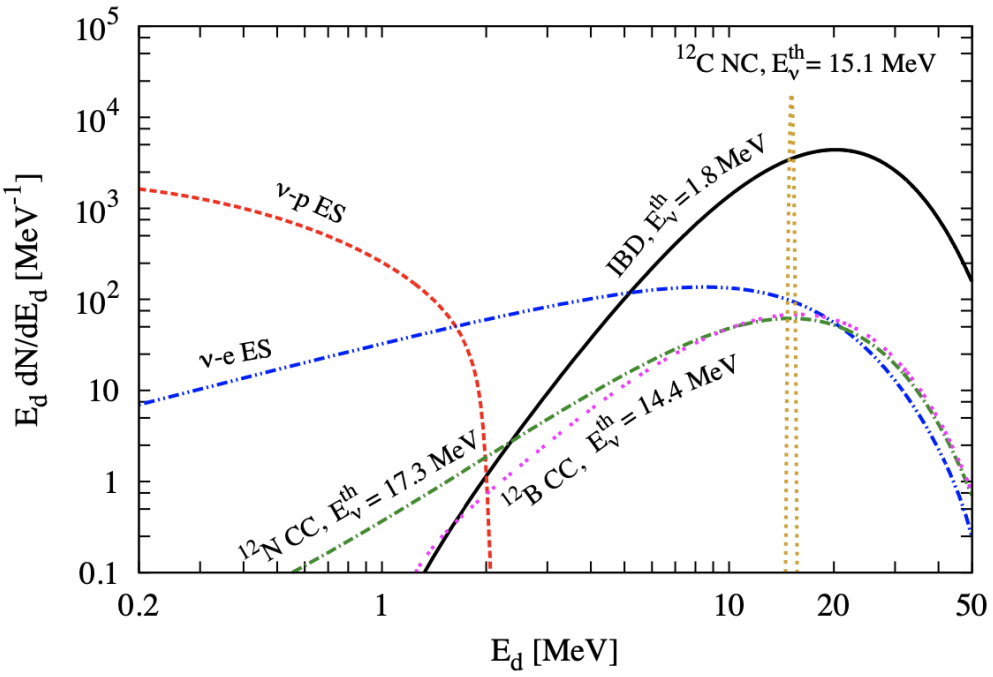

Figure 3.7: The neutrino event spectra with respect to the visible energy E_d in the JUNO detector for a SN at 10 kpc, where no neutrino flavor conversions are assumed. The average neutrino energies are $\langle E_{\nu_e} \rangle$ = 12 MeV, $\langle E_{\bar{\nu}_e} \rangle$ = 14 MeV and $\langle E_{\bar{\nu}_x} \rangle$ = 16 MeV. The main reaction channels are shown together with the threshold of neutrino energies: (1) IBD (black and solid curve), Ed = E 0.8 MeV; (2) Elastic neutrino-proton scattering (red and dashed curve), E_d stands for the recoil energy of proton; (3) Elastic neutrino-electron scattering (blue and double-dotted-dashed curve), E_d denotes the recoil energy of electron; (4) Neutral-current reaction on ^{12}C(orange and dotted curve),$E_d \approx$ 15.1 MeV; (5) Charged-current reaction on ^{12}C(ν_e,e)^{12}N (green and dotted-$\bar{\nu}_e, e^+$)^{12}B (magenta and dashed curve), $E_d = E_\nu$ 17.3 MeV; (6) Charged-current reaction ^{12}C(double-dotted curve), $E_d = E_\nu$ 13.9 MeV [33].

determination of the proton quenching factor and a low energy threshold are required to reconstruct neutrino energy and accumulate sufficient statistics. For JUNO, the proton quenching factor will be measured for the ultimately implemented scintillator ([33], p.74-76).

3.2 The DUNE experiment

3.2.1 Overview

The overbalance of matter over antimatter in the early universe, the dynamics of the supernova neutrino bursts (SNBs) that produced the heavy elements necessary for life, and whether protons eventually decay — these mysteries at the forefront of particle physics and astrophysics are key to understanding the early evolution of our universe, its current state, and its eventual fate. The Deep Underground Neutrino Experiment (DUNE) is an international world-class experiment dedicated to addressing these questions [34].
Experiments carried out over the past half century have revealed that neutrinos are found in three states, or flavors, and can transform from one flavor into another. These results indicate that each neutrino flavor state is a mixture of three different nonzero mass states, and to date offer the most compelling evidence for physics beyond the standard model. In a single experiment, DUNE will enable a broad exploration of the three-flavor model of neutrino physics with unprecedented detail. Chief among its potential discoveries is that of matter-antimatter asymmetries (through the mechanism of charge-parity symmetry violation (CPV)) in neutrino flavor mixing — a step toward unraveling the mystery of matter generation in the early universe. Independently, determination of the unknown neutrino mass ordering and precise measurement of neutrino mixing parameters by DUNE may reveal new fundamental symmetries of nature [34].

3.2.2 DUNE detector

To achieve its goals, the international DUNE experiment, hosted by the U.S. Department of Energy's Fermi National Accelerator Laboratory (Fermilab) in Illinois, comprises three central components: (1) a new, high-intensity neutrino source generated from a MW-class proton accelerator at Fermilab, (2) a massive far detector (FD) situated 1.5 km underground at the Sanford Underground Research Facility (SURF) in South Dakota, and (3) a composite near detector (ND) installed just downstream of the neutrino source [34]. The far detector will be a modular liquid argon time-projection chamber (LArTPC) with a fiducial (sensitive) mass of 40 kt of liquid argon (LAr), a cryogenic liquid that must be kept at 88 K (185°C). This detector will be able to uniquely reconstruct neutrino interactions with image-like precision and unprecedented resolution. The LBNF beamline at Fermilab will deliver the world's most intense neutrino beam to the near and far detectors in an on-axis configuration. The upgrade to the Proton Improvement Plan II (PIP-II), a leading-edge, superconduct-

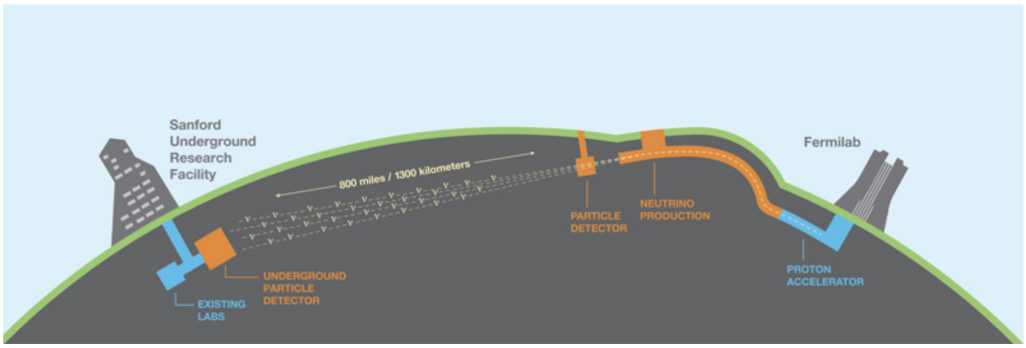

Figure 3.8: The configuration of the LBNF beamline at Fermilab, in Illinois, and the DUNE detectors in Illinois and South Dakota, separated by 1300 km [34].

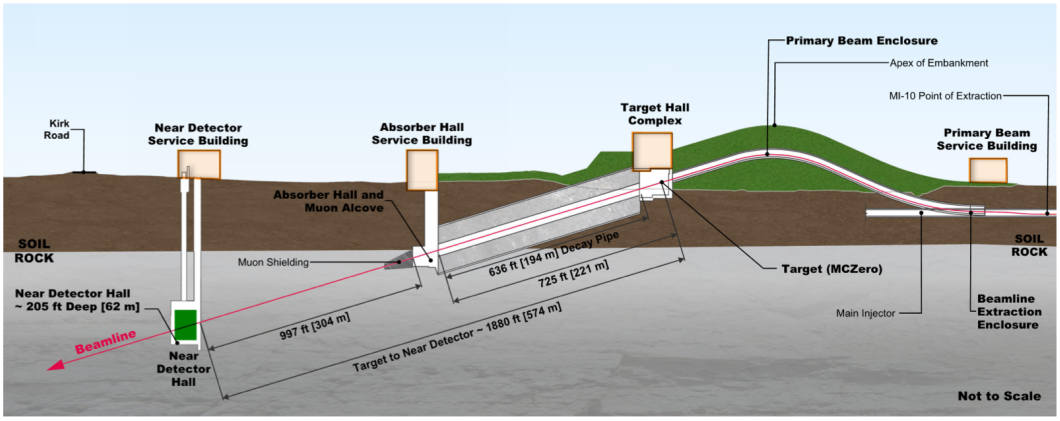

Figure 3.9: Neutrino beamline and DUNE near detector hall at Fermilab [34].

ing, linear proton accelerator under construction at Fermilab, will deliver between 1.0 and 1.2MW of proton beam power from the Fermilab Main Injector to LBNF, which will aim and focus the beam, whereupon the protons, in a wide energy band of 60 GeV to 120 GeV, will collide with a high-power production target, creating a secondary beam from which the intense neutrino flux will emerge, traveling in the direction of the DUNE detectors (Figure below). A further planned upgrade of the accelerator complex could provide up to 2.4 MW of beam power by 2030, potentially extending the DUNE science reach [34], [35].

As mentioned above, the LBNF project will provide the beamline and the conventional facilities (CF) for both detectors of the DUNE experiment. At the far site, SURF in South Dakota, LBNF will construct a facility to house and provide infrastructure for the DUNE 10 kt fiducial mass FD modules.

The DUNE FD will consist of four LArTPC detector modules, each with a LAr mass in the sensitive region of the cryostat (fiducial mass) of at least 10 kt, installed approx-

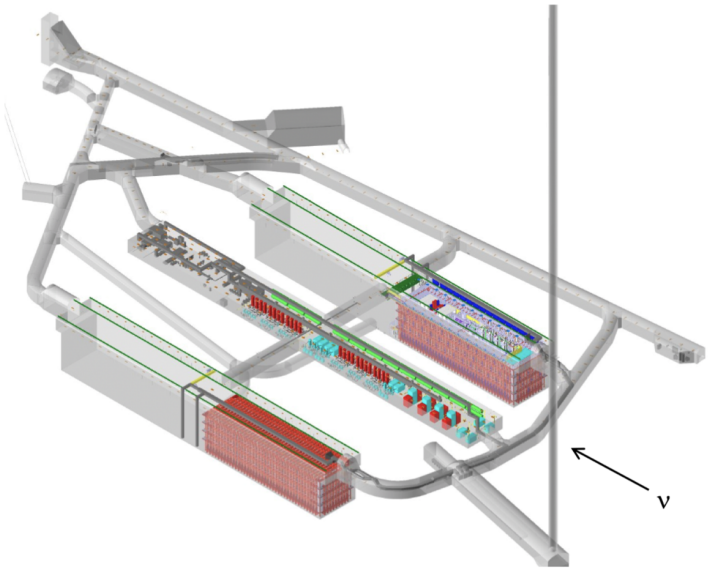

Figure 3.10: Underground caverns for the DUNE FD and cryogenics systems at SURF in South Dakota. The drawing shows the cryostats (red) for the first two FD modules in place at the 4850L. The Ross Shaft, the vertical shaft that will provide access to the DUNE underground area, appears on the right. Each cryostat is 65.8 m long (216 ft, approximately the length of two and a half tennis courts), 18.9 m wide, and 17.8 m tall (about three times as tall as an adult giraffe). The two detector caverns are each 144.5 m long, 19.8 m wide, and 28.0 m high, providing some room around the cryostats [34].

imately 1.5 km underground. excellent tracking and calorimetry performance, making it an ideal choice. Each LArTPC fits inside a cryostat of internal dimensions 15.1 m (w) x 14.0 m (h) x 62.0 m (l) containing a total LAr mass of about 17.5 kt. DUNE is planning for and currently developing two LArTPC technologies: single-phase (SP) in which all the detector elements inside the cryostat are immersed in liquid; and dual-phase (DP), in which some components operate in a layer of gaseous argon above the liquid ([34], p.25).
Argon is an excellent scintillator at a wavelength of 126.8 nm (UV), a property that both detector designs exploit. This fast scintillation light (photons), once shifted into the visible spectrum, is collected by photon detectors (PDs) in both designs. The light collection provides an initial start time (t_0) for every event recorded by the time projection chamber (TPC), indicating when the ionization electrons begin to drift. Comparing the time at which the ionization signal reaches the anode relative to this start time allows reconstruction of the event topology in the drift coordinate (i.e., horizontal and transverse to the beam for SP and vertical for DP); the precision of the measured t_0, therefore, directly corresponds to the precision of the spatial reconstruction in this direction [34].
An understanding of DUNE's capabilities would be impossible without some description of the Near Detector's (ND) crucial contribution to the experiment. The ND will serve as the experiment's control, constraining systematic errors and measuring the initial unoscillated ν_μ and ν_e energy spectra (and that of the corresponding antineutrinos). Comparing the measured neutrino energy spectra near the beam source, before any oscillation takes place, and again at the far site allows us to disentangle the different energy-dependent effects that modulate the beam spectrum and to reduce the systematic uncertainties to the level required for discovering CPV. Its other key role in this arena is to measure neutrino-argon interactions with high precision using both gaseous and liquid argon, which will further reduce the systematic uncertainties associated with modeling these interactions.

3.2.3 Detection of the supernova neutrinos with DUNE

Liquid argon has a particular sensitivity to the ν_e component of a supernova neutrino burst, via the dominant interaction, CC absorption of ν_e on ^{40}Ar,

$$\nu_e + {}^{40}\mathrm{Ar} \rightarrow e^- + {}^{40}\mathrm{K}^*$$

for which the observable is the e plus deexcitation products from the excited ^{40}K final state [Ref]. The $\bar{\nu_e}$ interaction,

$$\bar{\nu}_e + {}^{40}\mathrm{Ar} \rightarrow e^+ + {}^{40}\mathrm{Cl}^*$$

will also occur and can be tagged. Additional channels include NC interaction and ES on electrons.

$$\nu + {}^{40}\mathrm{Ar} \rightarrow \nu + {}^{40}\mathrm{Ar}^*$$

$$\nu + e^- \rightarrow \nu + e^-$$

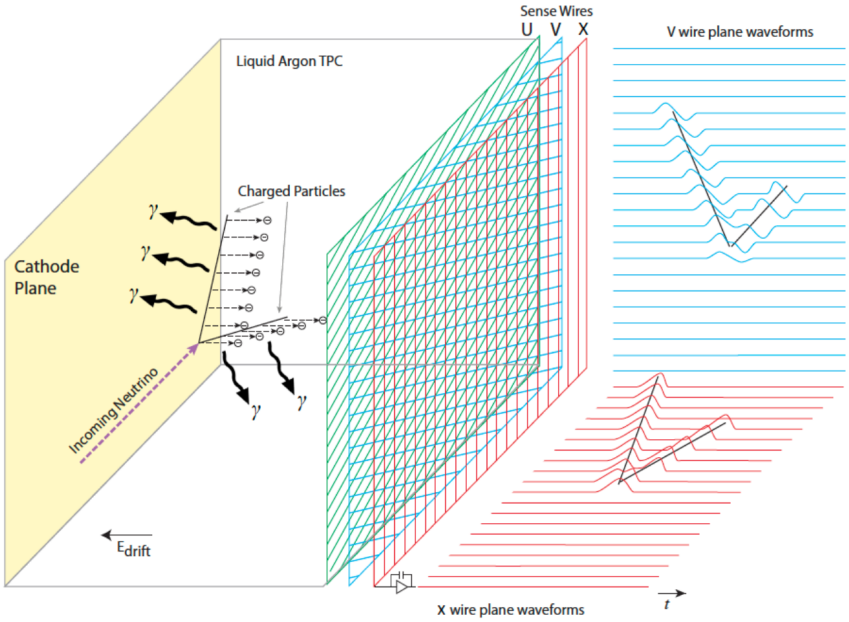

Figure 3.11: The general operating principle of the SP LArTPC. Negatively charged ionization electrons from the neutrino interaction drift horizontally opposite to the E field in the LAr and are collected on the anode, which is made up of the U, V and X sense wires. The right-hand side represents the time projections in two dimensions as the event occurs. Light (γ) detectors (not shown) will provide the t_0 of the interaction ([34], p.27).

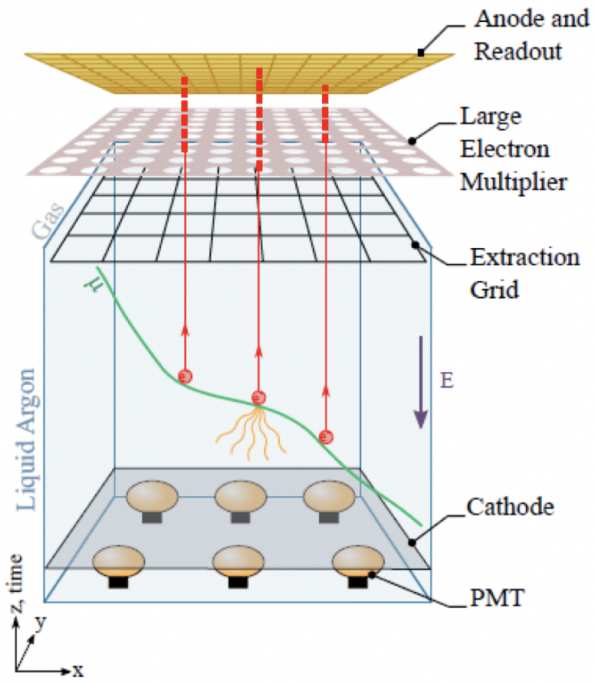

Figure 3.12: The general operating principle of the DP LArTPC. The ionization charges drift vertically upward in LAr and are transferred into a layer of argon gas above the liquid where they are amplified before collection on the anode. The light detectors (PMTs) sit under the cathode ([34], p.27).

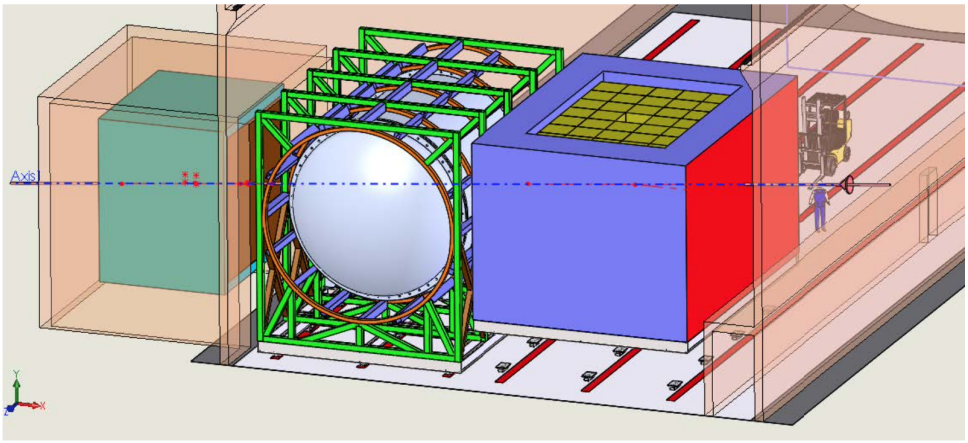

Figure 3.13: DUNE ND. The axis of the beam is shown as it enters from the right. Neutrinos first encounter the LArTPC (right), the MPD (center), and then the on-axis beam monitor (left) ([34], p.34).

Events from ν_e CC are likely to be accompanied by de-excitation products – gamma rays and/or ejected nucleons. Gamma rays are in principle observable via energy deposition from Compton scattering, which will show up as small charge blips in the time projection chamber. Gamma rays can also be produced by bremsstrahlung energy loss of electrons or positrons. The critical energy for bremsstrahlung energy loss for electrons in argon is about 45 MeV. Ejected nucleons may result in loss of observed energy for the event, although some may interact to produce observable deexcita- tions via inelastic scatters on argon. Such MeV-scale activ- ity associated with neutrino interactions has been observed in the ArgoNeuT LArTPC. ES on electrons will result in single scattered electron tracks, and single or cascades of gamma rays may result from NC excitations of the argon nucleus. Each interaction category has, in principle, a distinctive signature [36].
Expected event rates were calculated with the help of SNOwGLoBEs [[37]] and presented in a table below. All the information about the SNOwGLoBES you can find in the next chapter. It shows rates calculated for the dominant interactions in argon for the "Livermore" model [38] (included for comparison with literature), the "GKVM" model [39], and the "Garching" electron-capture supernova model [1]. No flavor transitions are assumed in the supernova or Earth; the GKVM model assumes collective effects in the supernova.

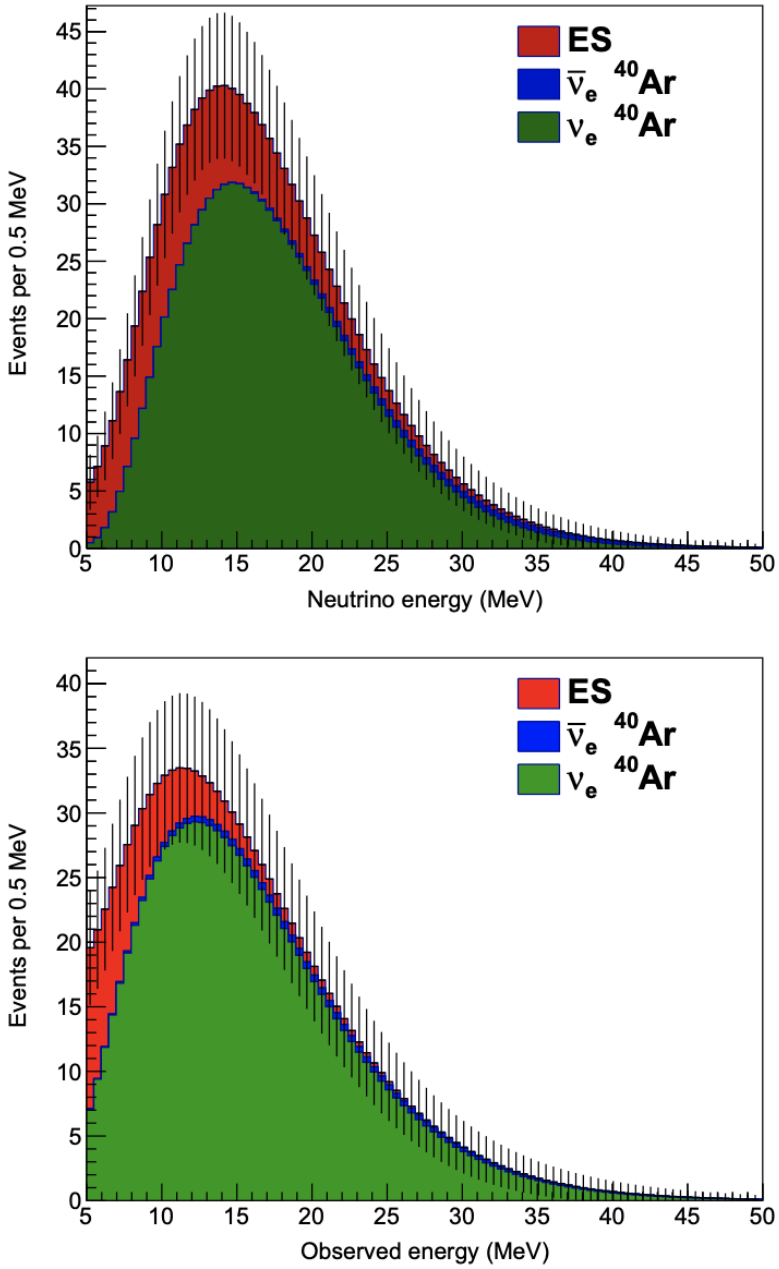

Figure 3.14: Top: Spectrum as a function of interacted neutrino energy com- puted with SNOwGLoBES in 40 kton of liquid argon for the electron- capture supernova ("Garching" model) at 10 kpc, integrated over time, and indicating the contributions from different interaction channels. No oscillations are assumed. Bottom: expected measured spectrum as a function of observed energy, after detector response smearing [36].

Channel	Livermore	GKVM	Garching
$\nu_e + {}^{40}Ar \rightarrow e^- + {}^{40}K^*$	2648	3295	882
$\bar{\nu_e} + {}^{40}Ar \rightarrow e^+ + {}^{40}Cl^*$	224	155	23
$\nu_x + e^- \rightarrow \nu_x + e^-$	341	206	142
Total	3213	3656	1047

Table 3.1: Event rates computed with SNOwGLoBES for different supernova models in 40 kton of liquid argon for a core collapse at 10 kpc [36].

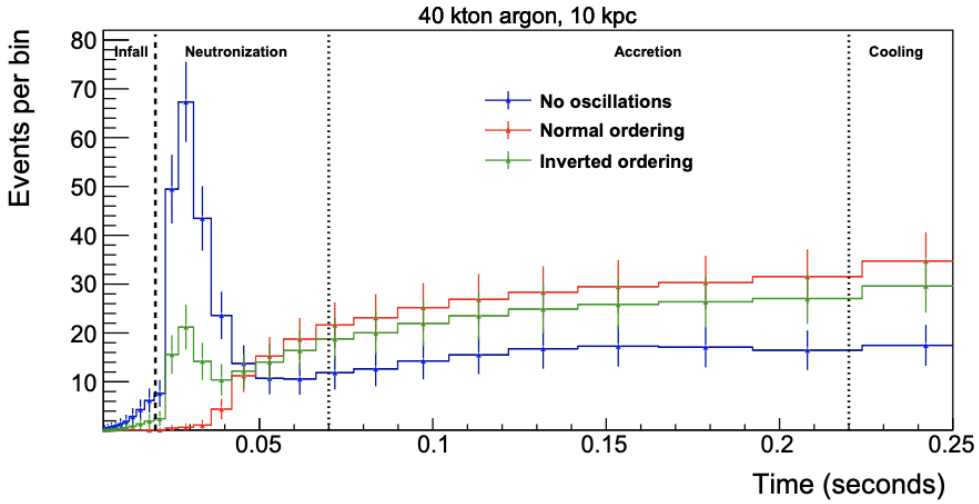

Figure 3.15: Expected event rates as a function of time for the electron- capture model in Garching model for 40 kton of argon during early stages of the event – the neutronization burst and early accretion phases [36].

3.3 IceCube

3.3.1 Overview

IceCube, the South Pole neutrino observatory, is a cubic-kilometer particle detector made of the ice of the Antarctic and located near the Amundsen-Scott South Pole Station. It was mainly designed to detect particles with energies in the multi-GeV to PeV range. Due to ice temperatures between 20°C to 43° C and the low radioactivity of the ice, the dark noise rates of the 5160 photomultiplier tubes forming the IceCube lattice are of order 500 Hz, which is particularly low for 10 inch photomultipliers. Therefore, IceCube can extend its searches to bursts of 10 MeV neutrinos lasting several seconds, which are expected to be produced by Galactic core collapse supernovae. By observing a uniform rise in all photomultiplier rates, IceCube can provide a particularly high statistical precision for the neutrino rate from supernovae

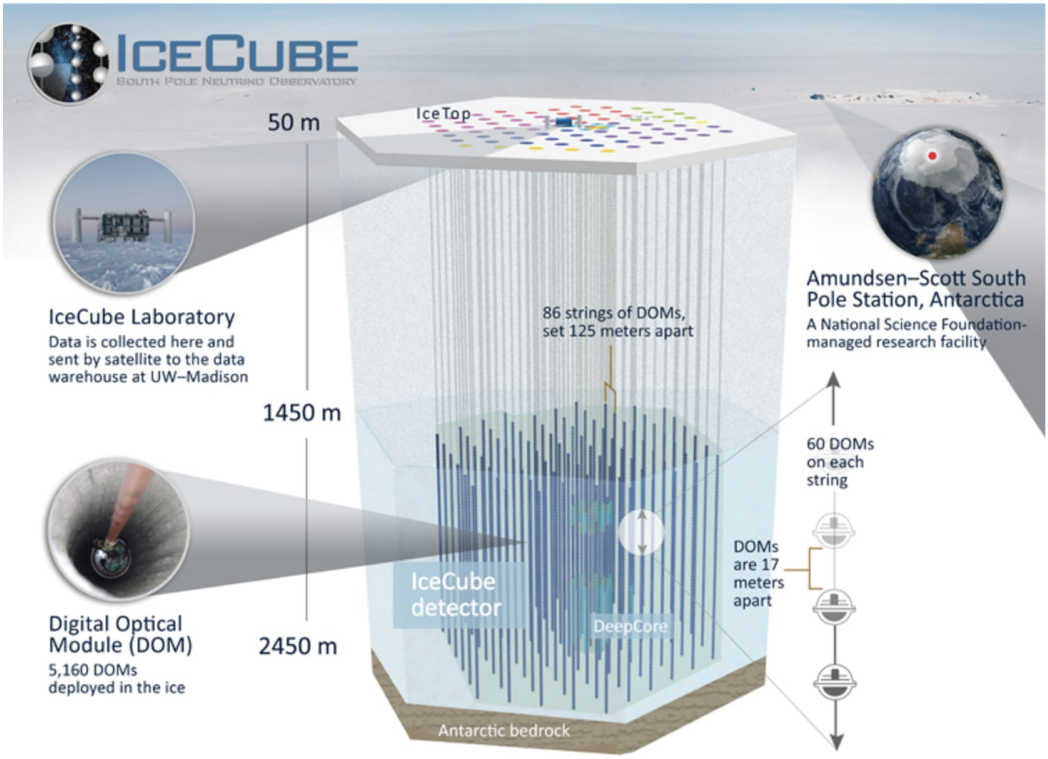

Figure 3.16: Icecube detector

in the inner part of our Galaxy ($\leq$ 20 kpc) [40]. And one can provide the spectral information to get the fluxes.

3.3.2 IceCube detector

IceCube is the first gigaton neutrino detector ever built and was primarily designed to observe neutrinos from the most violent astrophysical sources in our universe. Neutrinos, almost massless particles with no electric charge, can travel from their sources to Earth with essentially no attenuation and no deflection by magnetic fields.
The in-ice component of IceCube consists of 5,160 digital optical modules (DOMs), each with a ten-inch photomultiplier tube and associated electronics. The DOMs are attached to vertical "strings," frozen into 86 boreholes, and arrayed over a cubic kilometer from 1,450 meters to 2,450 meters depth. The strings are deployed on a hexagonal grid with 125 meters spacing and hold 60 DOMs each. The vertical separation of the DOMs is 17 meters.
Eight of these strings at the center of the array were deployed more compactly, with a horizontal separation of about 70 meters and a vertical DOM spacing of 7 meters. This denser configuration forms the DeepCore subdetector, which lowers the neu-

trino energy threshold to about 10 GeV, creating the opportunity to study neutrino oscillations.
IceTop consists of 81 stations located on top of the same number of IceCube strings. Each station has two tanks, each equipped with two downward facing DOMs. IceTop, built as a veto and calibration detector for IceCube, also detects air showers from primary cosmic rays in the 300 TeV to 1 EeV energy range. The surface array measures the cosmic-ray arrival directions in the Southern Hemisphere as well as the flux and composition of cosmic rays.
Developments in neutrino astronomy have been driven by the search for the sources of cosmic rays, leading at an early stage to the concept of a cubic-kilometer neutrino detector. Cosmic rays, which consist mainly of protons, are the highest energy particles ever observed, with energies over a million times those reached by today's particle accelerators on Earth [41]. Neutrinos are not observed directly, but when they happen to interact with the ice they produce electrically charged secondary particles that in turn emit Cherenkov light, as a result of traveling through the ice faster than light travels in ice.
The IceCube sensors collect this light, which is subsequently digitized and time stamped. This information is sent to computers in the IceCube Lab on the surface, which converts the messages from individual DOMs into light patterns that reveal the direction and energy of muons and neutrinos [41].

3.3.3 Detection of the supernova neutrinos with Icecube

The inverse beta decay (IBD) process $\bar{\nu}_e + p \rightarrow n + e^+$ is the dominant supernova neutrino interaction in ice. Its cross section depends approximately on the square of the anti-neutrino energy $E_{\bar{\nu_e}}$. Typically, only a single photon from each IBD reaches one of the DOMs. During a supernova, the increase in photon counts in individual DOMs will not be statistically significant, but the collective increase in counts across all DOMs produces a strong signal [4]. The signal does not allow for reconstruction of individual neutrino interactions or estimates of the energy, origin, and type of neutrino, but it provides detailed measurements of the neutrino flux versus time. There are also scattering procceses and interaction on ^{16}O, but the expected number of events is much less than for the IBD [40].
Expected rates for different reactions are presented in a Table 3.2:
Construction of IceCube finished in 2011, and since 2015 the trigger-capable uptime of the detector has averaged 99.7% around the clock. Due to the non-Poissonian character of the dark noise in the IceCube DOMs [47], the data acquisition system incorporates an artificial deadtime of $\tau = 250$ μs to reduce the dark rate R_{dark}(t) by $\approx 50\%$. The deadtime also lowers the detector count rate by a factor $0.87/(1 + \mathrm{R}_{dark}\ (\mathrm{t}\ )/\mathrm{NDOM}\cdot\tau\ )$, where NDOM is the number of participating optical modules. DOM rates are counted in 1.6384 ms time bins. A dedicated online software system (SNDAQ) rebins the data to 2 ms and searches the data stream for collective rate increases characteristic of a supernova [40].
When describing the sensitivity of a given neutrino detector to a core collapse super-

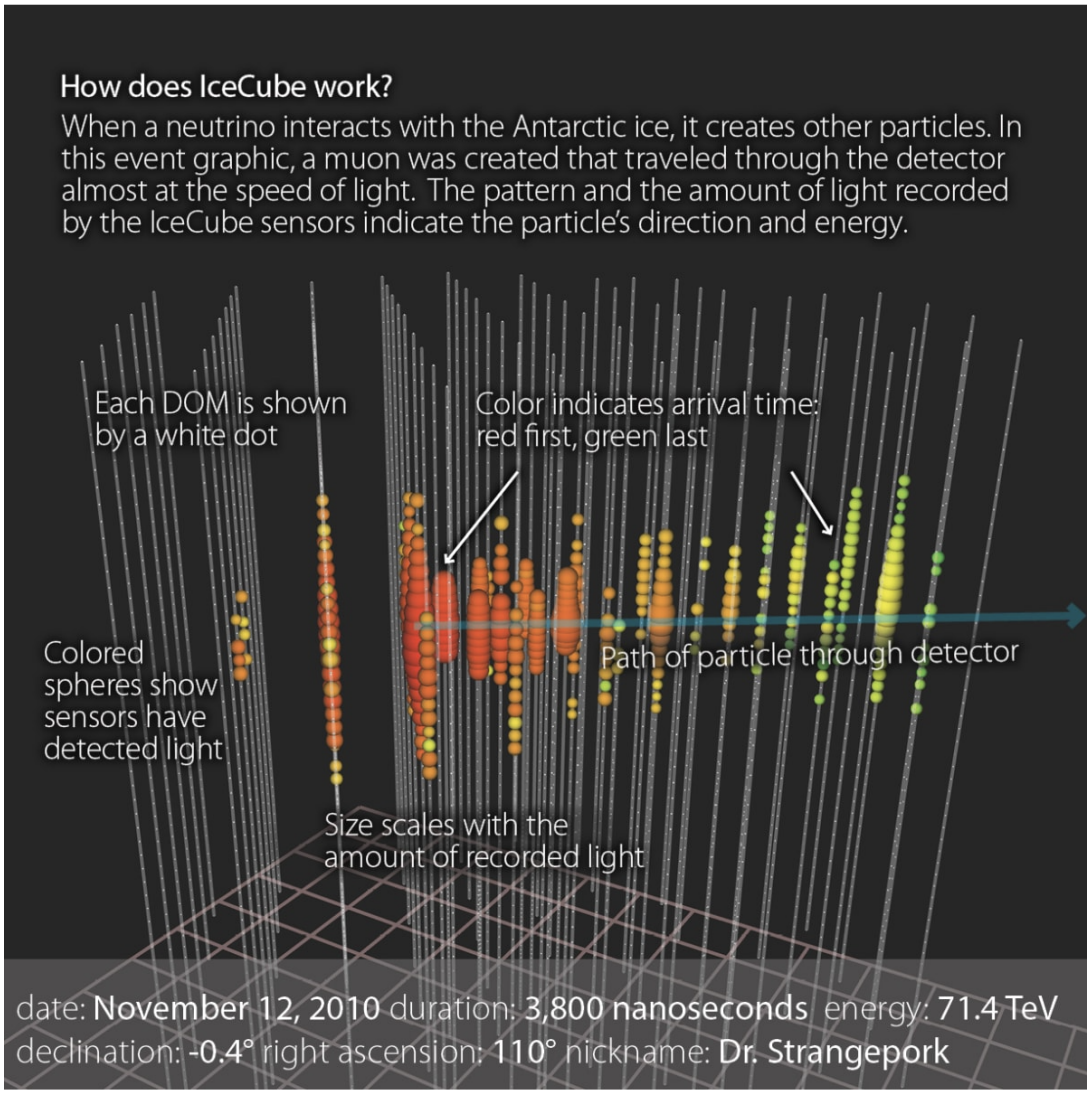

Figure 3.17: Detection of the neutrinos in Icecube is happening through detections of the Cherenkov light of the secondary particles.

Reaction	Targets	Signal hits	Signal fraction	Reference
$\bar{\nu_e} + p \rightarrow e^+ + n$	$6{\times}10^{37}$	134k(157k)	93.8%(94.4%)	Strumia & Vissani [42]
$\nu_e + e^- \rightarrow \nu_e + e^-$	3×10^{38}	2.35k(2.25k)	1.7% (1.4%)	Marciano & Parsa [43]
$\bar{\nu_e} + e^- \rightarrow \bar{\nu_e} + e^-$	3×10^{38}	660(720)	0.5% (0.4%)	Marciano & Parsa [43]
$\nu_{\mu+\tau} + e^- \rightarrow \nu_{\mu+\tau} + e^-$	3×10^{38}	700(720)	0.5% (0.4%)	Marciano & Parsa [43]
$\bar{\nu_{\mu+\tau}} + e^- \rightarrow \bar{\nu_{\mu+\tau}} + e^-$	3×10^{38}	600(570)	0.4% (0.4%)	Marciano & Parsa [43]
$\nu_e + {}^{16}O \rightarrow e^- + X$	$3{\times}10^{37}$	2.15k(1.50k)	1.5%(0.9%)	Kolbe et al. [44]
$\bar{\nu_e} + {}^{16}O \rightarrow e^+ + X$	$3{\times}10^{37}$	1.90k(2.80k)	1.3%(1.7%)	Kolbe et al. [44]
$\nu_{all} + {}^{16}O \rightarrow \nu_{all} + X$	$3{\times}10^{37}$	430(410)	0.3%(0.3%)	Kolbe et al. [44]
$\nu_e + {}^{17/18}O/{}^{2}_{1}H \rightarrow e^- + X$	$3{\times}10^{34}$	270(245)	0.2%(0.2%)	Haxton [45]

Table 3.2: Event rates computed with SNOwGLoBES for different supernova models in 40 kton of liquid argon for a core collapse at 10 kpc based on Garching model, assuming normal and inverted(in brackets) neutrino hierarchy [46].

nova, it is common to indicate its fiducial mass (or fiducial volume), as a means of describing how much detector material is available for detection to take place. This fiducial mass is normally closely tied to the physical mass of the detector material, making it relatively simple to visualize and estimate. However, in the case of IceCube, the array's great size and lack of well-defined borders makes the fiducial mass and volume of the detector somewhat ambiguous. IceCube has 5160 DOMs spread out over a volume of about 1km^3 [48]. However, as is illustrated in Figure 3.18 , the likelihood that a given event will be observed drops off with its distance to the nearest DOM, as well as the opacity of the ice in which it occurs. The distance from which an interaction event can be detected is also dependent on the energy of the incoming neutrino. As such, a high-energy cosmic ray neutrino may produce a signal across multiple detectors, allowing for the identification and reconstruction of single events, whereas the light produced by interactions with supernova neutrinos often fades below the detection threshold without triggering a single detector [48].
The estimation on the total number of events in Icecube for different models of supernova collapse you can find in Table 3.3 [49].

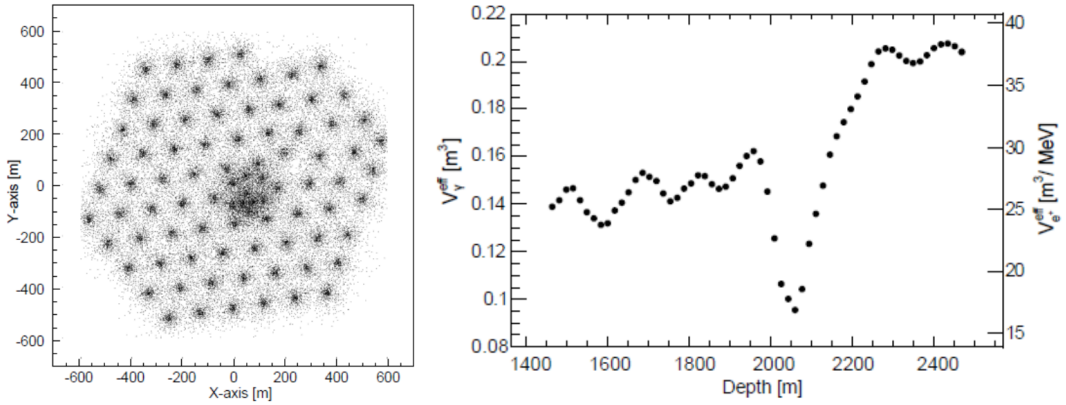

Figure 3.18: IceCube's sensitivity to low-energy neutrino interactions varies with the location of the event. Left: The spatial distribution of detected supernova neutrino interaction events, simulated using GEANT-3.21. Each dot represents a interaction event which was detected by a digital optical module. Right: The effective volume V_{γ}^{eff} for detecting Cherenkov photons with wavelength γ (300 - 600) nm as a function of depth in the ice.

Model	Progenitor mass ($M_{\odot}$)	ν's, t ¡ 380ms	ν's all times
Livermore	20	0.174 $\times 10^6$	0.79×10^6
Garching LS-EOS 1d	8-10	0.069×10^6	-
Garching WH-EOS 1d	8-10	0.078×10^6	-
Garching SASI 2d	15	0.106×10^6	-
1987A at 10kpc	15-20	-	$(0.57 \pm 0.18) \times 10^6$
O-Ne-Mg 1d	8.8	0.054×10^6	0.17×10^6
Quark star (full opacities)	10	0.067×10^6	-
Black Hole LS-EOS	40	0.395 $\times 10^6$	1.03×10^6
Black Hole SH-EOS	40	0.335 $\times 10^6$	3.40×10^6

Table 3.3: Number of recorded DOM hits in IceCube for various models of the supernova collapse and progenitor masses assuming a distance of 10 kpc, approximately corresponding to the center of our Galaxy. A normal neutrino hierarchy is assumed. [49].

4 SNOwGLoBeS

4.1 Introduction

In case of a Supernova explosion now or in the forseeable future, a number of neutrino detectors will be operating on the Earth. All of them will be scattered around the globe, they will have different mechanisms of detection, different detector media and energy resolution. And probably much more. And they don't and won't have a common simulations framework, which makes a multidetector analysis very difficult and hard to realise. The aim of this work was to perform such an analysis. Luckily there is a solution for this, which can give simulation results that reproduce the most important features of supernova neutrino detection of various detectors. And the name of the solution is SNOwGLoBES, developed mostly by the Duke university group [37]. This simulation framework for the neutrino detectors in case of a Supernova exlosion happening at 10 kpc distance was used in the analysis.

4.2 What is it?

SNOwGLoBES is a SuperNova Observatories with GLoBES [50]. It is a public software for computing interaction rates and distributions of observed quantities for supernova burst neutrinos in common detector materials.
To enable fast, informative studies of the physics potential of the detection of supernova neutrinos, was developed a simple software and database package to compute expected event rates by folding input fluxes with cross-sections and detector parameters. The output is in the form of interaction rates for each channel as a function of neutrino energy, and smeared rates as a function of detected energy for each channel (i.e. the spectrum that actually be observed in a detector). For this study it was chosen to do the event rate computation by using parameterized detector responses, making use of the GLoBES software. Only the front-end rate engine part of GLoBES was employed, and not the oscillation sensitivity part. GLoBES takes as input fluxes, cross sections, smearing matrices and post-smearing efficiencies. The smearing matrices include both interaction product spectra and detector response. Fig. 4.1 gives a schematic overview of the approach.
Although with this approach, information is lost with respect to a full event-by-event simulation using a neutrino interaction generator and detector simulation (correlations between energy and angle are lost, for example), nevertheless it offers a fast, simple method useful for many studies. Also, time-dependent fluxes are not supported explicitly; however time dependence can be straightforwardly handled by providing multiple

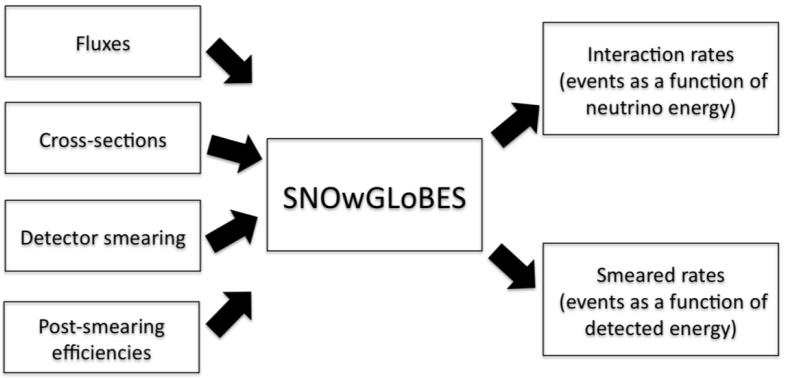

Figure 4.1: SNOwGLoBES data flow.

files with fluxes divided into different time bins. The supernova neutrino fluxes are given in units of neutrinos per cm^2 per energy bin for a supernova occurring 10 kpc away [50].

4.3 Channels of interaction and media

Cross-sections relevant for four detector materials are provided: water, scintillator, argon and lead. Distributions of interaction products are taken into account in the smearing matrices. Below you can find the description of all the detection channels [50]. Cross sections of the processes are presented on Fig. 4.2 - 4.5.

1. ***Inverse Beta Decay (IBD):*** IBD $\bar{\nu}_e + p \rightarrow n + e^+$ is dominant for detectors with free protons, such as water and scintillator.

2. ***Neutrino-Electron Elastic Scattering:*** The cross-sections for elastic scattering (ES) of neutrinos on electrons $\nu_{e,x} + e^- \rightarrow \nu_{e,x} + e^-$ (both NC and CC) are known to better than percent level. The electron ES interaction is relevant for all targets, although the scattered electrons may not be observable for some detector configurations (e.g. HALO).

3. ***Interactions with Oxygen:*** Interactions of the neutrinos on oxygen include the CC interactions $\nu_e + {}^{16}\mathrm{O} \rightarrow e^- + {}^{16}\mathrm{F}$, $\bar{\nu}_e + {}^{16}\mathrm{O} \rightarrow e^+ + {}^{16}\mathrm{N}$. They have different final states. These states include ejected nucleons and deexcitation gammas in addition to the produced lepton. For the NC interaction with ${}^{16}\mathrm{O}$, $\nu_x + {}^{16}\mathrm{O} \rightarrow \nu_x + {}^{16}\mathrm{O}^*$, deexcitation gammas are in principle observable. The cross-sections were used from reference [44].

4. ***Interactions with Carbon:*** Electron flavor neutrinos will interact with carbon nuclei via the CC interactions $\nu_e + {}^{12}\mathrm{C} \rightarrow e^- + {}^{12}\mathrm{N}$ and $\bar{\nu}_e + {}^{12}\mathrm{C} \rightarrow e^+ + {}^{12}\mathrm{B}$. An NC

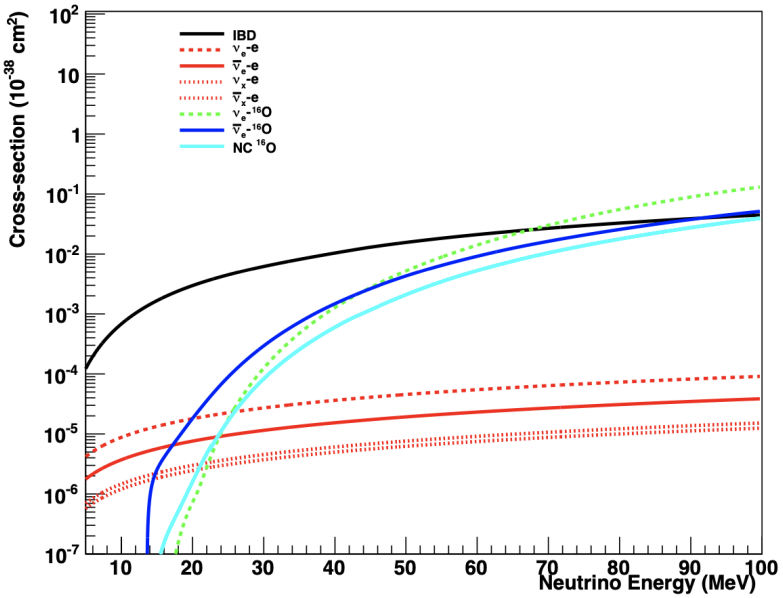

Figure 4.2: Cross sections for relevant processes in water.

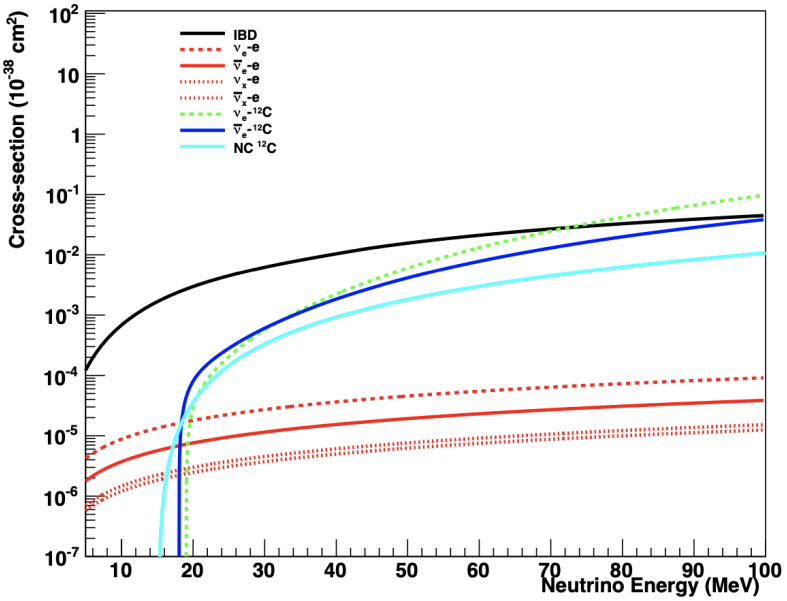

Figure 4.3: Cross sections for relevant processes in scintillator.

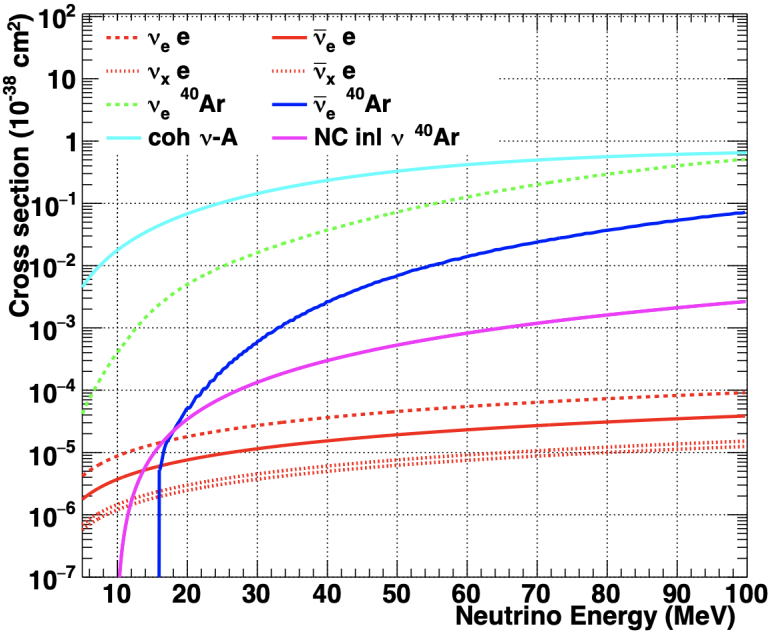

Figure 4.4: Cross sections for relevant processes in liquid argon.

excitation interaction, $\nu + {}^{12}\mathrm{C} \rightarrow \nu + {}^{12}\mathrm{C}^*$ also takes place; this interaction results in a 15.1 MeV deexcitation γ-ray which can be used to tag this interaction. The cross-sections from reference [51] for the CC interactions were used and the measurement from reference [52] for the NC cross-section.

5. ***Interactions with Argon:*** The CC interactions are included: $\nu_e + {}^{40}\mathrm{Ar} \rightarrow e^- + {}^{40}\mathrm{K}^*$ and $\bar{\nu}_e + {}^{40}\mathrm{Ar} \rightarrow e^+ + {}^{40}\mathrm{Cl}^*$. The cross sections for interactions in argon, from references [53], [54]. Also the NC inelastic $\nu + {}^{40}\mathrm{Ar} \rightarrow \nu + {}^{40}\mathrm{Ar}^*$ was added. This interaction is assumed to excite the ^{40}Ar nucleus to the 9.8 MeV level, from which it will de-excite directly to ground, emitting a 9.8 MeV γ.

6. ***Interactions with Lead:*** CC and NC cross-sections for both single and double neutron ejection channels were included: $\nu_e + {}^{208}\mathrm{Pb} \rightarrow e^- + {}^{208}\mathrm{Bi}^*$, $\nu_x + {}^{208}\mathrm{Pb} \rightarrow \nu_x + {}^{208}\mathrm{Pb}^*$, $\bar{\nu_x} + {}^{208}\mathrm{Pb} \rightarrow \bar{\nu_x} + {}^{208}\mathrm{Pb}^*$.

SNOwGLoBES supports several types of neutrino detectors: water cherenkov, scintillator, liquid argon and lead. And there is IceCube configuration [50].

1. ***Water cherenkov:*** Currently, two water Cherenkov configurations are provided. Both of them have 100kton of water in configuration, but they have different percentage of coverage of high quantum efficiency photomultiplier tubes(30% or 15%). Its response is similar to that of Super-Kamiokande I (or III, IV) or Super-Kamiokande II correspondingly [50].

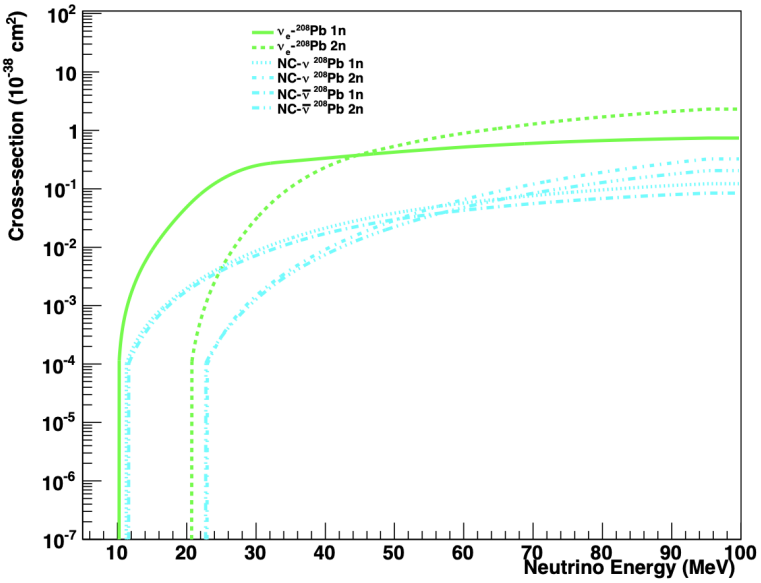

Figure 4.5: Cross sections for relevant processes in lead.

2. ***Scintillator:*** Three scintillator configurations are provided: **scint50kt**, representing 50 kton of generic scintillator (JUNO-like detector); and **novaFD** and **novaND**, which represent the NOνA far (14kt) and near (300t) detectors respectively. For the scint50kt smearing files one can create smearing matrices assuming customized resolution(for example $\frac{\sigma}{E} = \frac{3\%}{\sqrt{E(MeV)}}$ for JUNO) [50].

3. ***Liquid Argon:*** Currently one argon detector configuration is provided, **ar17kt**. For event rate estimates in liquid argon, it is assumed a detection threshold of 5 MeV, corresponding to a DUNE detector module. The energy resolution for the smearing matrices is from [56]: $(\frac{\sigma}{E})^2 = (\frac{11\%}{\sqrt{E(MeV)}})^2 + (2\%)^2$. For the CC channels in argon was included energy deposition of the leading lepton; in the detector response, it was also incorporated additional visible energy from deexcitation gammas [50].

4. ***Lead:*** Lead is a special case: for the type of detector configuration under consideration, HALO [55], electrons are practically invisible and only neutrons are observable. In practice, single and double neutron products from lead can be tagged and reconstructed; although no event-by- event energy information is available, spectral information can be inferred from the relative numbers of 1n and 2n events. The smearing files in SNOwGLoBES for this configuration are dummy unit matrices; efficiency of 36% for 1n channels and 56% for 2n channels is applied, although detailed reconstruction efficiencies for true 1n and 2n rates

would in practice need to be applied [50].

5. ***Icecube:*** The channels considered in this implementation of IceCube are the same as those which are considered in the Water Cherenkov experiment files which come pre-packaged with SNOwGLoBES v1.2 (see Table 4.1).

Interaction	n_{weight}
$\bar{\nu_e} + p \rightarrow e^+ + n$	1
$\nu_e + e^- \rightarrow \nu_e + e^-$	5
$\bar{\nu_e} + e^- \rightarrow \bar{\nu_e} + e^-$	5
$\nu_{\mu+\tau} + e^- \rightarrow \nu_{\mu+\tau} + e^-$	5
$\bar{\nu_{\mu+\tau}} + e^- \rightarrow \bar{\nu_{\mu+\tau}} + e^-$	5
$\nu_e + ^{16}O \rightarrow e^- + X$	0.5
$\bar{\nu_e} + ^{16}O \rightarrow e^+ + X$	0.5
$\nu_{all} + ^{16}O \rightarrow \nu_{all} + X$	0.5

Table 4.1: Interaction channels contributing to the supernova neutrino signal in IceCube [48].

Apart from random Poisson noise, there is also correlated noise, which is described in greater detail in [57]. There are different ways of mitigating the effect of this correlated noise, and which one is used will affect the final detection rate. An example is seen in [57], where an artificial deadtime $\tau = 250[\mu s]$ is introduced after each DOM hit, result in the detection rate being modified by a factor $\epsilon_{noise} \approx 0.87/(1 + \tau \cdot r_{SN}(t))$. A constant deadtime efficiency factor $\epsilon_{noise}(t) = 0.95$ is used. The noise rates in the IceCube DOMs average 540 Hz, and the artificial deadtime reduced this rate by roughly 50% [48].

4.4 Neutrino proton elastic scattering

Neutrino proton elastic scattering(PES) is one the most important channels of detection of the Supernova neutrinos in liquid scintillator. The contribution from all the neutrino-species will compensate for the loss in cross-section in comparison to the IBD one. Even though SNOwGLoBES has a lot of different cross-sections included, it didn't have the ν-p elastic scattering. The addition of the PES required several steps: implementing differential cross-section into the production of the smearing matrices (4.4.1), proton quenching (4.4.2) and change of the threshold (4.4.3).

4.4.1 Implementing PES cross section

The cross section for neutrino-proton elastic scattering is an important prediction [58] of the Standard Model, and it has been confirmed by extensive measurements at GeV energies (see, e.g., [59]). At low energies, the differential cross section as a function of

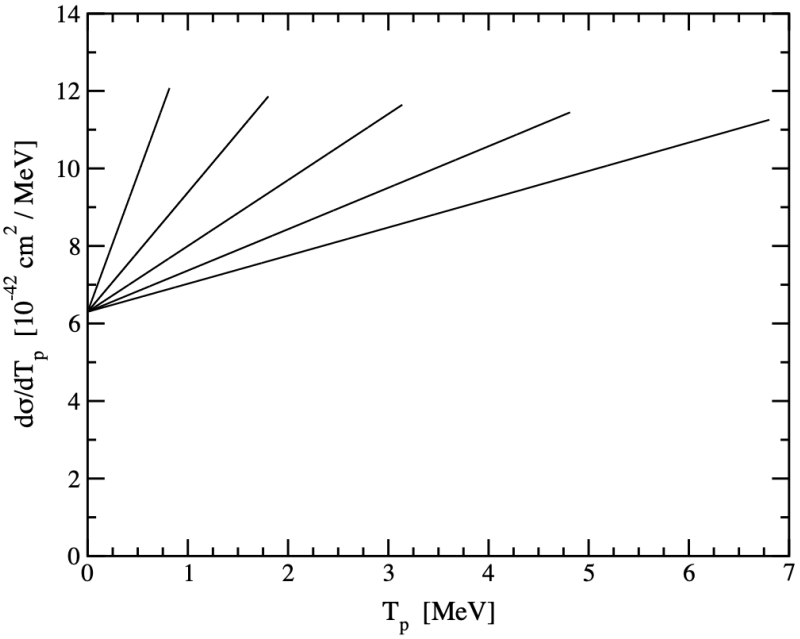

Figure 4.6: The differential cross section as a function of T_p for fixed E_ν. Note the rise at large Tp, indicating that large kinetic energies are preferred. From left to right, the lines are for E_ν=20,30,40,50,and 60 MeV [60].

neutrino energy E_ν and struck proton recoil kinetic energy T_p (and mass M_p) is [60]:

$$\frac{d\sigma}{dT_p} = \frac{G_F^2 M_p}{2\pi E_\nu^2}[(c_V + c_A)^2 E_\nu^2 + (c_V - c_A)^2 (E_\nu - T_p)^2 - (c_V^2 - c_A^2) M_p T_p] \qquad (4.1)$$

where coupling constants are:

$$c_V = \frac{1-4sin^2\Theta_W}{2} = 0.04$$
$$c_A = \frac{1.27}{2}$$

where the factor 1.27 is determined by neutron beta decay and its difference from unity is a consequence of the partially conserved axial current. For a neutrino energy E_ν, T_p ranges between 0 and T_{max}, where

$$T_p^{max} = \frac{2E_\nu^2}{M_p + 2E_\nu} \approx \frac{2E_\nu^2}{M_p}$$

The maximum is obtained when the neutrino recoils backwards with its original momentum E_ν, and thus the proton goes forward with momentum $2E_\nu$. The total cross section is [60]:

$$\frac{G_F^2 E_\nu^2}{\pi}(c_V^2 + 3c_A^2)$$

This cross-section was added to the create smearing matrix code, which was already existing in the Snowglobes. This reaction is going to be used for the JUNO-like detector configuration, the energy resolution used to create smearing matrices was set to $3\%/\sqrt{E(MeV)}$ since JUNO wants to achieve this level of precision. The detector response, i.e. of the neutrino-proton scattering is shown in Fig. 4.7.

4.4.2 Quenching

Low-energy protons lose energy very quickly by ionization. The energy loss rate dE/dx of nonrelativistic particles scales roughly as dE/dx $\sim z^2/\beta^2$ in this energy range [61], where z is the particle charge and β its velocity. In contrast to the usual 2 MeV/g/cm^2 for a minimum-ionizing particle, for few-MeV protons, dE/dx $\sim$ 100 MeV/g/cm^2. Thus even a 10 MeV proton will be brought to rest in less than about 0.1 cm. In a scintillator, there is generally an efficient transfer between the ionization loss of a charged particle and the detectable scintillation light observed by phototubes. For example, in KamLAND, there are approximately 200 detected photoelectrons per MeV deposited for a minimum-ionizing particle like an electron [62]. However, for highly ionizing particles like low-energy protons, the light output is reduced or quenched relative to the light output for an electron depositing the same amount of energy [60].
The observable light output E_{equiv} (i.e., equivalent to an electron of energy E_{equiv}) is given by Birk's Law [63]:

$$\frac{dE_{equiv}}{dx} = \frac{dE/dx}{1 + k_B(dE/dx)} \tag{4.2}$$

where kB is a constant of the scintillation material, and dE/dx is the energy deposition rate, in MeV/cm (and defined to be positive) . Therefore proton quenching factor can be calculated by integrating Eq.above with tables [64] of dE/dx for protons in the KamLAND oil-scintillator mixture [62]:

$$E_{equiv}(T_p) = \int_0^{T_p} \frac{dE}{1 + k_B(dE/dx)} \tag{4.3}$$

The observed energy in terms of the proton kinetic energy is shown in Fig. 4.9. Thus the proton quenching factor ($\frac{dE_{equiv}}{T_p}$) is thus roughly 1/2 at 10 MeV, 1/3 at 6 MeV, 1/4 at 3 MeV, and so on. The quenching factor was plotted and fitted (see Fig. 4.8, 4.9). To obtain the parameters of the curve, the following fit function was used:

$$f(x) = A + B \cdot \ln(Cx + D) \tag{4.4}$$

Best fit result gives values of the constants: A = -0.347, B = 0.196, C = 5.315, D = 6.454. Therefore this quenching factor was implemented to the SNOwGLoBES smearing code together with the neutrino-proton elasting scattering cross-section (Eq. 4.1). On the picture 4.10 and 4.11 you can see the result of applying the quenching parameter to the smearing matrix and hence the detector response. As it was expected the spectrum was shifted to the low energy area.

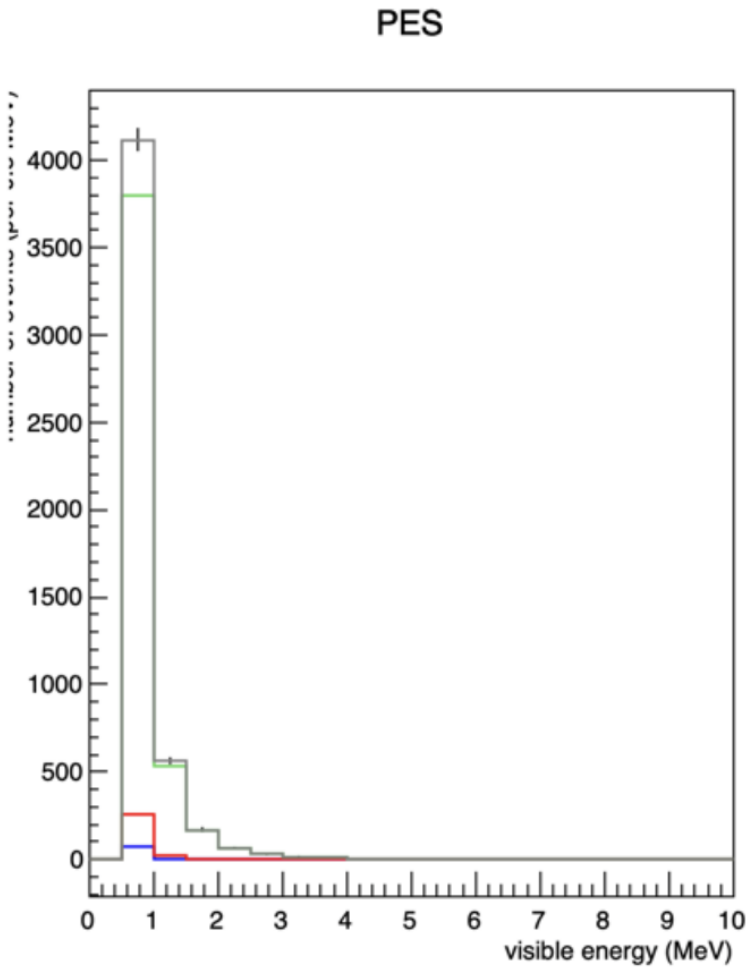

Figure 4.7: Example of a neutrino-proton spectrum simulated for the JUNO-like detector.

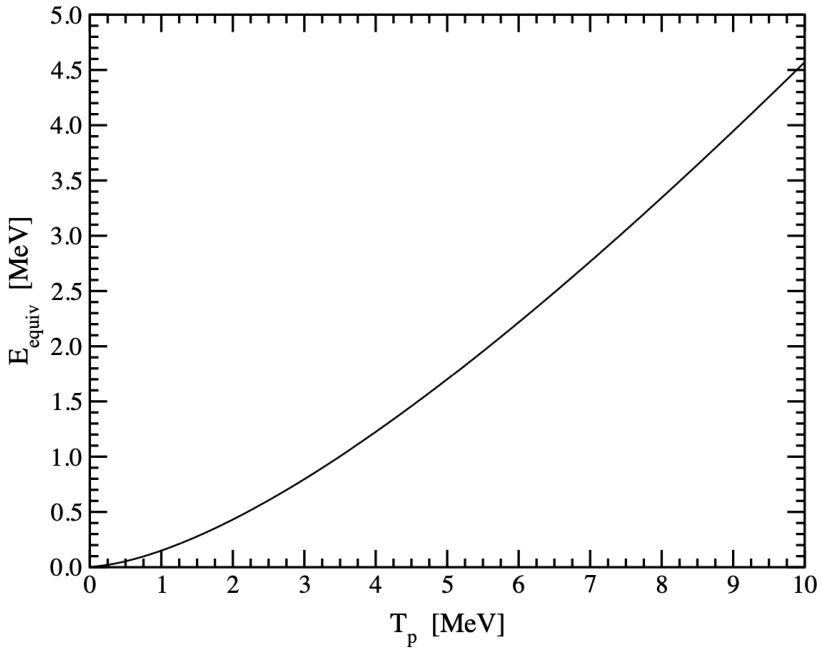

Figure 4.8: The quenched energy deposit as a function of the proton kinetic energy. The KamLAND detector properties are assumed.

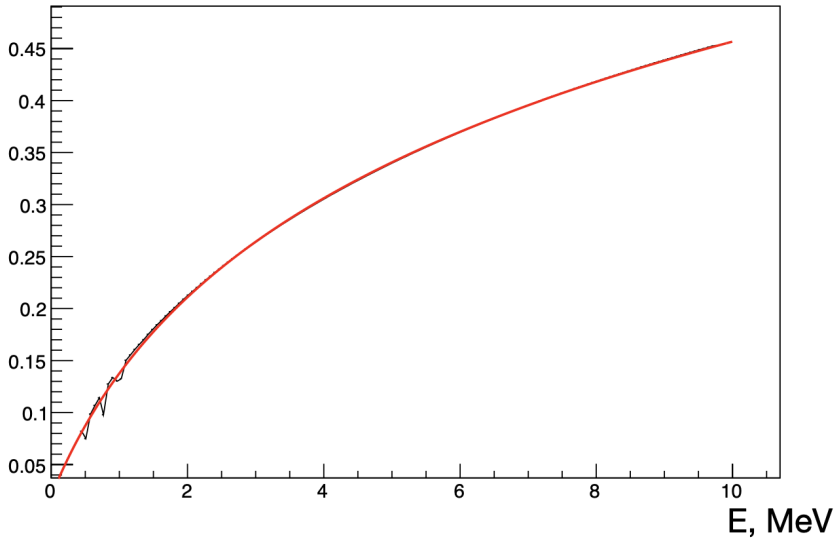

Figure 4.9: Fit of the quenching factor as a function of energy.

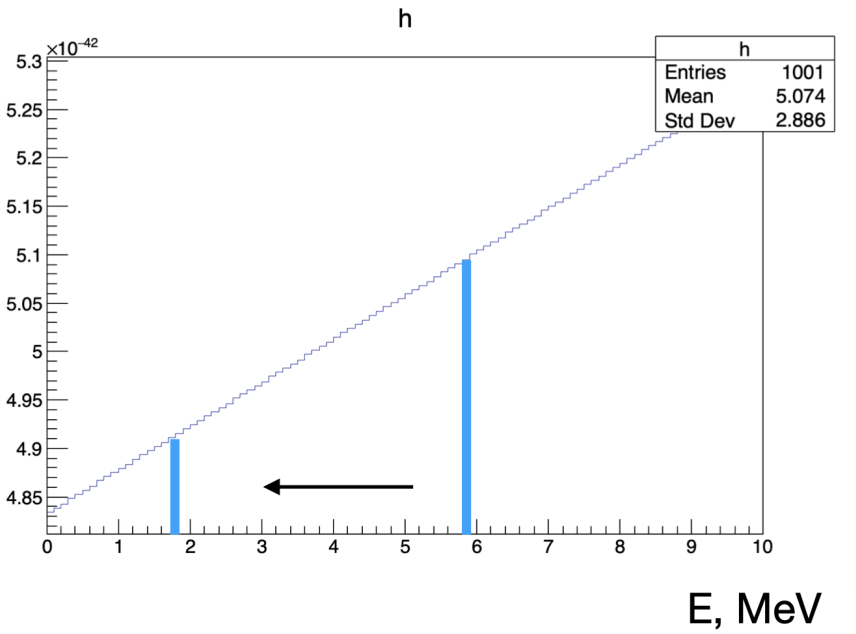

Figure 4.10: Applying quenching parameter brings higher energetic events to a lower energy area.

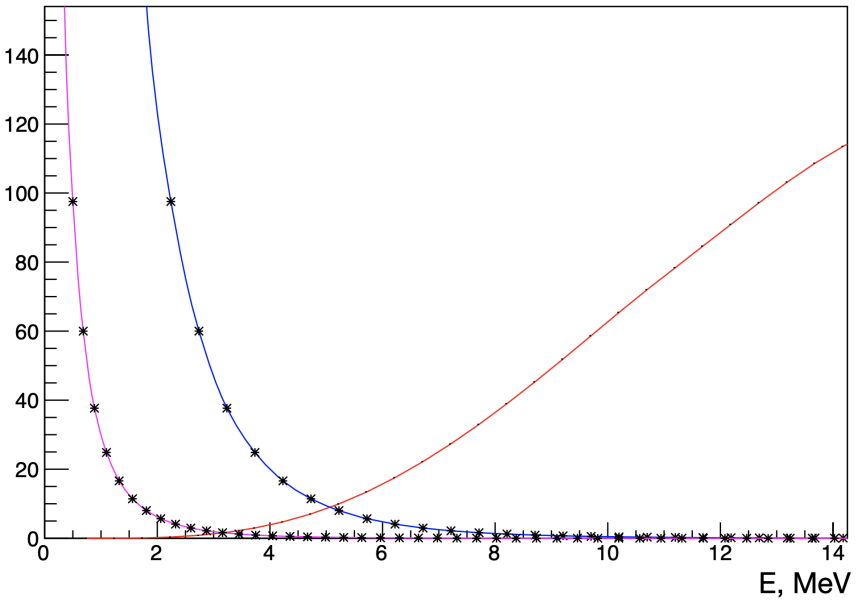

Figure 4.11: Neutrino proton scattering before(blue) and after(rose) quenching was applied. In red there is IBD.

4.4.3 Threshold change for the PES.

By default the SNOwGloBES has the energy range of 0.5-100 MeV. While most supernova neutrino events in other detection channels are happening in the 10 MeV range and thus not affected, the proton recoil energies and especially their quenched scintillation signals are close to an often below the 0.5 MeV thrreshold. The PES is the second largest channel of interaction in a sence of expected rates of detection and it has a lot of low energy events which could be seen by real JUNO detector, but not simulated by the SNOwGLoBES. To solve this obstacle and make the low energy events visible for the SNOwGLoBES the following was done. Using already updated code that produces smearing matrices for the simulations the PES spectrum in the matrices was shifted by one bin towards the higher energies, replacing the first bin with the NULL. One bin is exactly 0.5 MeV, hence all the missing and cutted by the threshold events should have appeared in the second bin. The smearing code has a possibility to set an energy threshold for a channel, for which the smearing matrix is being created. The PES rate crucially depends on both threshold and modeling of the quenching, hence in order to stay comparable to the JUNO Yellow Book [33], this threshold was adjusted to 0.4 MeV. On the picture below (Fig. 4.12) you can see an example of the shifted PES spectrum.

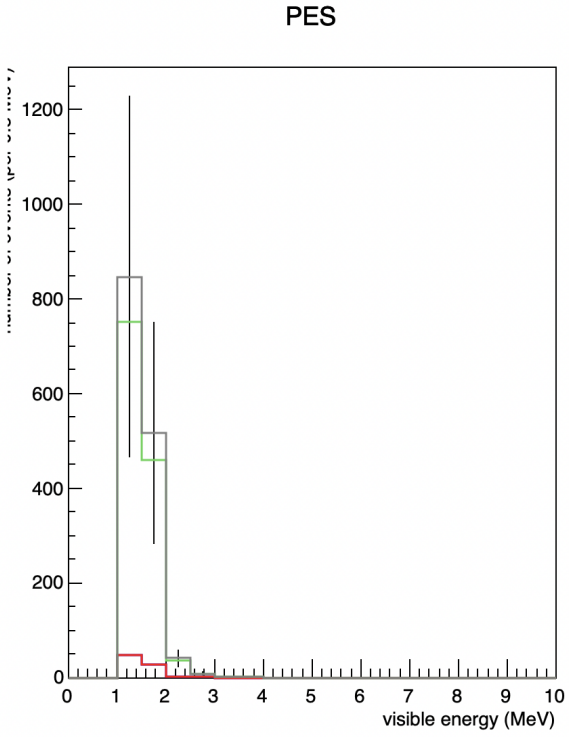

Figure 4.12: Example of a neutrino-proton spectrum simulated for the JUNO-like detector, shifted by one bin.

After applying all the changes, the output of the simulations for JUNO-like detector was compared with the JUNO yellow book [33] results (Table 4.2):

Mean energy	12 MeV	14 MeV	16 MeV
IBD (YB)	4300	5000	5700
PES (YB)	600	1200	2000
IBD (simul.)	4700	5700	6300
PES (simul.)	750	1224	2402

Table 4.2: Expected number of events vs mean energy of the spectra (JUNO YB vs SNOwGLoBES).

The numbers of events are very close. One could also calculate the ratio of IBD (events) / PES events and it stays comparable (Table 4.3):

Source	N_{IBD} / N_{PES}	N_{IBD} / N_{PES}	N_{IBD} / N_{PES}
SNOwGLoBES	6.26	4.5	2.61
JUNO YB	7.16	4.16	2.85

Table 4.3: IBD/PES number of events ratio for JUNO-like and JUNO simulations.

SNOwGLoBES doesn't provide precise simulations for the detectors, it only offers a good quantitative understanding of the detector responses, because basically all it knows about them are mass, target material and gaussian smearing of spectra. Hence we conclude that this result of upgrading SNOwGLoBES sufficiently accurate to be used in the further studies.

5 Fit procedure

5.1 Introduction

In the near future there will be plenty of neutrino experiments, that would be able to catch the supernova neutrino signal. They all have different media, sensitivity, energy resolution etc. And on top of that they don't have a common analysis framework to simulate and analyse their data. But to get the best possible outcome by analysing the data from the imminent supernova explosion, you should be prepared to use all of the detectors. They have different detection channels for neutrino flavors and spectral information, hence by combining them, one could achieve the precise determination of the neutrino flux parameters. In this work I discuss what you could achieve from the simultanious data analysis of JUNO, DUNE and IceCube-like detectors, based on the SNOwGLoBES as a tool to perform simulations of the neutrion signal in these experiments. In order to obtain information from the neutrino spectra, that could be used further, one should fit all these spectra. I don't talk about an analytical fit, but about the Monte-Carlo on Monte-Carlo fit. To perform this kind of analysis, the Asimov data set of various neutrino fluxes was created and used in SNOwGLoBES to get the correspondent detector responses. To describe many possible combinations of the neutrino spectra parameters, an array of values for the mean energy and γ was created. This array was used later in the fit procedure, in order to compare the input signal with the available set of simulated detector responses and fit it. A simulated supernova neutrino signal consists of a number of channels of interaction and all of them were fitted simultaneously. The simultaneuos fir was performed with common fit parameters to reproduce correctly correlations. Within the individual detectors the channels with similar signatures were fitted together (for example ν-e, ν-p scatterings and NC-interaction on ^{12}C in JUNO-like detector). For now the fit procedure for the neutrino flux is explained. Of course there is also the time component of the spectra, but the time dependence and time dependent fit will be included in the next chapter. Here the overall strategy of the flux fit procedure will be discussed.

5.2 Channels of interaction

Various detector media have different characteristical channels of interaction and detection, as it was showed in a chapter about the supernova neutrino detectors. Three detectors, which were used in analysis come with its own properties and offer diverse sensitivity on detection of the neutrino fluxes. Equiped with a liquid scintillator, the JUNO detector has a great sensitivity on $\bar{\nu_e}$ through the inverse beta decay(IBD); all

Channels	Interactions	Expected event rates (approx)
Inverse beta decay	$\bar{\nu}_e + p \rightarrow n + e^+$	5000
Proton elastic scattering	$\nu + p \rightarrow \nu + p$	1200
Electron elastic scattering	$\nu + e^- \rightarrow \nu + e^-$	360
Carbon CC	$\nu_e + {}^{12}\mathrm{C} \rightarrow e^- + {}^{12}\mathrm{N}$	90
Carbon CC	$\bar{\nu}_e + {}^{12}\mathrm{C} \rightarrow e^+ + {}^{12}\mathrm{B}$	110
Carbon NC	$\nu + {}^{12}\mathrm{C} \rightarrow \nu + {}^{12}\mathrm{C}^*$	390

Table 5.1: Channels of interaction in JUNO

the neutrino species interact through neutrino proton and neutrino electron scattering therefore these processes bring statistics and good sensitivity on ν_e and ν_x neutrinos. And ν_e and $\bar{\nu_e}$ are detected through the charge-current interaction on ^{12}C. IceCube's channel of interaction that gives most of the events is also IBD. For the standard supernova explosion at 10kpc distance millions of IBD events are expected, therefore it can significally improve the precision of the $\bar{\nu_e}$ spectrum parameters. On the other side IceCube doesn't provide event-by-event energy information. But using the rates of neutrinos one could get fluxes.
The DUNE experiment is very sensitive to ν_e via charge-current interaction on ^{40}Ar. Therefore it can supplement JUNO with $\bar{\nu_e}$ statistics.
Now let's take a bit closer look on the channels of interaction in every detector. You can find channels for JUNO, DUNE and IceCube in Tables 5.1, 5.2 an 5.3.
JUNO has six possible channels of detection of supernova neutrinos. IBD is the dominant one because the cross section of IBD is highest at low energies.
Positron-electron annihilation and energy deposition gives the prompt signal. In addition, there will be a delayed capture of the neutron on a free proton which will produce 2.2 MeV γs. The elastic scattering of neutrinos on protons is a promising channel to detect neutrinos of non-electron flavours. Although the total cross-section is about 4 times smaller than the IBD one, the contribution from all the neutrino-species will compensate for the loss in cross-section, especially the event rate, which is dominated by ν_x. And it is expected to be the second most important channel in JUNO regarding the supernova neutrinos. There is also ν-electron scattering process. In elastic scattering of ν_e on electrons, the scattered electrons carry the directional information of incident neutrinos, and thus can be used to locate the SN.
Charge-current (CC) interaction on ^{12}C is one of the advantages of the liquid scintillator detectors. It is advantagious because it has only clean energy information on ν_e in liquid scintillator. The subsequent beta decay of ^{12}N and ^{12}B will lead to a prompt-delayed coincidental signal. Due to different half-lifes it provides possibility to detect ν_e and $\bar{\nu_e}$ separately.
The neutral-current(NC) interaction on ^{12}C is important because it allows to probe neutrinos of non-electron flavour, because the signal would be dominated by ν_x, due to the fact, that the cross-section doesn't depend on the flavor of the neutrino.
DUNE on the other side is a liquid argon detector. It will have excellent sensitivity

Channels	Interactions	Expected event rates (approx)
Argon CC	$\nu_e + {}^{40}\mathrm{Ar} \rightarrow e^- + {}^{40}\mathrm{K}^*$	3300
Argon CC	$\bar{\nu}_e + {}^{40}\mathrm{Ar} \rightarrow e^+ + {}^{40}\mathrm{Cl}^*$	155
Argon NC	$\nu + {}^{40}\mathrm{Ar} \rightarrow \nu + {}^{40}\mathrm{Ar}^*$	210
Elastic scattering	$\nu + e^- \rightarrow \nu + e^-$	500

Table 5.2: Channels of interaction in DUNE

to ν_e via the charge-current interaction on ^{40}Ar. It is a taggable interaction since γs from $^{40}\mathrm{K}^*$ can be observed. The $\bar{\nu_e}$ interaction will also occur and can be tagged. The neutral current excitations are possible, although little information is currently available in the literature about cross sections and observables. Finally, there will be elastic scattering of neutrinos on electrons which again allows to probe all the neutrino species.
The channels considered for the IceCube detector are the same as those which are considered in the Water Cherenkov experiment. Main channel in terms of events is IBD as in scintillator detectors. But there is also neutrino electron scattering and interaction on ^{16}O. All channels you can see below:

Channels	Interactions	Expected event rates (approx)
Inverse beta decay	$\bar{\nu}_e + p \rightarrow n + e^+$	200000 - 10^6
ν electron elastic scattering	$\nu + e^- \rightarrow \nu + e^-$	40000
Oxygen CC	$\nu_e + {}^{16}O \rightarrow e^- + X$	7000
Oxygen CC	$\bar{\nu}_e + {}^{16}O \rightarrow e^+ + X$	5000
Oxygen NC	$\nu_{all} + {}^{16}O \rightarrow \nu_{all} + X$	100

Table 5.3: Channels of interaction in IceCube

Since the IceCube detects only a single photon per neutrino interaction it has almost no energy resolution, but can provide information on total number of detected events in a given time window. Because by providing the spectral information one can translate rates into fluxes.

$$\Phi = \frac{R}{N_p \cdot \sigma(E)} \tag{5.1}$$

This can not only offer a possibility to achieve great precision in determination of the neutrino flux parameters, but also give an opportunity to estimate some astrophysical quantities, which will be discussed later.

5.3 Creation of the preparational data set for the fit

As it was discussed in a Chapter 4, the mechanisms of SN neutrino production are distinct at three different stages of SN evolution, namely, the early-time neutronisation burst, the accretion phase and the cooling phase. However, the differential neutrino

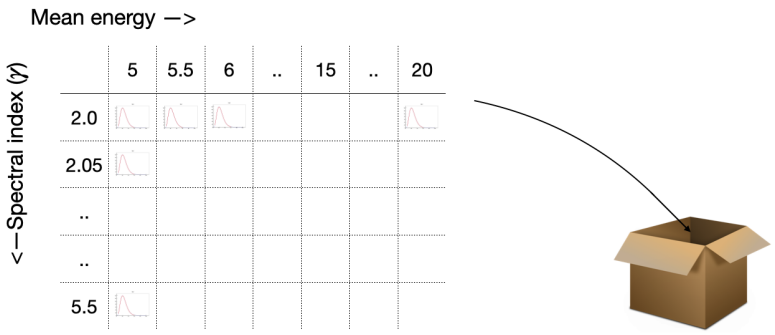

Figure 5.1: Array of models for the pre-simulated data set.

fluences or time-integrated neutrino energy spectra can be perfectly described by the Keil-Raffelt-Janka (KRJ) parametrisation [65].

$$\frac{dF_\alpha}{dE_\alpha} = \frac{3.5 \times 10^{13}}{\mathrm{cm^2 MeV}} \cdot \frac{1}{4\pi D^2} \frac{\epsilon_\alpha}{\langle E_\alpha \rangle} \frac{E_\alpha^{\gamma_\alpha}}{\Gamma(1+\gamma_\alpha)} \left(\frac{1+\gamma_\alpha}{\langle E_\alpha \rangle}\right)^{1+\gamma_\alpha} \exp[-(1+\gamma_\alpha)\frac{E_\alpha}{\langle E_\alpha \rangle}] \quad (5.2)$$

Where α denotes the neutrino flavour, E_α the energy of the neutrino, ϵ_α flavour-dependent total neutrino energy is given in units of $5 \cdot 10^{52}$ erg, $\langle \mathrm{E} \rangle$ - mean energy of the neutrino flux and γ is a spectral index.
It is being forward-folded with the cross-section and energy response of the detectors in order to do the fit of the observed event spectra in the detectors. Normalisation, the mean energy and the spectral index were free parameters in the fit. During the supernova explosion the mean energy and γ can vary in a wide range of values, depending on the conditions inside the dying star, like temperature, inner core size, etc.
A set of values for the mean energy was chosen in the range [5, 20] MeV with a step size of 0.5 MeV. The spectral index (i.e. γ) was varied in the range [2, 5.5] with a step size of 0.05 (see Fig. 5.1). Array of these models was used in the SNOwGloBES as an input and the data for all the detectors was simulated. Using SNOwGloBeS output, a histogram array, containing the visible energy spectra for every channel of neutrino interaction was created and pre-stored. That gave an Asimov data set which was used in a fit procedure. The input histograms were compared to this data set and the best possible parameters, which would fit the input were found. Log likelyhood minimisation was performed using MINUIT.
In order to make the fit better and more sensitive for the cases when the parameters were not on the grid of values, the interpolation method was applied. It means that the fit looks for the four closest histograms in the array and builds the result histogram using these four with the corresponding weights. You could see it on Fig. 5.3.

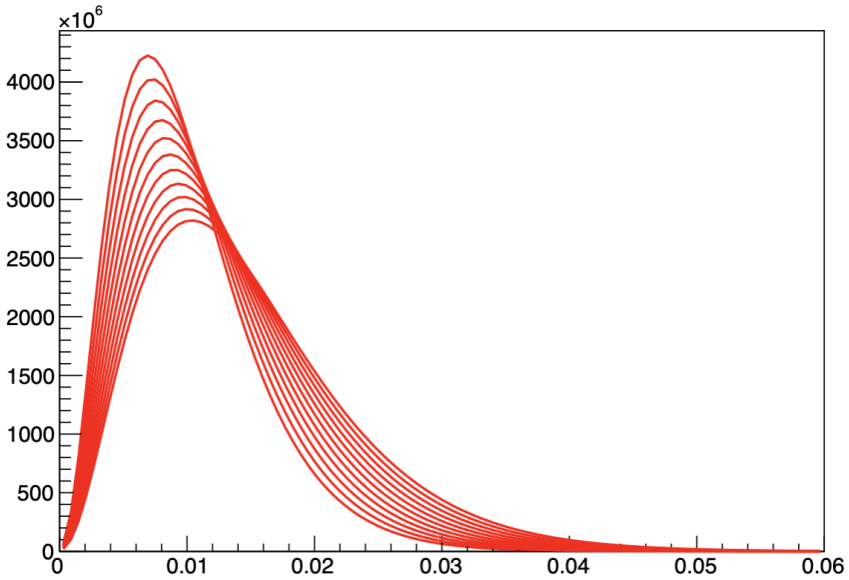

Figure 5.2: Example of the pre-simulated fluxes with the same normalisation but different γ and mean energy.

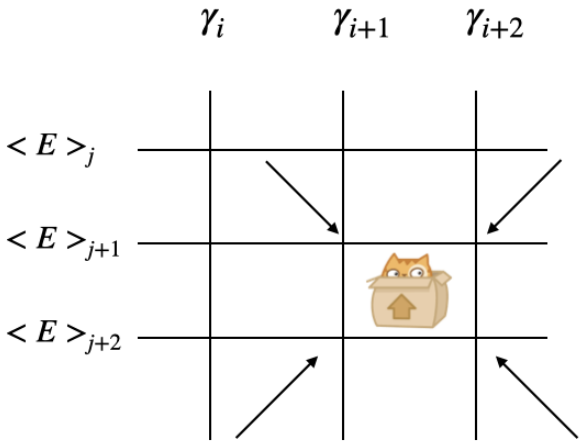

Figure 5.3: If the parameters of the input data were not on the grid of pre-simulated values, the interpolation method was applied.

Mathematically it is descibed as:

$$\begin{aligned}\text{FIT} = w_e w_\gamma \text{Hist}(\langle E\rangle_{j+1}, \gamma_{i+1}) + (1-w_e) w_\gamma \text{Hist}(\langle E\rangle_{j+2}, \gamma_{i+1}) + \\ + w_e(1-w_\gamma)\text{Hist}(\langle E\rangle_{j+1}, \gamma_{i+2}) + (1-w_e)(1-w_\gamma)\text{Hist}(\langle E\rangle_{j+2}, \gamma_{i+2})\end{aligned} \tag{5.3}$$

Corresponding weights are:

$$w_e = 1 - \frac{(E - \langle E\rangle_{j+1})}{\Delta E}$$

$$w_\gamma = 1 - \frac{\gamma - \gamma_{i+1}}{\Delta\gamma}$$

5.4 Fit procedure

The χ^2-analysis was performed. A nine degrees of freedom χ^2 analysis of the supernova signal was performed considering normalisations, average energies and pinching parameters for ν_e, $\bar{\nu_e}$ and ν_x fluxes. To make maximum use of all the interaction channels present for a single flavor, and to take into account correlations for channels sensitive to several neutrino flavors the simultaneous fit of all the channels was performed. In the JUNO detector, IBD and charged-current(CC) interactions on ^{12}C can be detected separately(because ^{12}C-CC is slower than IBD), but electron neutrinos and antineutrinos in CC-^{12}C were considered indistinguishable and were fitted as part of a common spectrum with two components. Neutrino-electron and neutrino-proton elastic scattering processes were fitted together with neutral current interaction events on ^{12}C as a sum of all neutrino spectra, because technically they are also indistinguishable and appear only as one spectrum, all single events without delayed decay.
DUNE-like detector data each channel of interaction was fitted as a sum of all involved neutrino species. For the IceCube-like detector the events detected for all of the channels were summed up and used as one value, or one bin in a histogram. As it was already mentioned, IceCube usually detects only single photon per neutrino interaction and it has almost no energy resolution, hence it was used as a giant calculator.
Therefore, a global fit was performed to the Asimov data sets returning median sensitivity and uncertainties.

5.5 Results

You can find the example accuracy, that can be reached for the neutrino spectra parameters Table 5.4 . The fit results using all three experiments are presented with relative uncertainties. The fitted spectra for different experiments you can see on Fig. 5.4, Fig. 5.5, Fig. 5.6 and Table 5.5.
As you see, all channels of interaction are being fitted very good. Fit results for ν_e are in blue, for $\bar{\nu}_e$ in red and for the ν_x the results are in green. Total fit is in grey. Fit procedure works smoothly in searching the parameters of the incoming neutrino flux. IceCube fit result histogram consists only of one bin, but that is because the sum of events from all the channels was used.

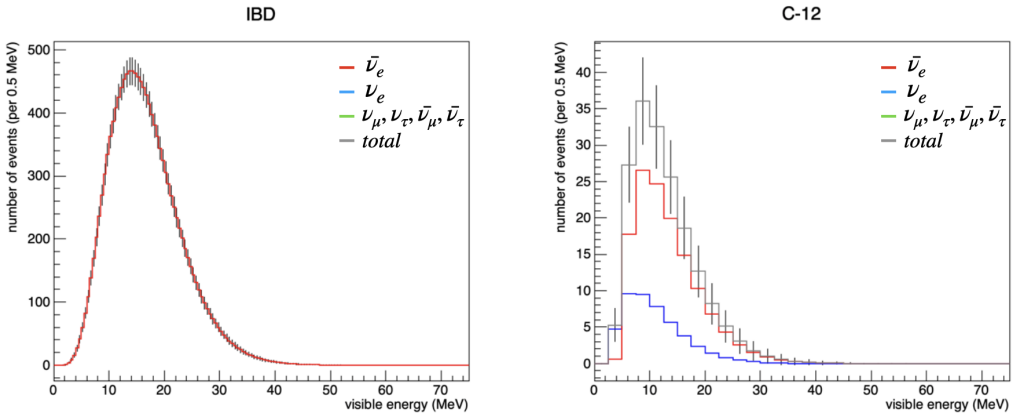

Figure 5.4: Fit results for IBD and CC-interaction on ^{12}C in JUNO

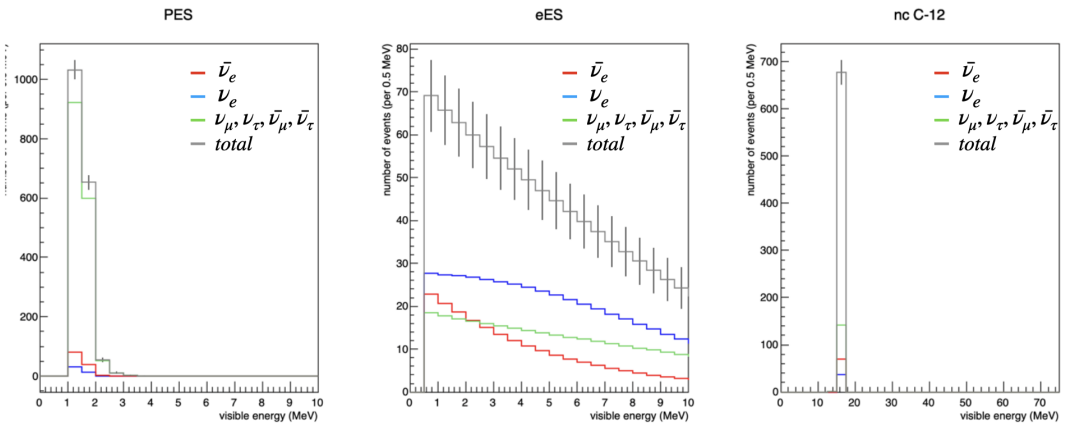

Figure 5.5: Fit results for neutrino-proton, neutrino-electron elastic scatterings and neutral-current interaction on ^{12}C in JUNO

Fit parameters	True values	Fit results	Relative uncertainty
E_{ν_e}, MeV	10	9.99 ± 0.56	5.6%
γ_{ν_e}	3.3	3.29 ± 0.51	15.5%
$Norm_{\nu_e}$	1	1.00 ± 0.06	5.9%
$E_{\bar{\nu_e}}$, MeV	11.5	11.49 ± 0.02	0.2%
$\gamma_{\bar{\nu_e}}$	3.5	3.49 ± 0.03	0.8%
$Norm_{\bar{\nu_e}}$	1	1.000 ± 0.003	0.3%
E_{ν_x}, MeV	13.5	13.50 ± 0.18	1.3%
γ_{ν_x}	3.5	3.50 ± 0.15	4.2%
$Norm_{\nu_x}$	1	0.99 ± 0.04	3.9 %

Table 5.4: Fit results. Example accuracy that can be reached for a generic model, using all three experiments.

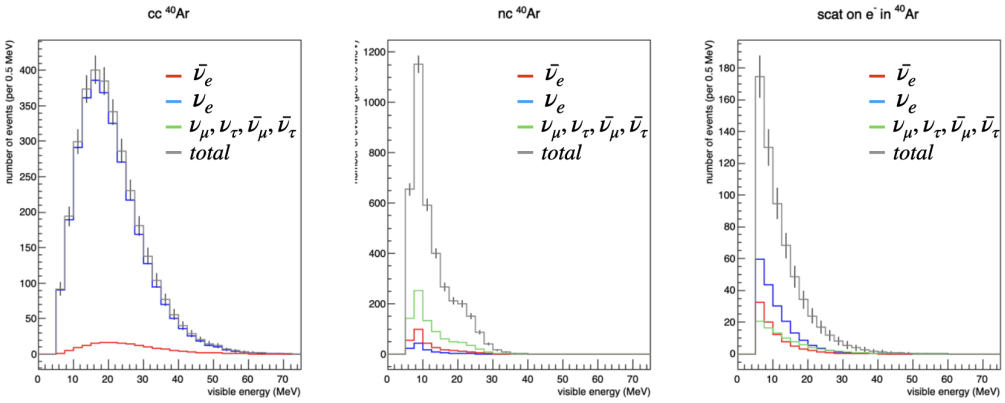

Figure 5.6: Fit results for charge and neutral current interaction on ^{40}Ar and scattering on electrons in DUNE

Channel	Initial values	Fit results
$\bar{\nu_e}$	1.09887e+06	1.09887e+06
ν_e	18798.6	18799.2
ν_x	4391.58	4294.47
Noise	540	540
Total	1.13577e+06	1.13538e+06

Table 5.5: Fit results in IceCube

It is interesting to understand the accuracy, at which different channels as well as different experiments constrain the fit parameters.
To estimate it and show how fit performes for different experiments, it was run separately for JUNO, for DUNE and for IceCube. On Fig.5.7, Fig.5.8 and Fig.5.9 you can

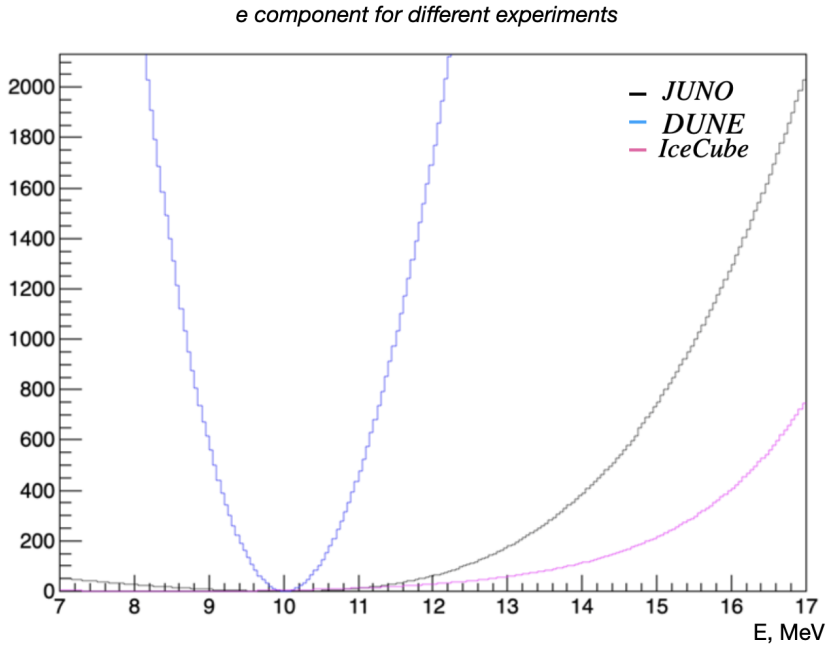

Figure 5.7: Mean energy χ^2 profile, e-component. Sensitivity of different detectors.

see the comparison for the χ^2-profile of mean energy for e, $\bar{e}$ and x components. We can cleary see, that the DUNE is the best experiment to determine the ν_e-spectrum parameters. It is also sensitive to the ν_x neutrinos, but not to the electron antineutrinos. On the other hand JUNO is most sensitive to the $\bar{\nu_e}$ and also has good sensitivity to the ν_x, because of the elastic scattering processes and ^{12}C-NC interaction. IceCube is very sensitive to the $\bar{\nu_e}$ too, which makes the uncertainties on the parameters even smaller.
The analysis showed that a degeneracy between the parameters doesn't prevent the precise determination of the supernova neutrino fluxes. This precision can give the possibility to define the neutrino flux parameters very well.
On the plots 5.10 and 5.11 you can see the 2D χ^2-profiles for different combinations of the experiments. To show the improvement, that addition of a single exepriment does, the fit was performed on JUNO-like data set, then on JUNO and DUNE, and finally on JUNO, DUNE and IceCube combined data set. It displays the correlation between mean energy and γ parameters and level of precision one could get on them. Circles represent 1, 2 and 3 σ deviations from the best fit value for mean energy and γ. You can basically see how step-by-step it improves the results first on ν_e, by adding DUNE data and then on $\bar{\nu_e}$ and ν_x after addition of the IceCube.

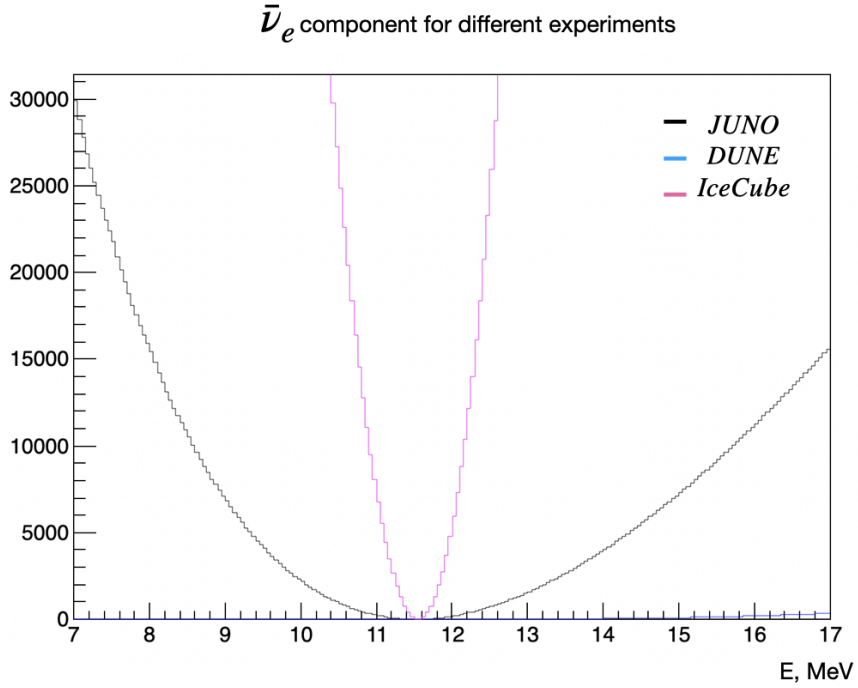

Figure 5.8: Mean energy χ^2 profile, $\bar{e}$-component. Sensitivity of different detectors.

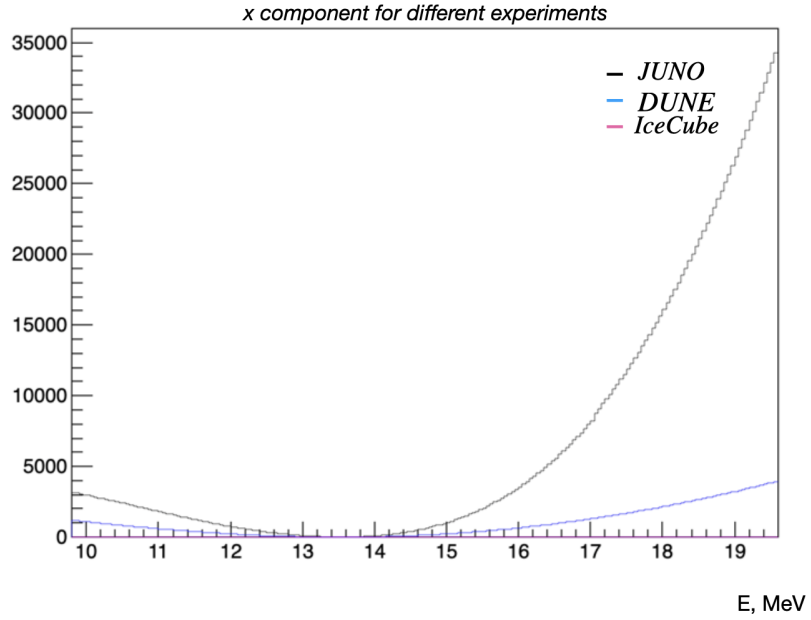

Figure 5.9: Mean energy χ^2 profile, x-component. Sensitivity of different detectors.

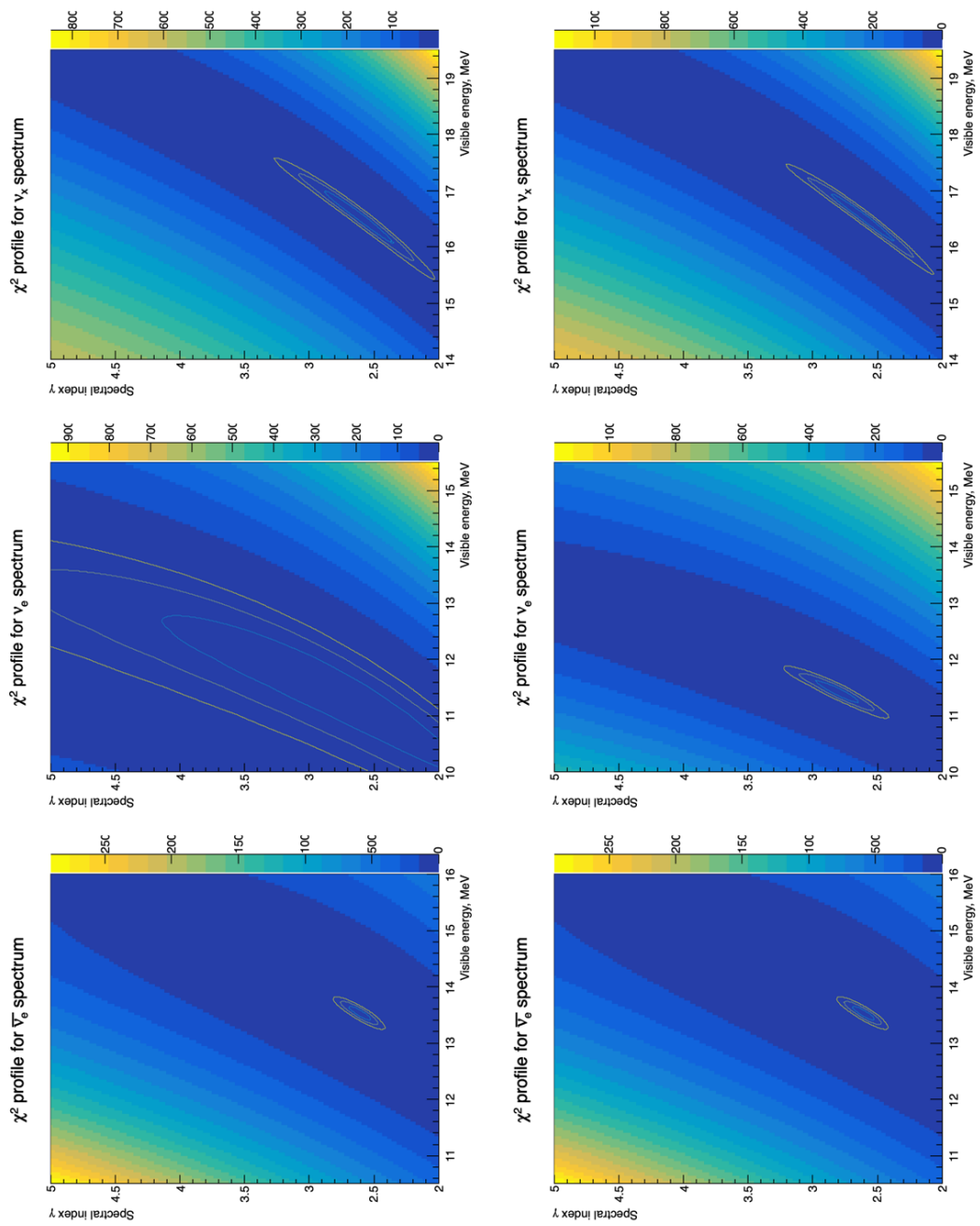

(a) χ^2-profile only JUNO

(b) χ^2-profile JUNO + DUNE data

Figure 5.10: 2D - χ^2-profiles.

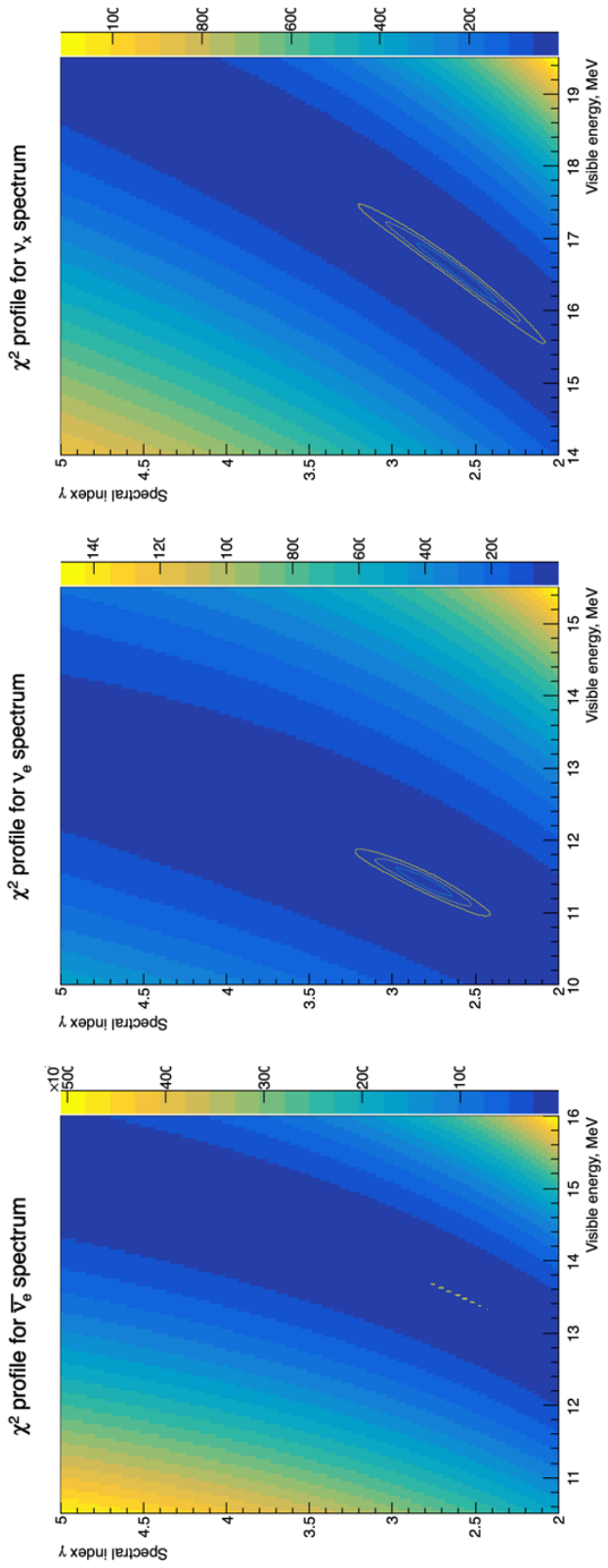

Figure 5.11: χ^2-profile JUNO + DUNE + IceCube

5.6 Energy of the SN explosion

The fit procedure described above can be used in order to estimate the energy of the supernova explosion and the uncertainties that come with it. In order to do that a SN explosion of total energy $3\cdot 10^{53}$ erg was simulated. It was done using SNOwGLoBES and hence the distance to the Earth is set to the canonical distance of 10 kpc. It was assumed that the energy is distributed equaly between all of the neutrino species, it means that each of the neutrino type got $0.5\cdot 10^{53}$ erg energy. The mean energies as well as the γ parameters were set equal for all species to 12 MeV (mean energy) and $3(\gamma)$ correspondingly. To evaluate the statistical uncertainty of the fit the following was done:

5.6.1 Uncertainties

On the step of creating the spectra with statistical fluctuation, the Poissonian uncertainty was introduced to the bins of all of the histograms. Hence the neutrino spectra became of more random shape, that could be obtained from the analysis of the real data. The Poissonian uncertainty was done using TRandom2 class of the ROOT. It was chosen because it allows to get new random values every time you run the code. This SN model of $3\cdot 10^{53}$ erg was ran 100 times through the fit procedure. And every time the random uncertainty of the bins was applied. To get the total energy of the explosion one should take the luminosity that was given to SNOwGLoBES to fit the input histogram and multiply it with the normalisation that you obtain from the fit procedure, along with the mean energy and γ parameters. And then one should sum it up for all the neutrino species. Every loop gave slightly different value for the total energy.

$$E_{total} = \sum_{f=1}^{6} n_f \cdot \langle E_f \rangle \tag{5.4}$$

where j is ν_e, $\bar{\nu_e}$ or ν_x neutrinos. Of course ν_x should be summed up 4 times. Total reconstructed energy of the neutrino species plotted below (Fig. 5.12). As before, in blue ν_e, in red $\bar{\nu_e}$ and ν_x is green.
As it was expected the best precision gives the $\bar{\nu_e}$ spectrum with 3.6 % relative error. The ν_e and ν_x spectra have 6% and 8.2% respectively. The relative error on the total energy is 7.1%.
To check that the fit was performed correctly, I checked the degeneracies between fit parameters such as normalisation and mean energy. Normalisation vs mean energy 2D plots were made. You can see them on Fig. 5.13, Fig. 5.14 and Fig. 5.15.
The plots show correctly that the nomalisation and the mean energy stay correlated during the fit procedure, with the spectra being smeared by the introduction of the Poissonian uncertainties in the bins.

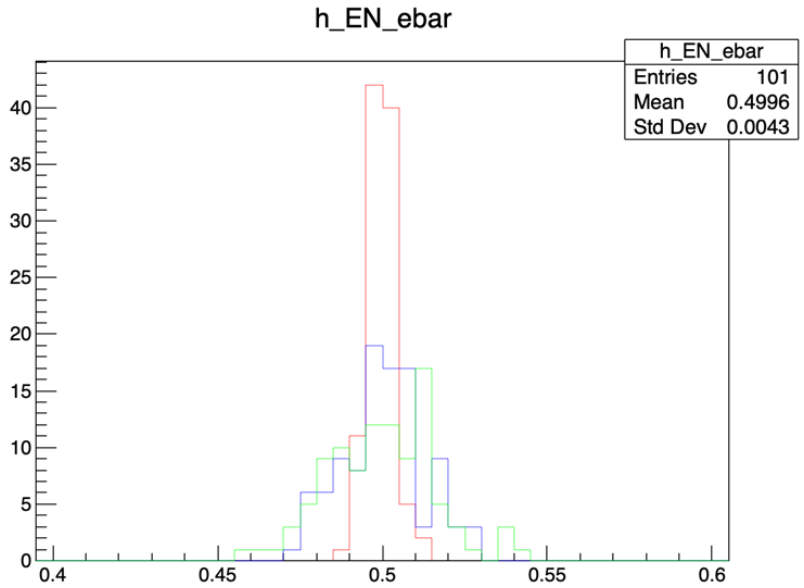

Figure 5.12: Uncertainties of the energy reconstruction for the neutrino fluxes. On the x axis erg·10^{53}.

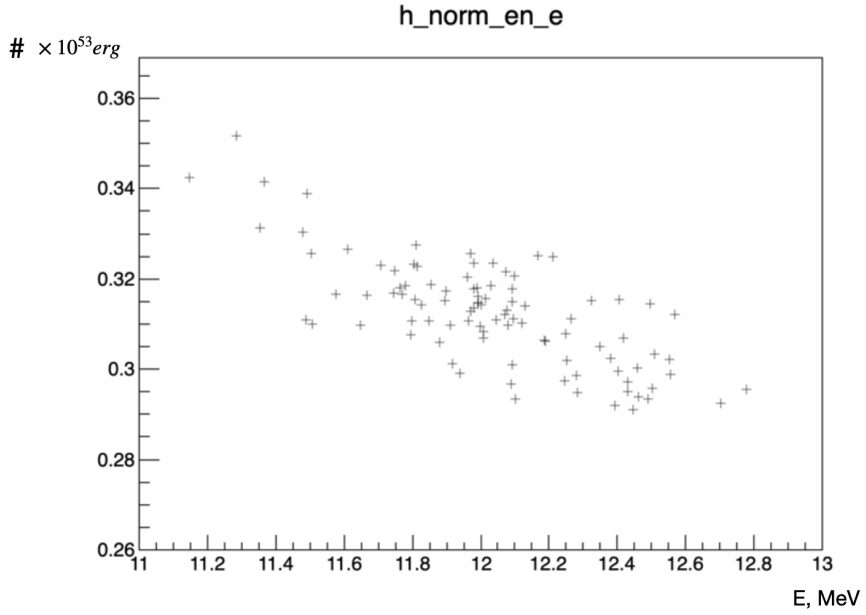

Figure 5.13: Normalisation vs mean energy for the ν_e spectrum.

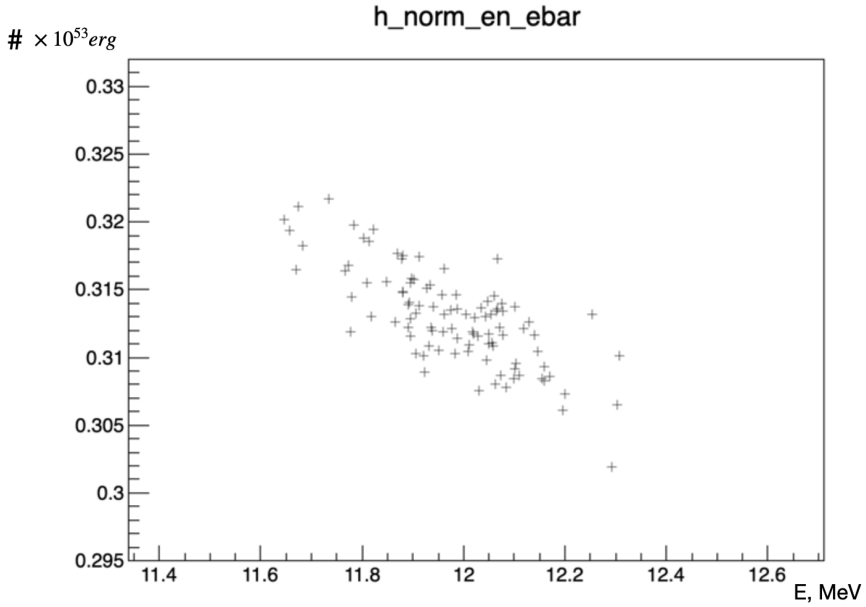

Figure 5.14: Normalisation vs mean energy for the $\bar{\nu_e}$ spectrum.

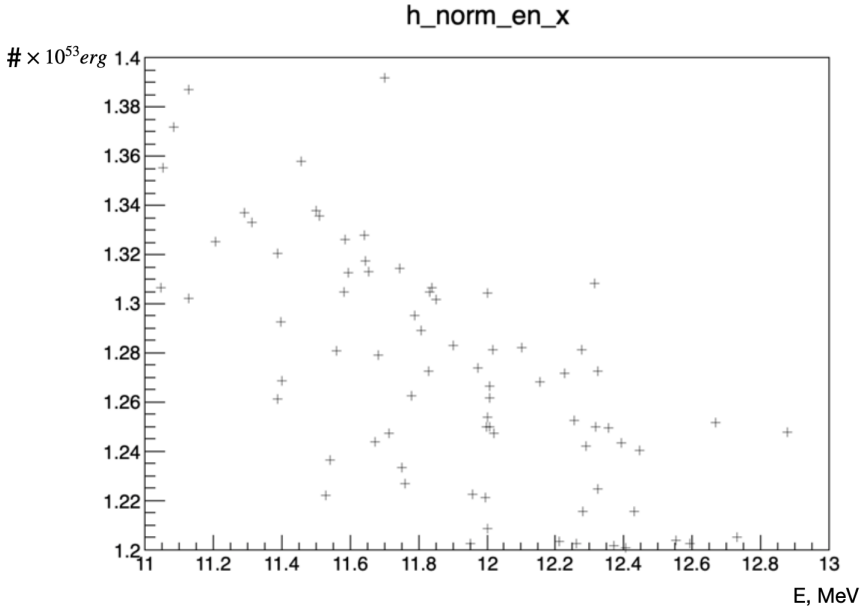

Figure 5.15: Normalisation vs mean energy for the ν_x spectrum.

6 Analysis of a time-dependent data

As it was already said in a previous chapter, the core-collapse supernova explosion doesn't happen in moment. It takes tens of seconds to go through different phases of the explosion and emit all neutrino flavors. The goal of this chapter is to build a fit procedure that would be able to fit the time evolution of the neutrino spectra. Following the death of the star, the mean energy, γ and normalisation behave differently in time. And it is very insightful to be able to predict and describe their behaviour, determine important time parameters of the spectra and to be able to estimate the errors of some astrophysical parameters of the supernova.

6.1 Introduction

The standard scenario of core-collapse SN explosion is the delayed, neutrino-driven explosion paradigm of Bethe and Wilson [66], [67]. The degenerate core of an evolved massive star becomes unstable by pressure loss due to electron absorption and photon dissociation on heavy nuclei. Usually this happens after completing all nuclear burning stages when the core consists of iron, the most tightly bound nucleus—the class of iron-core SNe. For the smallest progenitor masses of perhaps 6–8$M_{\odot}$, the dissociation begins before igniting the final burning stage when the oxygen- neon-magnesium core has become very degenerate—the class of electron-capture or O-Ne-Mg-core SNe. In both cases, the subsequent implosion on a near free-fall time is halted when nuclear density of around 3 $\times 10^{14}$ g cm^3 is reached and the equation of state stiffens. This sudden core bounce forms a shock wave that propagates outward, ramming into the high-Z material that keeps falling in at supersonic speed. Its dissociation absorbs energy and weakens the shock wave until it stagnates after reaching a radius of 100–200 km ([33], p.70).

Deleptonization burst: The absorption of electrons during infall produces a ν_e flux until the core reaches densities of around 10^{12} g cm^3. Afterwards neutrinos are trapped and the lepton number stored in the electron gas can no longer escape. Most of this trapped electron-lepton number will eventually escape by diffusion in the form of ν_e. However, a **prompt ν_e burst** or **deleptonization burst** lasting around 10 ms, is released when the shock wave passes through the edge of the iron core, dissociates iron, and allows the outer layers to deleptonize by $e + p \rightarrow n + \nu_e$.

In the neutrino-driven mechanism, there are two main phases of neutrino emission: *accretion* and *cooling*.

Accretion: A brief and very luminous neutrino emission, here termed accretion, that should involve a lower amount of neutrinos than in the cooling phase, 10-20% in energy. The accretion phase characterizes the neutrino-driven mechanism of the

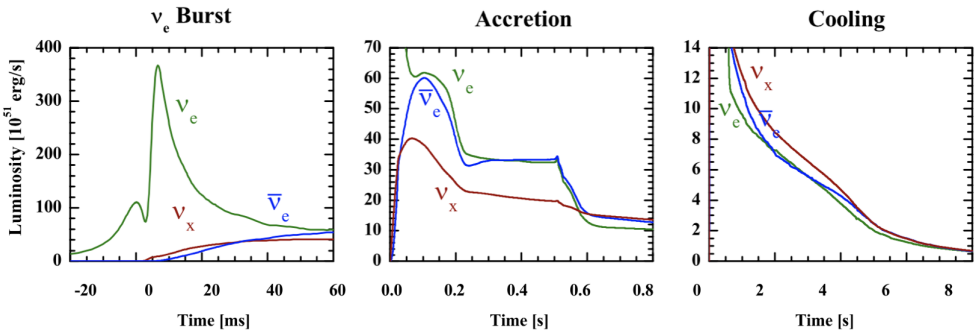

Figure 6.1: Time evolution of the luminosity throughout all the stages of the explosion [33].

explosion, and it is expected to occur in the first stage of neutrino emission. In this phase, the matter is rapidly accreting over the proto-neutron star through the stalled supernova shock wave. The two most important processes of neutrino emission are [2]:

$$e^- + p \to n + \nu_e \text{ and } e^+ + n \to p + \bar{\nu_e}$$

due to the abundant presence of nucleons and of quasi-thermal e^+e plasma. It lasts few tens to few hundreds of ms, depending on progenitor properties and other parameters. Neutrino emission is powered by accretion flow. Luminosities in ν_e and $\bar{\nu_e}$ perhaps as much as a factor of two larger than each of the ν_x fluxes. Pronounced hierarchy of average energies $\langle E_{\nu_e} \rangle < \langle E_{\bar{\nu_e}} \rangle < \langle E_{\nu_x} \rangle$, energies increasing until explosion. The luminosity drop at around 200 ms represents the infall of the Si/O interface—the accretion rate and therefore luminosity clearly drops afterwards ([33], p.72).
Cooling: A thermal phase, called cooling, occurring when the proto-neutron star cools quietly. This phase involves most of the emitted neutrinos, 80-90% in energy. When the explosion has taken off (here triggered between 500–600 ms by numerically quenching the accretion flow) the luminosity drops and is subsequently powered by cooling of the proto-neutron star. Approximate luminosity equipartition between species and $\langle E_{\nu_e} \rangle < \langle E_{\bar{\nu_e}} \rangle \approx \langle E_{\nu_x} \rangle$. Number flux of ν_e enhanced because of de-leptonization ([33], p.72).

6.2 Parametrisation of the flux

6.2.1 Accretion phase

After the bounce, the simulations indicate that the shock wave, propagating into the outer core of the star, looses energy and eventually gets stalled. It forms an accreting shock that encloses a region of dissociated matter and hot e^+e^- plasma, where the weak reactions $e^- + p \to n + \nu_e$ and $e^+ + n \to p + \bar{\nu_e}$ give rise to intense ν_e and $\bar{\nu_e}$

luminosities. This emission lasts a fraction of a second. The neutrons are treated as a transparent target, for only a small fraction of antineutrinos is expected to couple with the star. This is the accretion phase (suffix a in corresponding symbols). The parametrised $\bar{\nu_e}$ flux could be written in a form [2]:

$$\Phi_a^0(t, E_\nu) = \frac{1}{4\pi D^2} \frac{8\pi c}{(hc)^3} \times [N_n(t)\sigma_{e^+n}(E_\nu) g_{e^+}(\bar{E_{e^+}}(E_\nu), T_a(t))] \tag{6.1}$$

where D is the distance to the supernova, $N_n(t)$ is the number of target neutrons assumed to be at rest and the thermal flux of positrons:

$$g_{e^+}(E_{e^+}, T_a(t)) = \frac{E_{e^+}^2}{1 + exp[E_{e^+}/T_a(t)]} \tag{6.2}$$

is calculated at an average positron energy: $\bar{E_{e^+}}(E_\nu) = \frac{E_\nu - 1.293 MeV}{1 - E_\nu/m_n}$. Cross section for positron interactions in the energy range of interest E_ν = 5-40 MeV is

$$\sigma_{e^+n}(E_\nu) \approx \frac{4.8 \times 10^{-44} E_\nu^2}{1 + E_\nu/(260 MeV)} \tag{6.3}$$

The average energy of the antineutrinos is roughly given by 5 T_a and the spectrum is slightly non-thermal, mostly due to the presence of the cross section $\sigma_{e^+n}(E_\nu)$. For example, when T_a = 1.5, 2.5, 3.5 MeV, one gets $\langle E_\nu \rangle / T_a$ = 5.5, 5.2, 5.0 respectively with $\delta E_\nu / T_a$ = 0.39, 0.41, 0.41 where $\delta E_\nu = \sqrt{\langle E_\nu^2 \rangle - \langle E_\nu \rangle^2}$.
There are two time dependent quantities in Eq. 6.1: the number of neutrons N_n(t) and the positron temperature T_a(t). Temperature can be introduced in a way that it interpolates from an initial value to a final value:

$$T_a(t) = T_i + (T_f - T_i)(\frac{t}{\tau_a})^m with \begin{cases} T_i = T_a \\ T_f = 0.6 T_c \end{cases} \tag{6.4}$$

where T_a denotes the positron temperature at the beginning of accretion (to be contrasted with T_c, the antineutrino temperature at the beginning of the cooling phase). With this parametrization, the positron temperature reaches 0.6 T_c at t = τ_a. The power m = 1 – 2 mimics the behavior found in numerical simulations. The numerical simulations suggest the behaviour of the luminosity such as that, at least for t $\sim$ 0, decreases as 1/(1 + t/0.5 s) and is advocated by Lorerdo and Lamb [68]. Luminosity scales with the temperature as $N_n T_a^6$. Thus, one need to include an explicit factor $(T_a(t)/T_a)^6$. Therefore the number of neutrons exposed to thermal positrons is [2]:

$$N_n(t) = \frac{Y_n}{m_n} \times M_a \times (T_a/T_a(t))^6 \times \frac{j_k(t)}{1 + t/0.5s} \tag{6.5}$$

The fraction of neutrons being set to Y_n = 0.6. M_a is the initial accreting mass exposed to the positrons thermal flux. The time-dependent factor

$$j_k(t) = exp[-(t/\tau_a)^k] \tag{6.6}$$

is included to terminate the accretion phase at t $\sim \tau_a$. Factor k is set to be equal to 2, a choice that offers the advantage of leading to a reasonable, continuous luminosity curve, closer to the type of curves found in numerical simulations. Ultimately, the accretion phase involves 3 free parameters: M_a, T_a and τ_a. M_a is certainly lower than the outer core mass (about 0.6 $M_\odot$); T_a is expected to be in the few MeV range; and, finally, the accretion phase should last a fraction of a second, $\tau_a \sim 0.5$ s being a typical number.

6.2.2 Cooling phase

The forming proto-neutron star (with radius R_{ns}) evolves to a hot neutron star in the last phase of the SN collapse and this process is characterized by the emission of neutrinos and antineutrinos flux of all the species. This is the cooling phase (suffix c for the corresponding symbols).
A parameterization of the electron antineutrino flux, differential in the energy is [2]:

$$\Phi_c^0(t, E_\nu) = \frac{1}{4\pi D^2} \frac{\pi c}{(hc)^3} [4\pi R_c^2 g_{\bar{\nu_e}}(E_\nu, T_c(t))] \tag{6.7}$$

The time profile of the process is:

$$T_c(t) = T_c exp[-t/(4\tau_c)] \tag{6.8}$$

Eq. 6.7 describes an isotropic emission of antineutrinos from a distance D. The astrophysical free parameters are R_c, T_c, and τ_c: the radius of the emitting region (neutrino sphere), the initial temperature, and the time constant of the process. It is expected to have these parameters as: $R_c \approx R_{NS} = 10 - 20km$, $T_c = 3 - 6$ MeV, and $\tau_c =$ of order several seconds [2].
Putting all together the total flux is [69]:

$$\Phi_{\bar{\nu_e}}^0(t, E_\nu) = f_r(t)\Phi_a^0(t, E_\nu) + [1 - j_k(t)]\Phi_c^0(t, E_\nu) \tag{6.9}$$

where $f_r(t) = 1 - exp(-t/\tau_r)$ with the rising time scale τ_r further introduces an early-time fine structure, and $j_k(t) = exp[-(t/\tau_a)^k]$ (with k being an integer and equal to 2) is the time function interpolating the accretion and cooling phases of neutrino emission.
Given the flux $\Phi_{\bar{\nu_e}}(t, E_\nu)$, one can obtain the event rate R(t,E_e) by convolving it with the IBD cross section $\sigma_{IBD}(E_\nu)$.

$$R(t, E_e) = N_p \Phi_{\bar{\nu_e}}(t, E_\nu)\sigma_{IBD}(E_\nu)\eta(E_e) \tag{6.10}$$

Where N_p is the number of target protons in the detector, and the detection efficiency factor η(Ee) = 1 is taken for JUNO.

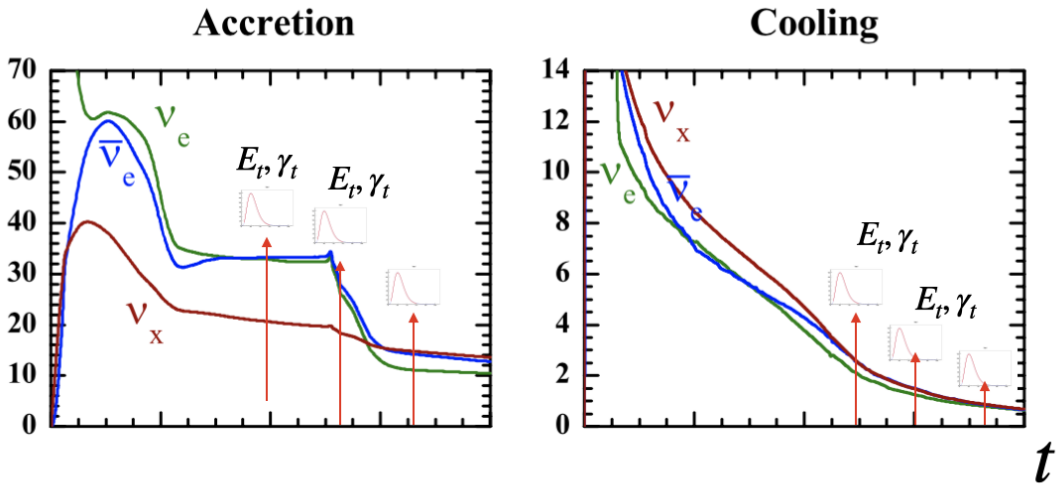

Figure 6.2: Bin by bin time dependent analysis approach

6.3 Spectral fits per time bin

SNOwGLoBES does not allow to perform time dependent analysis. Its output is already time integrated. Therefore it was chosen the approach to do bin by bin time analysis of the models of the SN-explosion. See Fig. 6.2.
For the given SN model it is known for every chosen time bin three crucial parameters: luminosity, mean energy and γ. Thus it is possible to feed single bins as independent models to SNOwGLoBES and its ouptup data would be the data to analyse and fit with the procedure descibed in chapter 5. As initial model to analyse was chosen a core-collapse SN-explosion of a star of 8.8 $M_\odot$ situated in Crab nebula [1]. Since it is convenient to show mean energy and γ time-dependent curves in logarythmic scale, it was chosen to use 27 time bins in three time regions [0.01-0.09 s], [0.1-0.9 s] and [1-9 s]. So after the first step of, i.e. fitting the single time bins one can get curves shown on Fig.6.3 , Fig.6.4 and Fig.6.5. The third curve used in this analysis was a normalisation curve, which represents the luminosity curve, obtaining it from the fit procedure.

6.4 Fit with the parametrised time-dependent flux

In order to make a combined fit of all these curves and get an estimation on the error of the astrophysical parameter, like R_c - the neutrino sphere, a complicated parametrised model was used. Parameters and formulas were motivated by Vissani model [2] and taking into account the simulation data of 8.8$M_\odot$ Supernova [1]. Each of the time-dependent curves, i.e. rate, mean energy and γ parameter got a mathematical description involving:

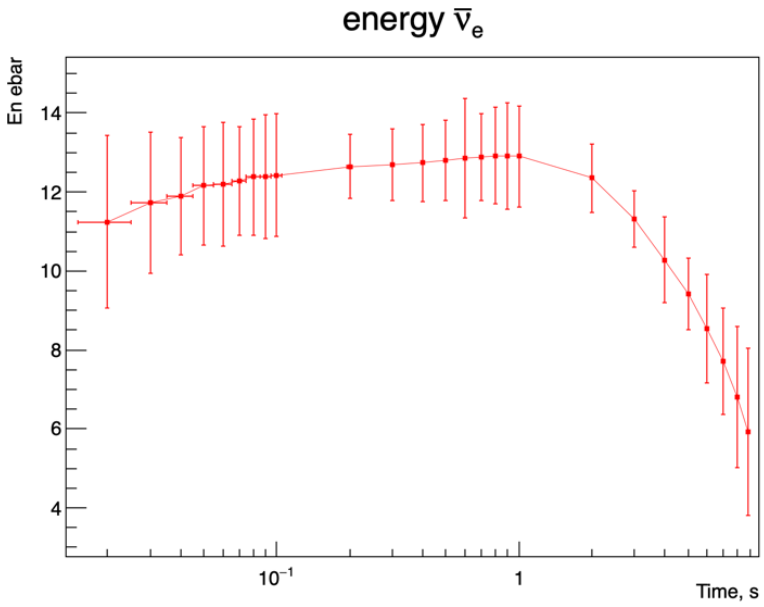

Figure 6.3: Mean energy time curve for the 8.8 $M_\odot$

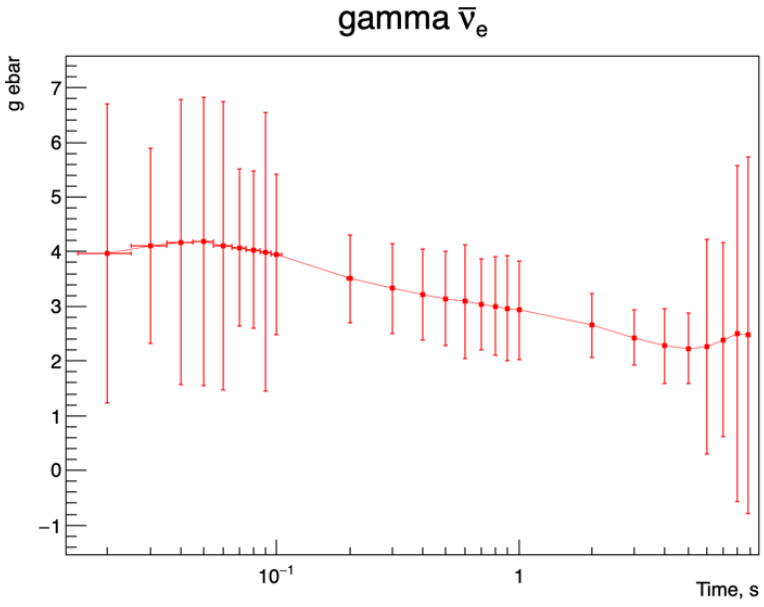

Figure 6.4: γ time curve for the 8.8 $M_\odot$

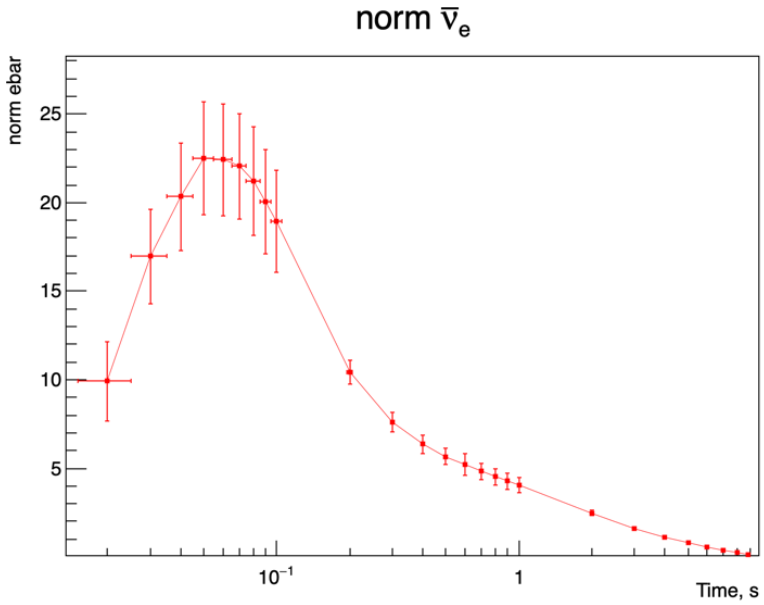

Figure 6.5: γ time curve for the 8.8 $M_\odot$

Parameters, that do not depend on neutrino flavor:

- duration of accretion phase
- duration of the neutronization burst

Other parameters could be subdivided into three categories, i.e. e, $\bar{e}$ and x. See Table 6.1.

In total there were 43 parameters to tune, which one can roughly divide into three subgroups: electron neutrino/antineutrino parameters and ν_x parameters. On the other hand the formulas consist of three time windows, or phases, describing, depending on the time variable, neutralization burst, accretion or cooling phase. Making separate mathematical specification and then summing them up helped to achieve good and precise fit of the time depending curves. The formulas one can find on Fig 6.6.
where $m_i = 4 \cdot gf1_i - 1 \cdot gf2_i - 3 \cdot gc_i$ and $n_i = 2 \cdot gf2_i - 4 \cdot gf1_i + 2 \cdot gc_i$. In order to describe better the mean energy curve, an additional flavor dependent stretch factor fac_a was introduced as $\tau_a = \tau_a \cdot \text{fac}_a$.
Now let's take a look on the result of the fit. Below you can see time dependent plots for normalisation, mean energy and gamma for all the three neutrino species. All of them were fitted simultainously.
In order to find best fit possible the χ^2 was used in a form: $\chi^2 = (\frac{f_{exp} - f_{fit}}{err_{exp}})^2$

$$\dot{N}_i = \frac{n_{n,i}}{\tau_n} \cdot exp(-\frac{t}{\tau_n}) + \quad n_{a,i} \cdot \frac{1}{\tau_a} \cdot (1 - exp(-\frac{t}{\tau_{r,i}})) \cdot exp(-\frac{t}{\tau_a}) + \quad n_{c,i} \cdot \frac{1}{\tau_{c,i}} \cdot (1 - exp(-\frac{t}{\tau_{r,i}})) \cdot exp(-\frac{t}{\tau_{c,i}})$$

$$E_i = (E_{n,i} - E_{a,i}) \cdot exp(-\frac{t}{\tau_n}) + \quad E_{a,i} + (E_{c,i} - E_{a,i}) \cdot (\frac{t}{\tau_a})^{m_{a,i}} + \quad E_{c,i} \cdot exp(-\frac{t - \tau_a}{\tau_{c,i}})$$

$$G_i = (g_{n,i} - g_{a,i}) \cdot exp(-\frac{t}{\tau_n}) + \quad g_{a,i} + (g_{c,i} - g_{a,i}) \cdot \frac{t}{\tau_a} + \quad g_{c,i} + m_e(\frac{t - \tau_a}{\tau_{c,i}}) + n_i(\frac{t - \tau_a}{\tau_{c,i}})^2$$

Initial burst (only e component) — Accretion phase — Cooling phase

Figure 6.6: Time dependent parametisation of the normalisation, mean energy and spectral index.

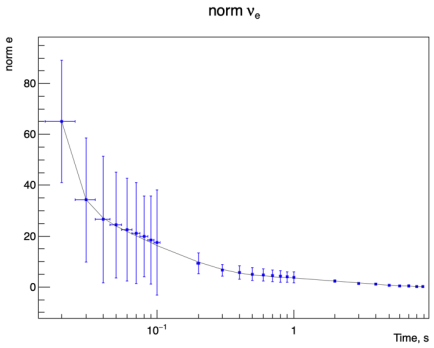

Figure 6.7: Fit of the normalisation(rate) for ν_e.

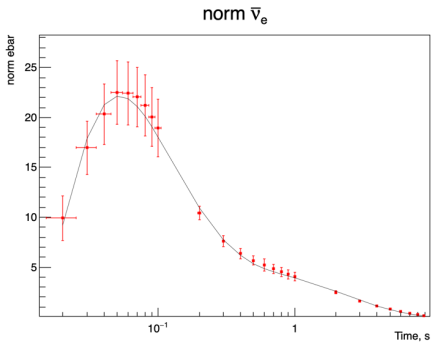

Figure 6.8: Fit of the normalisation(rate) for $\bar{\nu_e}$.

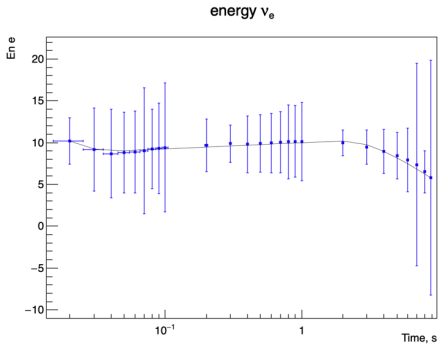

Figure 6.9: Fit of the mean energy for ν_e.

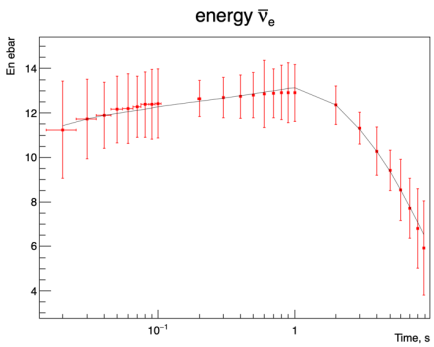

Figure 6.10: Fit of the mean energy for $\bar{\nu_e}$.

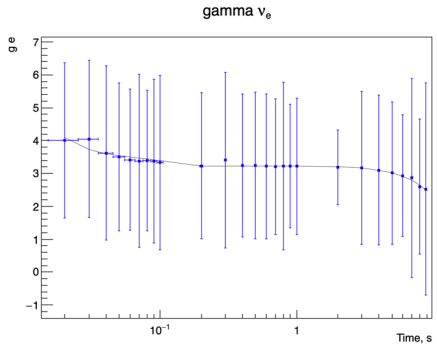

Figure 6.11: Fit of the γ for ν_e.

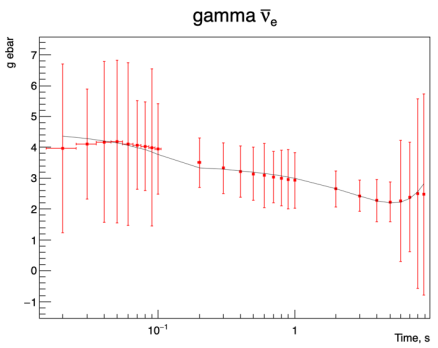

Figure 6.12: Fit of the γ for $\bar{\nu_e}$.

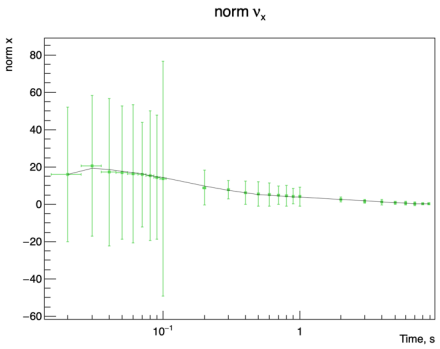

Figure 6.13: Fit of the normalisation(rate) for ν_x.

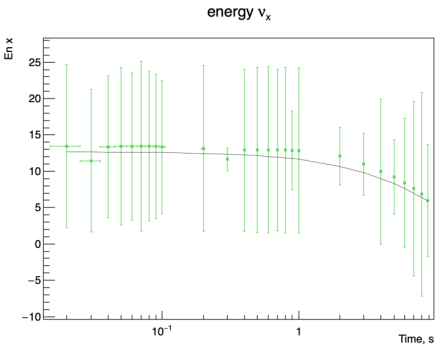

Figure 6.14: Fit of the mean energy for $\bar{\nu_x}$.

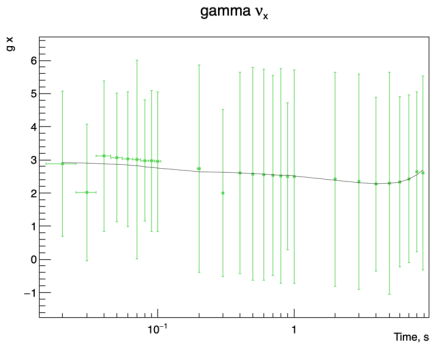

Figure 6.15: Fit of the γ for the $\bar{\nu_x}$.

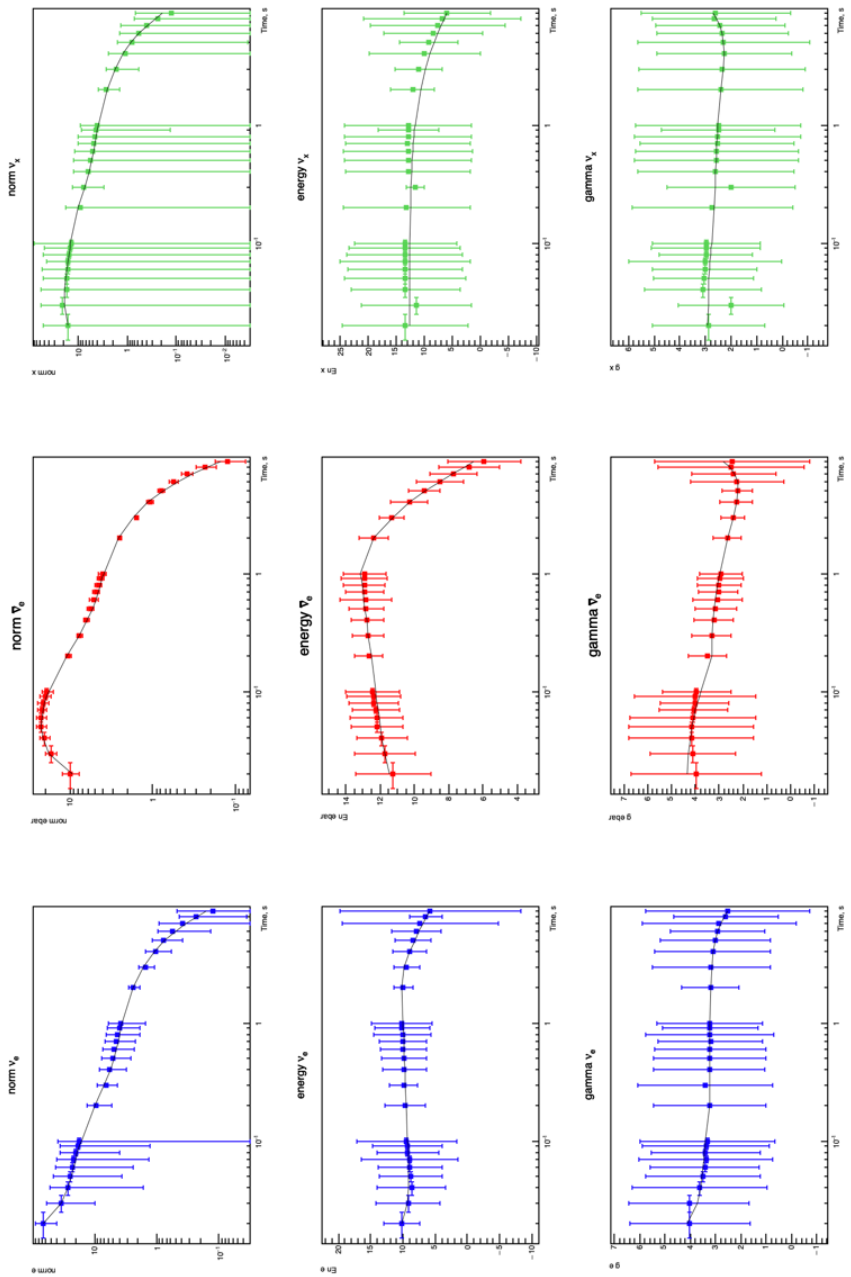

Figure 6.16: Result of the combined simultanous fit of all the time dependent curves. Logarithmic scale used.

Phase	Parameter	ν_e	$\bar{\nu_e}$	ν_x
Neutronization	initial energy	$E_{n,e}$	-	-
	initial γ	$g_{n,e}$	-	-
	stretch factor for neutronization time	fac_n	-	-
	normalistion	n_n	-	-
Accretion	initial energy of accretion phase	$E_{a,e}$	$E_{a,\bar{e}}$	$E_{a,x}$
	flavor dependent stretch factor(k from formula 7.6)	$fac_{a,e}$	$fac_{a,\bar{e}}$	$fac_{a,x}$
	power law parameter	$m_{a,e}$	$m_{a,\bar{e}}$	$m_{a,x}$
	initial γ	$g_{a,e}$	$g_{a,\bar{e}}$	$g_{a,x}$
	parameters to make the γcurve smooth	gf1, gf2	gf1, gf2	gf1, gf2
	rising time	$\tau_{r,e}$	$\tau_{r,\bar{e}}$	$\tau_{r,x}$
	normalisation	$n_{a,e}$	$n_{a,\bar{e}}$	$n_{a,x}$
Cooling	initial energy	$E_{c,e}$	$E_{c,\bar{e}}$	$E_{c,x}$
	cooling time	$\tau_{c,e}$	$\tau_{c,\bar{e}}$	$\tau_{c,x}$
	initial γ	$g_{c,e}$	$g_{c,\bar{e}}$	$g_{c,x}$
	stretch factor for cooling phase	fac_c	-	-
	normalisation	$n_{c,e}$	$n_{c,\bar{e}}$	$n_{c,x}$

Table 6.1: Parameters used in the fit, subdivided into categories.

As one can see, the analytical description fits very well the time dependent curves. Large errors of the initial bins can be explained by small number of events. First bins are only 0.01 s. and since SNOwGLoBES consumes fluences and not fluxes, the number of the produced events was normalised on the width of the time window. The growth of the error bars towards the last bins is also because of the lack of events, since at around 10 second this flux is almost faded. Electron antineutrino curves have the smallest error bars, because at first the JUNO-like experiment via IBD reaction, and then the Icecube-like experiment also via IBD provide a lot of $\bar{\nu_e}$. The electron component comes mainly from the reactions on argon from the DUNE-like experiment. It makes the nomalisation and mean energy values obtained from the fit in these time bins more precise, but still the errors stay rrelatively big. For the ν_x on has only scattering and neutral current reactions, where there is only sum of the spectra of all the neutrino species which can be fitted. Therefore the errors in all the time dependent ν_x curves stay big. And since the mean energy and gamma are anti-correlated, it is pretty difficult to get small error bars for both.

6.5 Measuring the temperature and radius of the PNS neutrino spheres

The time evolution of the neutrino flux parameters of the 8.8 $M_\odot$ supernova explosion model was fitted using the fit functions described in Sec. 6.4. The fit model is well able to reproduce the major features of the simulated neutrino signal. The time fit

allows to access physical parameters of SN explosion and here I treat one of the most straight-forward applications, i.e. temperature and radius of the neutrino spheres. As it was already said, there were 43 parameters in total. The tables with all the values an you can see below. Accretion time fit value is: τ_a 0.14 +/- 0.01, and other parameters arer divided into three columns: ν_e, $\bar{\nu_e}$ and ν_x, please look at Table 6.2 and Table 6.3:

Par	ν_e	Par	$\bar{\nu_e}$
fac_a	17 +/- 9	$fac_{a,\bar{e}}$	9 +/- 2
$E_{a,e}$	5.0 +/- 0.4	$E_{a,\bar{e}}$	8.2 +/- 0.1
$E_{c,e}$	10.3 +/- 0.5	$E_{c,\bar{e}}$	13.2 +/- 0.1
$m_{a,e}$	0.07 +/- 0.03	$m_{a,\bar{e}}$	0.08 +/- 0.01
$\tau_{c,e}$	2.5 +/- 0.4	$\tau_{c,\bar{e}}$	2.4 +/- 0.1
$E_{n,e}$	8 +/- 5	–	–
τ_n	0.007 +/- 0.007	–	–
$g_{a,e}$	3.6 +/- 1.1	$g_{a,\bar{e}}$	4.4 +/- 1.5
$g_{c,e}$	3.2 +/- 0.1	$g_{c,\bar{e}}$	3.4 +/- 0.1
$g_{n,e}$	4.6 +/- 5.3	–	–
$gf1_e$	3.2 +/- 0.1	$gf1_{\bar{e}}$	2.86 +/- 0.04
$gf2_e$	3.18 +/- 0.08	$gf2_{\bar{e}}$	2.5 +/- 0.1
fac_n	1.2 +/- 1.8	–	–
$\tau_{r,e}$	5.07e-05 +/- 0.04	$\tau_{r,\bar{e}}$	0.019 +/- 0.003
fac_c	4.5 +/- 0.6	–	–
$n_{c,e}$	13.3 +/- 1.6	$n_{c,\bar{e}}$	14.2 +/- 0.3
$n_{a,e}$	112 +/- 36	$n_{a,\bar{e}}$	36.7 +/- 3.4
$n_{n,e}$	0.7 +/- 0.3	–	–

Table 6.2: Parameters of the ν_e and $\bar{\nu_e}$ time evolution spectra (all the detectors)

Snowglobes can only provide the detector responses for a fixed 10 kpc distance (and doesn't have any distance uncertainties, if you want to change it), and from the fit procedure come the uncertainties of the fit only. But let us include the space distance uncertainty. The flux of the neutrinos in case of the supernova explosion is proportional to the radius of the neutrino sphere over the distance to the supernova squared (Eq. 6.7):

$$\Phi \propto \frac{R_{NS}^2}{D^2} \tag{6.11}$$

This relation can be used to differ the PNS radius based on the measured neutrino flux and distance from the SN:

Par	ν_x
$fac_{a,x}$	0.02 +/- 0.16
$E_{a,x}$	11.5 +/- 1.5
$E_{c,x}$	12.7 +/- 1
$m_{a,x}$	12 +/- 7
$\tau_{c,x}$	2.6 +/- 0.8
$g_{a,x}$	2.9 +/- 0.9
$g_{c,x}$	2.7 +/- 0.2
$gf1_x$	2.5 +/- 0.1
$gf2_x$	2.3 +/- 0.1
$\tau_{r,x}$	0.003 +/- 0.033
$n_{c,x}$	14.6 +/- 3.6
$n_{a,x}$	4 +/- 3

Table 6.3: Parameters of the ν_x time evolution spectra (all the detectors)

$$R_{NS} \approx \frac{D}{\sqrt{\Phi}} \approx D \cdot \Phi^{-1/2}$$

The corresponding uncertainty can be obtained from standard (gaussian) error propagation:

$$\Delta R = \sqrt{(\frac{1}{\sqrt{\Phi}})^2 \cdot \Delta D^2 + (-\frac{1}{2} \cdot \Phi^{-3/2} \cdot D)^2 \cdot \Delta\Phi^2} = \\ = \sqrt{(\frac{R}{D} \cdot \Delta D)^2 + (-\frac{1}{2} \cdot \frac{R}{\Phi})^2)\Delta\Phi^2}$$

Therefore the relative uncertainty on the radius of the neutrino sphere would be:

$$\frac{\Delta R}{R} \approx \sqrt{(\frac{\Delta D}{D})^2 + (\frac{1}{2}\frac{\Delta\Phi}{\Phi})^2}$$

Flux normalisation measurements will be limited by the uncertainty of the distance to the supernova. Within our galaxy, i.e. Milky Way, the uncertainties can be on the scale of 10-25 % or more, but in some cases, some additional studies of the features, like in case of the SN1987A can reduce it. Such large errors mostly come from the fact, that the Cepheids are being used to determine the distances up to $\propto$ 5Mpc, and they are too faint to use them in direct measurements. For SN1987A the spread of the ring coming from the explosion allowed to reduce it up to 2.3%. So the neutron star radius R_c can be constrained with the accuracy of the distance determination. On our case, since we have flavour dependent normalisation parameters $\text{norm}_{c,i} \approx R_c$, we can speak more about neutrino spheres, i.e. where the emitting of the neutrinos happened.
Let us assume that we have two cases. First case would be that we know the uncertainty of the distance with good precision, let's say 2 %. And the second case would be with the error of 25%. Results you can find in the Table 6.4:

Par	ΔD / D = 2 %	ΔD / D = 25 %
R_e/R_e	6 %	26 %
$R_{\bar{e}}/R_{\bar{e}}$	2.2 %	25 %
R_x/R_x	13 %	28 %

Table 6.4: Relative uncertainties on the radii R_i of the neutrino spheres depending on the distance from astronomical observation uncertainty ΔD / D

It is clear, that in case of the supernova explosion of around 8.8 $M_\odot$ at the typical 10 kpc distance, the crucial role in reducing the error on the neutron star radius will be played the distance determination.
It is also interesting to see the precision of the fit and estimations on the radii, if you take only two detectors, namely JUNO and IceCube, which are able to determine $\bar{\nu_e}$ component very good. On the picture below (Fig. 6.17) you can see the result of the fit.
It is able to fit all the curves very well, but the values of the parameters differ a bit. And fit cannot really determine ν_e parameters and some of the time related parameters, because it is closely connected to ν_e curves development. The complete overview of the values you can see in Table 6.5 and 6.6.

Par	ν_e	Par	$\bar{\nu_e}$
fac_a	13 +/- 18	$fac_{a,\bar{e}}$	4 +/- 3
$E_{a,e}$	5.0 +/- 0.4	$E_{a,\bar{e}}$	7.4 +/- 1.8
$E_{c,e}$	11.4 +/- 2.5	$E_{c,\bar{e}}$	13.0 +/- 0.2
$m_{a,e}$	0.2 +/- 0.2	$m_{a,\bar{e}}$	0.07 +/- 0.06
$\tau_{c,e}$	2.1 +/- 0.6	$\tau_{c,\bar{e}}$	2.11 +/- 0.02
$E_{n,e}$	6.8 +/- 7.5	–	–
τ_n	0.4 +/- 0.4	–	–
$g_{a,e}$	3.5 +/- 1.6	$g_{a,\bar{e}}$	4.7 +/- 0.2
$g_{c,e}$	3.9 +/- 1.0	$g_{c,\bar{e}}$	3.5 +/- 0.2
$g_{n,e}$	3.4 +/- 1.5	–	–
$gf1_e$	3.2 +/- 0.8	$gf1_{\bar{e}}$	2.88 +/- 0.14
$gf2_e$	2.8 +/- 0.9	$gf2_{\bar{e}}$	2.44 +/- 0.13
fac_n	1.0 +/- 7.4	–	–
$\tau_{r,e}$	5.2e-05 +/- 0.01	$\tau_{r,\bar{e}}$	0.023 +/- 0.008
fac_c	9.3 +/- 0.5	–	–
$norm_{c,e}$	11.7 +/- 4.4	$norm_{c,\bar{e}}$	13.9 +/- 0.2
$norm_{a,e}$	149 +/- 77	$norm_{a,\bar{e}}$	68 +/- 108
$norm_{n,e}$	0.001 +/- 32	–	–

Table 6.5: Parameters of the ν_e and $\bar{\nu_e}$ time evolution spectra (JUNO and IceCube case)

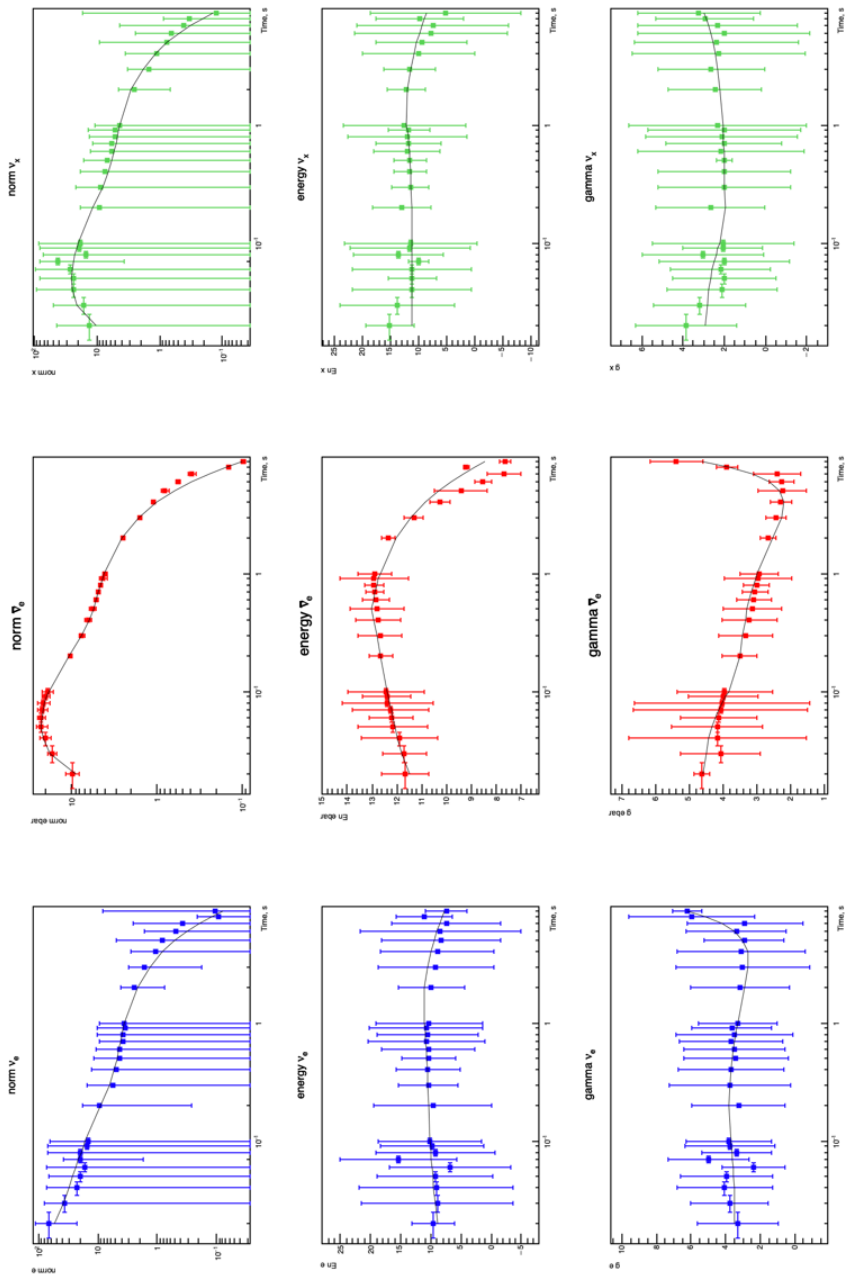

Figure 6.17: Combined JUNO and IceCube result of the combined simultanous fit of all the time dependent curves. Logarithmic scale used.

Par	ν_x
$fac_{a,x}$	11 +/- 12
$E_{a,x}$	11.1 +/- 1.5
$E_{c,x}$	12.3 +/- 2.1
$m_{a,x}$	1 +/- 9
$\tau_{c,x}$	2.3 +/- 1.5
$g_{a,x}$	3 +/- 1
$g_{c,x}$	2.0 +/- 0.5
$gf1_x$	2.1 +/- 0.6
$gf2_x$	2.3 +/- 1.6
$\tau_{r,x}$	0.01 +/- 0.04
$norm_{c,x}$	15.3 +/- 6.1
$norm_{a,x}$	3.3 +/- 6.1

Table 6.6: Parameters of the ν_x time evolution spectra(JUNO and IceCube case)

In Table 6.7 you can find the results for the relative uncertainties in case of two detectors.

Par	ΔD / D = 2 %	ΔD / D = 25 %
R_e/R_e	19 %	31 %
$R_{\bar{e}}/R_{\bar{e}}$	2.3 %	25 %
R_x/R_x	20 %	32 %

Table 6.7: Relative uncertainties on the radii R_i of the neutrino spheres (JUNO and IceCube case)depending on the distance from astronomical observation uncertainty ΔD / D

Using the same Vissani parametrisation and results of the fit, one can also estimate the temperature of the PNS neutrino spheres. It can be done by using the E_c parameter from the parametrisation. The temperature of the neutrinos is roughly 5 times less than the mean energy value, and the final state temperature (at cooling phase) is T_f = 0.6 T_c.

$$T_a(t) = T_i + (T_f - T_i)(\frac{t}{\tau_a})^m, with \begin{cases} T_i = T_a \\ T_f = 0.6 \cdot T_c \end{cases} \tag{6.12}$$

Therefore it is straight-forward to estimate it. The results you can see in the Table 6.8:

Par	ν_e	$\bar{\nu_e}$	ν_x
T_i	3.4±0.2	4.40±0.04	4.2±0.3

Table 6.8: Temperature estimations and uncertainties on the PNS neutrino spheres (all detectors).

The same can be done for the two detectors case. The analysis of the JUNO and IceCube data gives the estimation on the temperature of the PNS neutrino spheres presented in Table 6.9.

Par	ν_e	$\bar{\nu_e}$	ν_x
T_i	3.8±0.9	4.33±0.08	4.1±0.7

Table 6.9: Temperature estimations and uncertainties on the PNS neutrino spheres. (JUNO + IceCube case)

7 Conclusions

A galactic core-collapse supernova is an amazing astrophysical event that cannot be missed. In case of an explosion many of the questions about its nature could be answered. It can reveal the explosion mechanism and leave us with a neutron star or a black hole. The spectra of the neutrinos will be able to indicate how the supernova evolves in time before its death and how much energy of the explosion is carried by the neutrinos. Many fascintaing pecularities and properties of this astrophysical event can be investigating, like cooling time, duration of the accretion phase, initial temperature of the PNS etc. and they allow us to understand the physics behind one of the brightest occasion in the universe.
This thesis is mostly dedicated to the development of the analysis tools for the neutrino burst of a galactic supernova. The tools permit to perform a multidetector sensitivity studies for a selection of existing and upcoming neutrino detectors, namely JUNO, DUNE and IceCube, in case of a supernova explosion. Such an analysis profits from the large variety of the interaction channels for all the neutrino species, which become accessible due to the different taget materials. The huge potential of the liquid scintillators was shown in the last years by Borexino and KamLand experiments, achieving world-leading results in the observation of solar, reactor and geo-neutrinos. The upcoming JUNO detector will be mostly sensitive to the $\bar{\nu_e}$ and ν_x neutrinos. DUNE is liquid argon detector, which suits particularly good for detection of the ν_e-neutrinos and constraing the parameters of its spectrum. IceCube is a long-time operating neutrino observatory, made of a cubic-kilometer antarctic ice. Even though it was designed to detect particles with energies in the multi-GeV to PeV range, it can give a time envelope of $\bar{\nu_e}$ interaction rate. With the spectral information by JUNO, one can translate rates into fluxes.
First part of the work was setting up the framework for the simulation of the data of JUNO, DUNE and IceCube-like detectors. For that purpose the SNOwGLoBES was chosen, the public software for computing interaction rates and energy spectra for supernova neutrinos in various detector materials. In order to upgrade it to the needs of the study, the neutrino-proton scattering process in JUNO was included into the simulation chain. The proton recoils detection depends strongly on the characteristics of the liquid scintillator, such as quenching. To make the simulation more precise and make them be closer to the real detector response, a quenching model, based on the KamLAND scintillator was introduced.
The neutrino flux, coming from the supernova explsion could be described by the standard parametrisation with three parameters: mean energy, γ - the spectral index and luminosity/flux normalisation(equation 5.1). A fit procedure was developed to obtain the supernova neutrino spectra parameters simultaneously from all experiments

included in the analysis.
The χ^2 analysis of the time-integrated fits of fluences showed that the JUNO-like detector can tell a lot about the $\bar{\nu}_e$ and ν_x parameters based on IBD and PES channels, but has basically no information about the ν_e-flux parameters. This is compensated by adding the DUNE-like detector into the fit procedure. χ^2-profiles shown on Fig. 5.10 - 5.11 display the evolution of determination of the parameters and the input of the experiments. The addition of IceCube-like detector gives excellent precision for the $\bar{\nu}_e$ flux, but changes almost nothing for other neutrino species. The individual and combined contributions of the three detectors to the χ^2-profiles for the mean energy of the three flavors is shown in Fig. 5.7 - 5.9.
The determination of the flux parameters gives also the opportunity to estimate the total energy of the explosion and its statistical uncertainties. This was evaluated for a representative SN scenario with equally distributed energy between neutrino species and equal mean energy and γ was simulated, namely $E_i = 0.5 \cdot 10^{53}$ erg, $\langle E \rangle = 12$ MeV and $\gamma = 3$. In order to obtain statistical uncertainties, an ensemble of 100 data sets of the three detectors including Poissonian smearing was created. The distribution of the reconstructed energies is presented on Fig. 5.12.: the best precision gives the $\bar{\nu}_e$ spectrum with the 3.6% uncertainty, the ν_e has 6% and the ν_x 8.2% uncertainty on the reconstructed energy (excluding distance uncertainties).
The neutino signal of a core-collapse supernova explosion evolves over ten seconds. A time-resolved analysis is especialy interesting to confirm or deny the models of the supernova collapse and estimate the astrophysical parameters of a proto-neutron star. In order to fit the time dependent neutrino spectra, the following procedure was applied. The quasi-continous neutrino light curves were converted to a binning logarithmic in time that provide sufficient event statistics per bin for a spectral fit to be applicable. Therefore you obtain the evolution of the neutrino spectra parameters in time. To fit these time behaviours one should do the second step. An adapted analytical model for time development of the mean energy, γ and Φ was used, based on the work of F.Vissani et al. [2].
This description was applied to the model of the supernova explosion corresponding to the Crab nebula of a 8.8 $M_\odot$. In the analysis presented here, this collapse was set to the canonical distance of 10 kpc. All the curves of the neutrino flux parameters were fitted simultaneously. The results are shown on Fig. 6.7 - 6.17. The fit can perfectly reproduce all the time-dependent curves of the neutrino fluxes. It fits neutronization, accretion and cooling phases of the explosion. Best fit values and uncertainties are listed in the tables 6.1 - 6.3.
Using the flux and distance information, obtained from the fit and astronomical observations correspondigly, one can also estimate the uncertainty at which the radius of the neutrino sphere can be determined.
This depends crucially on the distance uncertainty. Within the Milky Way the distance uncertainties are of the order of 25%, but it is possible to reduce it, using visible features of the collapse, 2 % in case of SN1987A. This estimation was done for the three detector case, which shows that they are able to determine the radii of the neutrino spheres to: 6% for ν_e, 2.2% for $\bar{\nu}_e$ and 13% for ν_x. In case of the big

uncertainty on the astronomical distance to the supernova (25%), the uncertainties on the radii of the neutrino spheres stay in a range of 25-32%, which wouldn't allow a precise measurement. It is clear that the distance determination plays crucial role. Using the same parametrisation and fit results, the temperatures of the PNS neutrino spheres was estimated. All the detectors estimate the temperatures at: $T_{\nu_e} = 3.4 \pm 0.2$ MeV, $T_{\bar{\nu_e}} = 4.40 \pm 0.04$ MeV, $T_{\nu_x} = 4.2 \pm 0.3$ MeV.
As it was already mentioned in this work, the combined analysis of the supernova signal is crucial in order to determine with percent level precision the parameters of the neutrino spectra and some astrophysical parameters. Therefore adding other neutrino detectors would improve the results. HyperKamiokande could be one of the candidates. This ultra-large Water-Cherenkov detector could bring even more to the $\bar{\nu_e}$ spectrum parameters determination. The other candidate could be HALO experiment. Lead has a large neutron excess, which strongly inhibits the proton to neutron transitions due to Pauli blocking. In contrast, the reaction involving the electron neutrino in heavy elements has a large enhancement from the nuclear Coulomb effect in comparison to lighter elements. The suppression of electron antineutrinos and the enhancement of electron neutrinos make HALO uniquely sensitive to electron neutrinos and complementary to the water Cherenkov and scintillator detectors, which are primarily sensitive to electron anti-neutrinos. It is also sensitive to the ν_x due to the NC-intercation on Pb. Therefore it can improve the precision on ν_e and ν_x neutrino spectra. Of course the effect of flavor oscillation on fluxes and spectra of the neutrinos should be studied. Even though it wouldn't change the algorithms presented in this work, one would need to do all the simulations for the detectors with oscillations included, to describe better the real neutrino signal. It is worth mentioning that one could find time-dependent features of the spectra, like SASI (Standing Accretion Shock Instabilities). They are interesting to investigate in order to understand the dynamic of the collapse and its connection not only to the rate of the neutrinos, but also to the gravitational waves, which potentionally could be detected.

8 Bibliography

Bibliography

[1] Hüdepohl L, Müller B, Janka HT, Marek A, Raffelt GG. Neutrino signal of electron-capture supernovae from core collapse to cooling. Phys Rev Lett. 2010 Jun 25;104(25):251101. doi: 10.1103/PhysRevLett.104.251101. Epub 2010 Jun 22. PMID: 20867357. **arXiv:0912.0260** [astro-ph.SR]

[2] G. Pagliaroli, F. Vissani, M. L. Costantini and A. Ianni, Astropart. Phys. **31** (2009), 163-176 doi:10.1016/j.astropartphys.2008.12.010 [arXiv:0810.0466 [astro-ph]].

[3] C. L. Cowan, Jr. et al. ,Detection of the Free Neutrino: a Confirmation.Science124,103-104(1956).DOI:10.1126/science.124.3212.103

[4] Carlo Giunti and Chung W.Kim, Fundamentals of neutrino physics and astrophysics.

[5] K. Scholberg, Ann. Rev. Nucl. Part. Sci. **62** (2012), 81-103 doi:10.1146/annurev-nucl-102711-095006 [arXiv:1205.6003 [astro-ph.IM]].

[6] W.Baade and F.Zwicky, *Phys. Rev.,* 46, 76-77, 1934.

[7] S. Chandrasekhar, *An Introduction to the study of Stellar Structure*, University of Chicago Press, 1938.

[8] F. Manucci et al., *Astron. Astrophys.*, 433, 807-814, 2005, astro-ph/0411450.

[9] G.A. Tammann, 1982, Supernovae: a Survey of Current Research, Cambridge, England, June 29-July 10, 1981, p.371-403.

[10] K.U Ratnatunga and S. van den Bergh, *Astrophys. J.*, 343, 713-717, 1989

[11] R.G. Strom, 1990, NATO Advanced Study Institute on Neutron Stars: Their Birth, Evolution, Radiation and Winds, Erice, Sicily, Italy, September 5-17, 1988, p.253.

[12] R.A. Muller et al., *Astrophys. J*, 384, L9-L13, 1992.

[13] E. Cappellaro et al., *Astron. Astrophys.*, 273, 383, 1993, astro-ph/9302017.

[14] S. van den Bergh, *Comments on Astrophys.*, 17, 125-130, 1993.

[15] G.A. Tammann, W. Loeffer, and A. Schroder, *Astrophys. J. Suppl.*, 92, 487-493, 1994.

[16] R.G. Strom, *Astron. Astrophys.*, 288, L1-L4, 1994.

[17] E. Cappellaro et al., *Astron. Astrophys.*, 322, 431-441, 1997, astro-ph/9611191.

[18] F.X Timmes, R. Diehl, and D.H. Hartmann, 1997, astro-ph/9701242.

[19] P.M. Dragicevich, D.G. Blair, and R.R. Burman, *Mon. Not. Roy. Astron. Soc.*, 302, 693-699, 1999.

[20] E. Cappellaro and M.Turrato, 2000, astro-ph/0012455, The Influence of Binaries on Stellar Population Studies, Brussels 21-25 Aug. 2000.

[21] B.C. Reed, *Astronomical J.*, 130, 1652-1657, 2005, astro-ph/0506708.

[22] E.N. Alekseev and L.N. Alekseeva, *J. Exp. Theor. Phys.*, 95, 5-10, 2002, astro-ph/0212499.

[23] R. Narayan, 1987, Ap. *J.*, **319**, 162.

[24] John N. Bahcall, Neutrino Astrophysics, Cambridge University Press.

[25] A. Heger, C. L. Fryer, S. E. Woosley, N. Langer and D. H. Hartmann, Astrophys. J. **591** (2003), 288-300 doi:10.1086/375341 [arXiv:astro-ph/0212469 [astro-ph]].

[26] A. Burrows, S. Reddy and T. A. Thompson, Nucl. Phys. A **777** (2006), 356-394 doi:10.1016/j.nuclphysa.2004.06.012 [arXiv:astro-ph/0404432 [astro-ph]].

[27] Burbidge, E.M., G.R. Burbidge, W.A.Fowler, and F. Hoyle (1957) *Rev. Mod. Phys.*, **29**, 547.

[28] L. Zhan, Y. Wang, J. Cao and L. Wen, Phys. Rev. D **78**, 111103 (2008) [arXiv:0807.3203 [hep-ex]].

[29] L. Zhan, Y. Wang, J. Cao and L. Wen, Phys. Rev. D **79**, 073007 (2009) [arXiv:0901.2976 [hep-ex]].

[30] Yifang Wang, talk at ICFA seminar, (2008). `http://www-conf.slac.stanford.edu/icfa2008/Yifang_Wang_102808.pdf`

[31] Jun Cao, talk at Neutrino Telescope, (2009). `http://neutrino.pd.infn.it/NEUTEL09/Talks/Cao.pdf`

[32] Y. F. Li, J. Cao, Y. Wang and L. Zhan, Phys. Rev. D **88**, 013008 (2013) [arXiv:1303.6733 [hep-ex]].

[33] F. An *et al.* [JUNO], J. Phys. G **43** (2016) no.3, 030401 doi:10.1088/0954-3899/43/3/030401 [arXiv:1507.05613 [physics.ins-det]].

[34] B. Abi *et al.* [DUNE], JINST **15** (2020) no.08, T08008 doi:10.1088/1748-0221/15/08/T08008 [arXiv:2002.02967 [physics.ins-det]].

[35] V. Hewes *et al.* [DUNE], Instruments **5** (2021) no.4, 31 doi:10.3390/instruments5040031 [arXiv:2103.13910 [physics.ins-det]].

[36] Abi, B., Acciarri, R., Acero, M.A. et al. Supernova neutrino burst detection with the Deep Underground Neutrino Experiment. Eur. Phys. J. C **81**, 423 (2021). https://doi.org/10.1140/epjc/s10052-021-09166-w

[37] SNOwGLoBES. `http://www.phy.duke.edu/~schol/snowglobes`

[38] T. Totani, K. Sato, H. E. Dalhed and J. R. Wilson, Astrophys. J. **496** (1998), 216-225 doi:10.1086/305364 [arXiv:astro-ph/9710203 [astro-ph]].

[39] J. Gava, J. Kneller, C. Volpe and G. C. McLaughlin, Phys. Rev. Lett. **103** (2009), 071101 doi:10.1103/PhysRevLett.103.071101 [arXiv:0902.0317 [hep-ph]].

[40] R. Cross *et al.* [IceCube], PoS **ICRC2019** (2020), 889 doi:10.22323/1.358.0889 [arXiv:1908.07249 [astro-ph.HE]].

[41] Icecube neutrino observatory. `https://icecube.wisc.edu/science/icecube/`

[42] A. Strumia and F. Vissani, Phys. Lett. B **564** (2003), 42-54 doi:10.1016/S0370-2693(03)00616-6 [arXiv:astro-ph/0302055 [astro-ph]].

[43] W. J. Marciano and Z. Parsa, J. Phys. G **29** (2003), 2629-2645 doi:10.1088/0954-3899/29/11/013 [arXiv:hep-ph/0403168 [hep-ph]].

[44] Kolbe, E., Langanke, K., & Vogel, P. 2002, Phys. Rev. D, 66, 13007

[45] Haxton, W. C., & Robertson, R. G. H. 1999, Phys. Rev. C, 59, 515

[46] IceCube sensitivity for low-energy neutrinos from nearby supernovae. A&A 535, A109 (2011), DOI: 10.1051/0004-6361/201117810

[47] IceCube Collaboration, R. Abbasi et al., Astron. Astrophys. **535** (2011) A109.

[48] F. Malmenbeck *et al.* [IceCube], [arXiv:1909.00886 [astro-ph.HE]].

[49] Lutz Köpke (for the IceCube Collaboration). Supernova Neutrino Detection with IceCube. arXiv:1106.6225, [**astro-ph.HE**]

[50] snowglobes1.2.pdf `https://github.com/SNOwGLoBES/snowglobes`

[51] E. Kolbe, K. Langanke and P. Vogel, Nucl. Phys. A **652** (1999), 91-100 doi:10.1016/S0375-9474(99)00152-9 [arXiv:nucl-th/9903022 [nucl-th]].

[52] B. Armbruster et al. Measurement of the weak neutral current excitation C-12(nu(mu) nu'(mu))C*-12(1+,1,15.1-MeV) at E(nu(mu)) = 29.8- MeV. *Phys. Lett.*, B423:15–20, 1998.

[53] I. Gil Botella and A. Rubbia, JCAP **08** (2004), 001 doi:10.1088/1475-7516/2004/08/001 [arXiv:hep-ph/0404151 [hep-ph]].

[54] E. Kolbe, K. Langanke, G. Martinez-Pinedo and P. Vogel, J. Phys. G **29** (2003), 2569-2596 doi:10.1088/0954-3899/29/11/010 [arXiv:nucl-th/0311022 [nucl-th]].

[55] C A Duba *et al.* 2008 J. Phys.: Conf. Ser. **136** 042077

[56] S. Amoruso *et al.* [ICARUS], Eur. Phys. J. C **33** (2004), 233-241 doi:10.1140/epjc/s2004-01597-7 [arXiv:hep-ex/0311040 [hep-ex]].

[57] The IceCube Collaboration: R. Abbasi et al. ASTRONOMY & ASTROPHYSICS, 535:109 (2011).

[58] S. Weinberg, Phys. Rev. D **5**, 1412 (1972).

[59] L.A. Ahrens et al., Phys. Rev. D **35**, 785 (1987).

[60] J. F. Beacom, W. M. Farr and P. Vogel, Phys. Rev. D **66** (2002), 033001 doi:10.1103/PhysRevD.66.033001 [arXiv:hep-ph/0205220 [hep-ph]].

[61] D. E. Groom et al., Eur. Phys. J. C 15, 1 (2000).

[62] A. Suzuki, in Lepton and Baryon Number Violation Par- ticle Physics, Astrophysics, and Cosmology, eds. H.V. Klapdor-Kleingrothaus and I.V. Krivosheina (Institute of Physics, Philadelphia, 1999); S. J. Freedman, G. Gratta, et al., Proposal for US Participation in KamLAND, March 1999; A. Piepke, Nucl. Phys. Proc. Suppl. **91**, 99 (2001)

[63] W. R. Leo, Techniques for Nuclear and Particle Physics Experiments, Second Edition (Springer-Verlag, Berlin, 1994).

[64] NIST PSTAR Database: `https://physics.nist.gov/PhysRefData/Star/Text/`

[65] M. T. Keil, G. G. Raffelt and H. T. Janka, Astrophys. J. **590** (2003), 971-991 doi:10.1086/375130 [arXiv:astro-ph/0208035 [astro-ph]].

[66] H. A. Bethe and J. Wilson, R., Astrophys. J. **295**, 14 (1985).

[67] H. A. Bethe, Rev. Mod. Phys. **62**, 801 (1990).

[68] T. J. Loredo and D. Q. Lamb, Phys. Rev. D **65** (2002), 063002 doi:10.1103/PhysRevD.65.063002 [arXiv:astro-ph/0107260 [astro-ph]].

[69] J. S. Lu, J. Cao, Y. F. Li and S. Zhou, JCAP **05** (2015), 044 doi:10.1088/1475-7516/2015/05/044 [arXiv:1412.7418 [hep-ph]].